1-23-2017

Catalytic Upgrading of Biogas to Fuels: Role of Reforming Temperature, Oxidation Feeds, and Contaminants

Nada Elsayed
University of South Florida, nadahelsayed@gmail.com

Catalytic Upgrading of Biogas to Fuels:

Role of Reforming Temperature, Oxidation Feeds, and Contaminants

by

Nada H. Elsayed

A dissertation submitted in partial fulfillment
of the requirements for the degree of
Doctor of Philosophy
Department of Chemical and Biomedical Engineering
College of Engineering
University of South Florida

Co-Major Professor: John N. Kuhn, Ph.D.
Co-Major Professor: Babu Joseph, Ph.D.
Scott Campbell, Ph.D.
Sylvia Thomas, Ph.D.
Matthew M. Yung, Ph.D.

Date of Approval:
January 17, 2017

Keywords: Biogas Reforming, Low Metal Loading, Pt and Pd Catalysts, Alternative Fuels, Waste-to-Energy, Greenhouse Gas Emissions

DEDICATION

I dedicate this to my family who are truly my backbone. To my wonderful parents Salwa and Hamdy, I would be nowhere without your unconditional love and encouragement. To my amazing husband Mostafa, thank you for always being there, supporting and loving me. And finally to my boys Adam and Noah, I love you beyond words.

ACKNOWLEDGMENTS

I would like to acknowledge first and foremost Dr. John Kuhn for all of his help, patience and guidance throughout my Ph.D. I would also like to acknowledge Dr. Joseph for his valuable input and direction. I would also like to thank all of my committee members (Dr. Yung, Dr. Campbell, and Dr. Thomas) for giving me time and feedback. I would like to acknowledge all the present and previous members of the Heterogeneous Catalysis & Materials Chemistry Group. Dr. Yolanda A. Daza, Debtanu Maiti, Ummuhan Cimenler, as well as my undergrad mentees Nathan Roberts and Anthony Elwell.

I would also like to acknowledge the funding sources that made this research possible. I would like to acknowledge funding from the Hinkley Center for Solid and Hazardous Waste Management, NASA's Dissertation Improvement Fellowship administered by the Florida Space Grant Consortium, and the Graduate Students Success Fellowship that is administered by the USF School of Graduate Studies.

TABLE OF CONTENTS

LIST OF TABLES iv

LIST OF FIGURES vi

ABSTRACT viii

CHAPTER 1: INTRODUCTION 1
1.1 Biomass 2
1.2 Methane Emissions 3
1.3 Municipal Solid Waste Biomass 4
1.4 Types of Methane Reforming 6
1.5 Landfill Gas Cleanup Technologies and Motivation 8
1.6 Catalyst System 9
1.6.1 Ceria-Zirconia Oxide Support 9
1.6.2 Nickel Catalysts 10
1.6.3 Magnesium 11
1.6.4 Noble Metals 11

CHAPTER 2: LOW TEMPERATURE DRY REFORMING OF METHANE OVER PT-NI-MG/CERIA-ZIRCONIA CATALYSTS 15
2.1 Introduction 15
2.2 Experimental 18
2.2.1 Materials and Synthesis 18
2.2.2 Catalyst Characterization 19
2.2.3 Catalytic Testing 20
2.3 Results and Discussion 22
2.3.1 Characterization 22
2.3.2 TP-Rxn Results 29
2.3.3 Steady-State Reaction Results 31
2.4 Conclusion 35

CHAPTER 3: COMPARISON OF PD-NI-MG/CERIA-ZIRCONIA AND PT-NI-MG/ CERIA-ZIRCONIA CATALYSTS FOR SYNGAS PRODUCTION VIA LOW TEMPERATURE REFORMING OF MODEL BIOGAS 37
3.1 Introduction 37
3.2 Experimental Section 39
3.2.1 Synthesis and Materials 39
3.2.2 Catalyst Characterization 40

3.2.3 Catalytic Testing 42
3.3 Results and Discussion 43
3.3.1 Characterization 43
3.3.2 TP-Dry Reforming 49
3.3.3 Steady-State Dry Reforming (470-430°C) 50
3.3.4 Post-Reaction Characterization 52
3.4 Conclusion 53

CHAPTER 4: EFFECT OF SILICON POISONING ON CATALYTIC DRY REFORMING OF SIMULATED BIOGAS 54
4.1 Introduction 54
4.2 Experimental Procedure 58
4.2.1 Synthesis and Materials 58
4.2.2 Catalyst Characterization 59
4.2.3 Catalytic Testing 60
4.3 Results and Discussion 61
4.3.1 Characterization 62
4.3.1.1 Temperature Programmed Reduction (TPR) 62
4.3.1.2 N_2 Physisorption Analyses 63
4.3.1.3 Scanning Electron Microscopy Coupled with Energy Dispersive Spectroscopy (SEM/EDS) 65
4.3.1.4 FT-IR Spectroscopy 67
4.3.1.5 XRD 67
4.3.2 Dry Reforming 68
4.4 Summary and Conclusion 73

CHAPTER 5: SYNGAS PRODUCTION AND REACTANT CONVERSION USING PT-NI-MG/CERIA-ZIRCONIA AND PD-NI-MG/CERIA-ZIRCONIA CATALYSTS AND EFFECT OF GHSV ON LOW TEMPERATURE BI-REFORMING OF MODEL BIOGAS 75
5.1 Introduction 75
5.2 Experimental 79
5.2.1 Materials and Synthesis 79
5.2.2 Catalyst Characterization 80
5.2.3 Catalytic Testing 82
5.3 Results and Discussion 83
5.3.1 Equilibrium Conversions 83
5.3.2 Experimental Results 84
5.3.3 DRIFTS 88
5.3.4 Steady-State Reaction Studies (600-400°C) 90
5.3.5 Conditions (Feed Composition) Effect of Feed 92
5.3.6 Time on Stream Study 93
5.4 Conclusion 94

CHAPTER 6: CONCLUSIONS AND FUTURE WORK 96
6.1 Conclusions 96

6.2 Future Work 98
6.2.1 Gas Cleanup and Cost Analysis 98
6.2.2 FTS Catalyst Components Suitable For Combined Process 99

REFERENCES 101

APPENDIX A: COPYRIGHT PERMISSIONS 110
A.1 Permission for Use of Material in Chapter 1 110
A.2 Permission for Use of Material in Chapter 2 111
A.3 Permission for Use of Material in Chapter 3 112

APPENDIX B: CALCULATIONS 113
B.1 Assumptions and Calculations for Chapter 4 113

LIST OF TABLES

Table 1.1 Biomass conversion to second generation biofuels: Overview, advantages and disadvantages of various technologies/processes 14

Table 2.1 Surface, bulk properties, reduction temperatures and CO_2 adsorption data 24

Table 2.2 Temperature-programmed reaction results for the various catalysts 30

Table 2.3 Activation energies of different metal-based catalysts 33

Table 2.4 Literature comparison of apparent activation energies and turnover frequencies (TOFs) at T=450°C for selected catalysts 35

Table 3.1 Surface area, pore properties, CO_2 desorption data and reduction temperature 45

Table 3.2 Dry reforming 10% and 50% conversion temperatures and H_2:CO ratio at T=450°C 51

Table 3.3 Turnover frequencies, rates, and apparent activation energies of select catalysts (at given temperatures and P=1 atm) 52

Table 4.1 Properties of selected volatile methyl siloxanes[a] 57

Table 4.2 Mass gain of silica 62

Table 4.3 Specific surface areas (SSA)[a] and bulk properties 64

Table 4.4 EDS quantitative data (in Wt%, carbon-free basis) for fresh 0.16Pt and NiMg catalysts compared to the 6M-Pt and 6M-NiMg catalysts 66

Table 4.5 Methane and carbon dioxide 10% (X_{10}) and 50% (X_{50}) conversion temperatures 69

Table 5.1 Physiochemical properties 86

Table 5.2 Comparison of steam reforming alone vs. dry reforming vs. bi-reforming reaction data at 500°C and 1 atm 87

Table B1 Mass gain of silica and error calculations 114

Table B2 Effect of changing GHSV (h^{-1}) 114

Table B3 Effect of changing initial siloxane amount 115

LIST OF FIGURES

Figure 1.1 Objectives of this research effort (denoted by dashed lines) and place in overall WTE process 13

Figure 2.1 BJH pore size distribution of all samples 23

Figure 2.2 XRD pattern of catalysts 25

Figure 2.3 TPR profiles of catalysts 26

Figure 2.4 TPD-CO_2 of reduced catalysts 28

Figure 2.5 Dry reforming activity trends 31

Figure 2.6 CH_4 and CO_2 conversion from 100.5 hr stability test 32

Figure 3.1 Temperature-programmed reduction (TPR) profiles as represented by water formation (m/z 18) 44

Figure 3.2 BJH pore size distribution curves 47

Figure 3.3 X-ray diffraction patterns of Pd (A) and Pt (B) catalysts 48

Figure 3.4 TPD-CO_2 (m/z = 44) of reduced Pd (A) and Pt (B) catalysts 48

Figure 3.5 Hydrogen and carbon monoxide formation over 0.13Pd (A/B) and 0.16Pt (C/D) with respect to temperature 50

Figure 4.1 Temperature-programmed reduction (TPR) profiles as represented by water formation (m/z 18) 63

Figure 4.2 SEM images of fresh vs. 6M catalysts 65

Figure 4.3 IR spectra of Pt and NiMg catalysts 67

Figure 4.4 X-ray diffraction patterns of 0.16Pt and NiMg catalysts 68

Figure 4.5 Hydrogen and carbon monoxide formation with respect to temperature 71

Figure 4.6 TPR profiles of 1M-NiMg catalysts at 600°C calcination and 800°C calcination..... 72

Figure 4.7 Effect of silica addition on CH_4 and CO_2 conversion 73

Figure 5.1 Sensitivity study and H_2:CO ratio with respect to temperature (300°C-600°C) at 1 atm using a feed composition in Kmol CH_4=3, CO_2=1 and H_2O=2 83

Figure 5.2 DRIFTS spectra of 0.16Pt and 0.13Pd catalysts..... 89

Figure 5.3 H_2:CO ratio with respect to temperature at different GHSV (h^{-1})..... 91

Figure 5.4 CH_4 percent conversion with respect to temperature at different GHSV (h^{-1}) 92

Figure 5.5 CO_2 percent conversion with respect to temperature at different GHSV (h^{-1}) 93

Figure 5.6 Time-on-stream study of 0.16Pt sample at T=500°C and P=1atm..... 94

ABSTRACT

Global energy demands are constantly increasing and fossil fuels are a finite resource. The shift towards alternative, more renewable and sustainable fuels is inevitable. Furthermore, the increased emissions of greenhouse gases have forced a pressing need to find cleaner, more environmentally friendly sources of fuel. Biomass energy is a promising alternative fuel because it offers several important advantages. It is a renewable energy form, it comes from many sources and produces biogas (CH_4 and CO_2). Furthermore, it can have a zero carbon footprint; this is due to the fact that the carbon produced is from the same carbon used to make the biomass. In addition, by replacing fossil fuels, the emissions of CH_4 and CO_2 (both greenhouse gases) is reduced. Biomass-derived syngas (H_2 and CO) can be utilized as a feedstock for many important industrial processes such as methanol synthesis, ammonia synthesis and Fischer-Tropsch synthesis (FTS) to produce long chain hydrocarbon fuels.

Municipal solid waste (MSW) biomass is considered as the source of the biomass for this dissertation work. MSW accounts for 20% of man-made methane emissions making it an attractive source for utilization. However, methane reforming to synthesis gas (H_2 and CO) typically occurs at temperatures higher than 600°C making it economically challenging at the smaller scale of MSW conversion processes.

This dissertation effort focused on formulating low precious metal loaded heterogeneous catalysts that can reform methane at low temperature (T<500°C) making the process more industrially viable. The effect of select contaminants (siloxanes) in the biogas on the reforming

catalysts was studied through accelerated poisoning. Finally, the syngas ratio was improved by combining low temperature dry reforming with steam reforming (termed bi-reforming).

The catalyst system used for this dissertation study was comprised of 1.34wt%Ni-1.00wt%Mg on a Ceria-Zirconia oxide support (0.6:0.4 ratio respectively). The catalysts were doped with platinum (0-0.64% by mass) and compared to palladium doped catalysts (0-0.51% by mass). The ratio chosen for the support, $Ce_{0.6}Zr_{0.4}$, was determined to be the best ratio in terms of activity and surface area by previous studies done in this group [1]. Nickel has been widely studied as methane reforming catalyst [2-6]. Alone, nickel atoms are prone to carbon deposition especially during methane decomposition, however, coupling NiO with MgO helps to reduce carbon deposition by reducing agglomeration of Ni crystallites, thereby improving catalyst lifetime [2, 7]. Furthermore, addition of small amounts of noble metals such as Pt or Pd help to drive the reduction of the catalyst to lower temperatures and enhance catalytic activity.

Different metal loadings of Pt and Pd were tested to determine the optimum catalyst that will reform methane at low temperatures, is resistant to deactivation and produces a high syngas ratio (~2:1) which is necessary for processes such as FTS. Preliminary results have shown that in general Pt is superior in this catalyst system for low temperature reforming of methane. It consistently had syngas ratios near the desired ratio compared to Pd, it did not deactivate with extended time on stream and overall had higher turnover frequencies. This catalyst system has potential to make industrial reforming of methane from biomass feedstock more economically viable.

CHAPTER 1: INTRODUCTION

With increasing population, it is estimated that global energy demands will continue to rise and top 820 quadrillion BTU in the next thirty years. That is more than a 56% increase from today's demand of 524 quadrillion BTU according to the International Energy Outlook of 2013 [8]. Most of the demand will continue to be fulfilled from non-renewable fossil fuels. In the US alone, 14.3 billion barrels of fossil fuels are presently being consumed annually. Current US proved oil reserves are about 19.1 billion barrels [9] and world reserves about 1342 billion barrels. Given the current rising trend in energy consumption, the world reserves would be exhausted in just over 40 years. With the inevitable depletion of fossil fuels and the alarming increase in demand, alternative fuel sources are no longer optional, but are now a necessity. Alternative fuels that are currently under investigation or are being used include solar energy, wind energy, biomass energy, and hydrogen energy to name a few. Although each type of alternative fuel mentioned offers advantages, there are also severe limitations preventing it from being used on a wider scale. For instance, solar energy is intermittent and highly dependent on geographic location. Other alternative energy forms suffer from issues of transportation and storage.

Waste to energy (WTE) routes offer several attractive advantages. In addition to being sustainable as well as renewable, WTE fuels also have the potential to reduce emissions of two major greenhouse gases mainly methane and carbon dioxide. Furthermore, WTE fuels specifically biofuels can have zero carbon emissions. This is a result of reutilizing the carbon in the biomass which was produced from CO_2 in the atmosphere. This same carbon which forms carbon dioxide,

is used to make synthesis gas (H_2 and CO) and other hydrocarbons in combined processes potentially resulting in zero environmental emissions.

Biomass-derived biogas conversion to liquid fuels is considered as a potential alternative fuel source for a variety of reasons as previously mentioned. In addition to the possibility to become a carbon neutral energy source as well as reduce emissions of CH_4 and CO_2, upon reforming, the produced syngas can be used as a feedstock for many industrial chemicals including Fischer Tropsch Synthesis (FTS) to produce liquid hydrocarbons. The goal of this dissertation is to reform biogas at low temperatures to syngas using novel low metal loading heterogeneous catalysts and determine the effect of select impurities on the reforming catalysts. The produced syngas can then be used through an unconventional route to upgrade (the original biogas) using noble metal-doped composite catalysts to liquid hydrocarbon fuels using FTS in a combined intensified process.

1.1 Biomass

Biomass produces biogas (CH_4 and CO_2) through several pathways. Table 1.1 outlines various routes of biomass to second generation biofuels as well as the main advantages and limitations of each. Biomass can come from industrial residues, animal wastes, municipal solid waste (MSW), sludge digesters and agricultural crops. Depending on the source of the biomass, the produced biogas which is roughly equal parts of the two major greenhouse gases methane and carbon dioxide, can also have some contaminants such as the case with MSW derived biomass [10].

Biomass also possesses the attractive quality of being a carbon neutral energy source since the carbon dioxide produced is largely the same that was used to create the biomass forming a closed carbon cycle as mentioned earlier. That is one of the main advantages of utilizing biomass

as an energy source versus fossil fuels which generates new greenhouse gases according to NREL [11]. Biomass has been used as an energy form from prehistoric times when wood was burned for energy. Furthermore, biomass has the potential to largely replace the heavily depended-upon fossil fuels and can be utilized in three useful ways. Biomass can be converted to liquid fuels termed biofuels which is the main focus of this dissertation effort. However it can also be directly burned for electricity (biopower) or can be reprocessed into chemicals (bioproducts)[11].

CH_4 and CO_2, the two most abundant greenhouse gases, are the primary components of biogas as previously mentioned and have been increasingly emitted into the earth's atmosphere. According to the key world energy statistics, CO_2 emissions have been steadily increasing for the past 45 years, with more than 31.7 GT of CO_2 emitted in 2012 [12]. At the current rate, it is expected that emissions can reach 45 GT by 2040 which may devastatingly and irreversibly increase the earth's temperature by 2°C [12]. Therefore, it is crucial to find ways to decrease emissions of CO_2. Furthermore, methane, which is the second most abundant greenhouse gas is more powerful than CO_2 in that it is able to trap energy much more efficiently into the earth's atmosphere [13]. In fact, over a 100 year period, pound for pound, methane has an effect 25 times greater on the earth's atmosphere than CO_2 [13]. Therefore, methane is a gas that should be mitigated and considered for its harmful effects just like CO_2.

1.2 Methane Emissions

In 2014, methane (CH_4) accounted for 11% of all emitted greenhouse gases [13]. CH_4 comes from a variety of different sources. More than 33% of man-made CH_4 emissions comes from petroleum and natural gas processes. Enteric fermentation accounts for the second largest portion of emissions at 22%. Landfills account for 20% of all CH_4 emissions. Coal mining accounts for 9% of emissions and the remaining 14% comes from wastewater treatment and other smaller

sources [13]. Natural sources such as wildfires, termites and wetlands also contribute to CH_4 emissions, although at a smaller scale. According to the Inventory of U.S. Greenhouse Gas Emissions and Sinks published on the EPA's website, more than 700 million metric tons of CO_2 equivalent CH_4 was released into the atmosphere in 2014 [13] with an expectation that this number will continue to rise.

As a result of the increased awareness to the potential hazardous effect of CH_4 emissions on the global community, many initiatives have been placed to help mitigate emissions. In 2010, the Global Methane Initiative was launched with the support of more than 38 nations to find solutions to curb CH_4 emissions. Because methane is produced from many sources, reduction of emissions varies and can be source specific. In industry, new equipment can reduce undesired leaks. Capturing and storing methane for energy is also an option especially in coal mines. However, finding safe long term storage is a challenge. The EPA has put the Natural Gas STAR Program as well as the Coalbed Methane Outreach Program in place to provide a guide to industry on how to reduce emissions. For emissions resulting from agriculture, the EPA has initiated the AgSTAR program which encourages the storage and reutilization of the generated CH_4 through means such as anaerobic digestion [13].

1.3 Municipal Solid Waste Biomass

In the case of biodegradable municipal solid waste dumped in landfills, the generated biogas, called landfill gas (LFG), has the same composition of methane and carbon dioxide as other types of biogases but also has some impurities. Biogas derived from MSW has the same potential as an energy source. The EPA has recently set limits on emissions of CH_4 from landfills [10] as part of the landfill methane outreach program (LMOP). As a result of the program, CO_2 and CH_4 emissions from landfills have been reduced by 39.5MMTCO_2e in 2014 [14]. Although

the LMOP initiative has curbed emissions of both CO_2 and CH_4, there is still a very long way to go before emissions are overall reduced to an acceptable limit that does not contribute to global warming. According to the EPA [15], 20% of CH_4 anthropogenic emissions come from landfills as previously discussed. It is estimated that the US generates more than 250 million tons of municipal solid waste (MSW) per year which mostly go to landfills [10]. That is roughly equivalent to 4.3 lb/day of waste per person which is expected to increase with the growing population. Biomass, the biodegradable component of MSW (and primary source for biogas) accounts for about 215 billion cu.ft/year.

A typical small to midsize landfill containing 1 million tons of MSW will produce 12,232m^3/day of LFG and will continue at this level of production for 20-30 years [16]. Currently less than 15% of MSW is utilized for energy. However LFG is instead used in three main ways, the gas gets flared, or burned for electricity or the CH_4 gets condensed (CNG). Most of these are inefficient ways of utilizing the full potential of LFG. For instance, burning the gas for electricity is only about 40% efficient [17]. Furthermore, the incineration process produces more pollutants and greenhouse gases. Condensing the CH_4 may be useful for industrial uses, however it still leaves the issue of the carbon dioxide unresolved. Reforming LFG to H_2 and CO (syngas) is one attractive route to reduce greenhouse gas emissions and generate a usable feedstock. Syngas can be used as a feedstock for ammonia as well as methanol synthesis and can be upgraded to long chain hydrocarbons such as diesel and jet fuel using Fischer Tropsch synthesis (FTS) (reaction 1.5 below). Furthermore, upgrading landfill gas has many environmental benefits including reduction of greenhouse gas emissions, improving air quality and reducing fossil fuel dependence.

1.4 Types of Methane Reforming

There are several different routes for reforming of CH_4 which are widely used in industry to produce syngas. Reforming of CH_4 can be done using CO_2 as the oxidant, termed dry reforming, which is shown as reaction (1) (DRM). Methane dry reforming is attractive due to the lower cost and the lower H_2:CO ratios (≤1-1.5) produced making it more viable for use in FTS [2, 7, 18-20]. However, for the endothermic dry reforming of methane reaction, high temperatures (T>600°C) are a necessity for reaching desirable H_2:CO (syngas) ratios for FTS.

$$CH_4 + CO_2 = 2CO + 2H_2 \qquad \Delta H° = 247.3\ {}^{kJ}/_{mol} \qquad (1.1)$$

$$CH_4 + H_2O = CO + 3H_2 \qquad \Delta H° = 206.3\ {}^{kJ}/_{mol} \qquad (1.2)$$

$$CH_4 + {}^{1}/_{2}\,O_2 = CO + 2H_2 \qquad \Delta H° = -35.6\ {}^{kJ}/_{mol} \qquad (1.3)$$

$$CO + H_2O = CO_2 + 3H_2 \qquad \Delta H° = -41\ {}^{kJ}/_{mol} \qquad (1.4)$$

$$nCO + \left(n + {}^{1}/_{2}\,m\right)H_2 = C_nH_m + nH_2O \qquad \Delta H° = -X\ {}^{kJ}/_{mol\ CO\ conv} \qquad (1.5)$$

The produced syngas can then be utilized for fuel synthesis of hydrocarbon as well as oxygenate fuels and chemicals when combined with steam reforming (reaction 1.2) or the WGS reaction (reaction 1.4). The endothermic dry reforming reaction readily occurs at high temperatures as previously stated [21]. However, that also adds to the overall cost of the process on an industrial scale, as CH_4 is commonly parasitically combusted to generate the heat. The DRM reaction is thermodynamically predicted to not occur at temperatures below 350°C with coking being the only possible pathway at such low temperatures [7, 22]. Low temperature dry reforming of CH_4 has the potential to decrease the cost making it industrially more feasible. A desired H_2:CO of 2:1 is necessary for FTS to produce longer chain hydrocarbons (C10+) [23-25], though lower values are desirable for alcohols, acetic acid, and alkenes [26]. One of the targets of this

dissertation work is to lower the temperature of CH_4 dry reforming using novel low metal loading catalysts.

Steam alone is also used to reform methane in a process called steam reforming (SRM) (reaction 1.2). Steam reforming usually produces very high H_2:CO ratios (>3) versus other types of reforming as a result of the water gas shift reaction simultaneously occurring (reaction 1.4) [27]. Coupling dry reforming with steam reforming (bi-reforming, reactions 1.1 and 1.2) and/or partial oxidation of CH_4 (tri-reforming, reactions 1.1-1.3) can improve the H_2:CO ratio [1, 28, 29] and help adjust it to the desired ratio. High syngas ratios are not suitable for fuel producing techniques such as FTS because they favor the methanation reaction [2]. Bi-reforming at low temperatures yielded much higher syngas ratios compared to dry reforming alone using the catalyst systems used in this study and will be discussed in greater detail in chapter 5. Other less frequently used reforming techniques include oxy-steam reforming of methane (OSRM), partial oxidation of methane (POM), autothermal reforming of methane (ATR) and oxy- reforming of methane (ORM).

This work demonstrates low temperature reforming activity, stability, and the components required for an active catalyst. The reforming temperature is affected by both the support and the catalyst used.

Many supports have been investigated for dry reforming of methane including silica, alumina, $(Ce,Zr)O_2$ and perovskites [19, 30, 31]. Using noble metal catalysts can help drive the reaction to lower temperatures making it more economically feasible and also open possibilities for intensified processes. Coupling low temperature ($T<500°C$) dry reforming with heat from solar energy as an example can help reduce or eliminate the need for heating by natural gas combustion [32]. The current work focuses on low temperature reforming of CH_4, as a model of biogas derived

from municipal solid waste biomass, using Pt or Pd doped nickel magnesium catalysts on a ceria-zirconia oxide support. The effect of contaminants (mainly siloxanes) in the biogas on the reforming catalyst was studied through accelerated poisoning and the syngas ratio was improved through combining dry reforming with steam reforming (bi-reforming).

1.5 LFG Cleanup Technologies and Motivation

As discussed earlier, the source of biomass considered for this research effort is MSW. LFG derived from MSW contains a variety of impurities that must be cleaned prior to the reforming process. Otherwise these contaminants rapidly build up in equipment (engines, turbines, etc.) causing it to fail as well as deactivate reforming catalysts and are harmful to the environment. Contaminants present in LFG include siloxanes, sulfides, halides and mercury compounds. Siloxanes are compounds that have silicon, oxygen and methyl groups. Depending on the chain length, siloxanes can be linear or cyclic. Siloxanes decompose to silica, which then deposits onto the equipment and/ or catalyst causing irreversible damage. To protect the equipment from the extensive damage these siloxanes can cause, engine manufacturers have decreased the allowable siloxane concentration limits to maintain warranty from 10 mg/m^3 to 2.8 mg/m^3 [33]. This fueled the need to have efficient cleaning processes.

Currently, industrial contaminant removal can be categorized into three main areas, adsorption, absorption and chilling [34]. Adsorption is further subcategorized into fixed bed and fluidized bed adsorption. In fixed bed adsorption, there are usually two parallel adsorbers with regenerable adsorbant that are interchanged. While in fluidized bed adsorption, the process is continuous and is more suited for higher volatile organic matter concentrations. It is also sometimes referred to as temperature swing adsorption. Where biogas flows to one adsorber of

activated carbon for purification while contaminants are simultaneously desorbed and exhausted in a second adsorber [34].

The second major type of contaminant removal is absorption which is also a continuous process that can be either chemical or physical. Chemical absorption utilizes strong acids and bases such as sulfuric acid or sodium hydroxide. Physical absorption is done using absorbents as well as organic solvent [34]. Packed or spray columns are the most widely used for siloxane absorption. However, gas flow rate plays a key role in amount of siloxane removed. Where at higher flowrates, the siloxanes can flow out of the solvent and back into the gas defeating the process of removal [35].

The final major technology used for contaminant removal is gas chilling. Removal is done at a temperature less than -25°C where larger siloxanes and chillers sometimes operate as condensers [34]. However, all of these removal technologies add high operating costs to the process such as frequently replacing scrubbing beds. Equipment manufacturers are implementing more stringent warranty guidelines for allowable VMS levels. For instance, in 2002, engine manufacturers had an allowable siloxane levels of 10-15 mg/m^3. However by 2008, that number decreased to 2.8 mg/m^3 [33]. This in turn forces the need for higher contaminant removal levels and better technologies which still need to be developed to make the process economical.

1.6 Catalyst System

1.6.1 Ceria-Zirconia Oxide Support

The catalysts developed for this study are nickel magnesium catalysts (1.00-1.34 weight% of each) supported on ceria zirconia (0.6:0.4 mass ratio) and doped with either platinum (0-0.64% by mass) or palladium (0-0.51% by mass). Many supports have been investigated for reforming of methane. Studied supports have included different silicates, ceria, alumina, zirconia, lanthanum

oxide, perovskites, titanium dioxide and magnesium oxide [1, 2, 6, 19, 20, 30, 31, 36-40]. For this work, a mixed ceria-zirconia oxide support $(Ce_{0.6}Zr_{0.4})O_2$ was chosen for a variety of reasons. Literature shows that ceria has a high oxygen storage capacity (OSC) which is useful for the reaction in enhancing the reducibility within the fluorite lattice [41]. In addition, oxygen vacancies in the support help reduce coking [42].

The ratio chosen for this work was also shown to have the highest catalyst activity and stability versus other compositions [1, 31]. Adding zirconia which has a smaller ionic size, helps create a lattice strain which in turn causes high oxygen mobility that help improve the redox properties [42, 43]. In addition, $(Ce,Zr)O_2$ is thermally stable at high temperatures [31, 41]. The addition of zirconia to ceria also helps to shift the oxygen vacancies to the more stable surfaces (111) and (110). This oxygen shift aids in moving the reduction equilibrium to the right by utilizing bulk oxygen which in turn significantly favors bulk reduction [44].

1.6.2 Nickel Catalysts

Nickel has been used as a catalyst for many chemical reactions such as methane reforming, including dry, steam as well as tri reforming, hydrogenation of CO, and cellulose decomposition [1, 2, 27, 39, 45-47]. Nickel offers various advantages over other metal catalysts including abundance, high activity and low cost [3, 7, 27, 48, 49].

Furthermore Ni supported on Ce-Zr has been shown by Laosiripojana et al. to convert methane at temperatures between 650°C and 900°C using steam reforming [41]. Tri reforming of methane using Ni catalysts supported on ceria zirconia has been shown to produce a syngas ratio of 1.5-2 at ~850°C by Song and Pan [50]. Walker et al. [1] had a similar observation of syngas ratios between 1.7-2.3 at 800°C using a $Ce_{0.6}Zr_{0.4}$-8%wtNi8%wtMg catalyst.

However, one major drawback for Ni catalysts is that they suffer from rapid deactivation via coke formation and sintering [2, 7, 49, 51]. Carbon deposits on Ni to form fibers especially in dry reforming reactions [2]. This is the result of the decomposition of methane allowing carbon atoms to attach onto the nickel surface forming layers [2, 52]. The length between Ni-Ni bonds increases as carbon atoms adsorb thereby allowing deeper penetration until more layers of graphitic carbon form eventually deactivating the catalyst [7].

It has been shown by Laosiripojana et al. that Ni supported on Ce-ZrO_2 displayed higher resistivity to coke formation compared to other supports with a Ce to Zr ratio of 3:1 for steam reforming. This was attributed to the high oxygen storage capacity (OSC) of Ce-ZrO_2 which help initiate redox reactions of the present species thereby reducing carbon deposition from methane decomposition. In addition, the catalyst remained stable with no activity loss even after 10 hours on stream at 900°C and 3kPa [41].

1.6.3 Magnesium

Adding MgO to NiO creates a solid solution [2]. From TPO studies of Ni/MgO to Ni/SiO_2 and Ni/TiO_2 done by Bradford and Vannice, it was determined that MgO interaction with Ni helps reduce the formation of coke on the surface by several orders of magnitude compared to other supports [2]. In addition, MgO helps add basicity to the catalyst which also reduces the agglomeration of Ni particles.

1.6.4 Noble Metals

Noble metals such as Ru, Rh, Pt, Pd have been investigated as dopants to nickel catalysts for methane reforming [53-55]. Noble metals dissociatively adsorb hydrogen. In addition, there's evidence in the literature to support that noble metals and Ni can help reduce the $CeZrO_2$ support through hydrogen spillover [56].

Furthermore, addition of noble metals such as Pt and Pd helps the catalyst to reduce at lower temperatures [20, 53, 56]. This is due to noble metals' high affinity for hydrogen atoms which in turn reduces the amount of carbon deposits. In addition, noble metals affect the basicity of the catalyst thereby changing the amount of CO_2 adsorbed. This effect is caused by a shift in surface coverage that allows for more stability to intermediates formed after CH_4 decomposition and CO disproportionation [7, 20].

Overall, this dissertation effort focused on two important challenges in the waste-to-energy (WTE) field as shown in Figure 1.1. The first is economy of scale addressed by lowering the initial reforming temperature through novel heterogeneous catalysts. The second is effect of contaminants on the reforming catalyst using LFG as a feed.

Chapter 2 discusses the synthesis and characterization of low temperature dry reforming of methane catalysts. Several loadings of Platinum on Nickel-Magnesium catalysts supported on a Ceria-Zirconia oxide support were tested. Chapter 3 discusses Palladium doped Nickel-Magnesium catalysts and compares them to Platinum doped Nickel-Magnesium catalysts, both on a Ceria-Zirconia oxide support, for low temperature dry reforming. Chapter 4 addresses the effect of silicon poisoning through accelerated deactivation studies on both the Platinum low temperature reforming catalyst and the high temperature reforming catalyst comprised of Nickel-Magnesium only supported on a Ceria-Zirconia oxide support. Chapter 5 discusses improving the syngas ratio through bi-reforming and explores the effect of GHSV on both the Platinum and Palladium low temperature catalysts. Finally Chapter 6 includes overall conclusions and recommendations for future work.

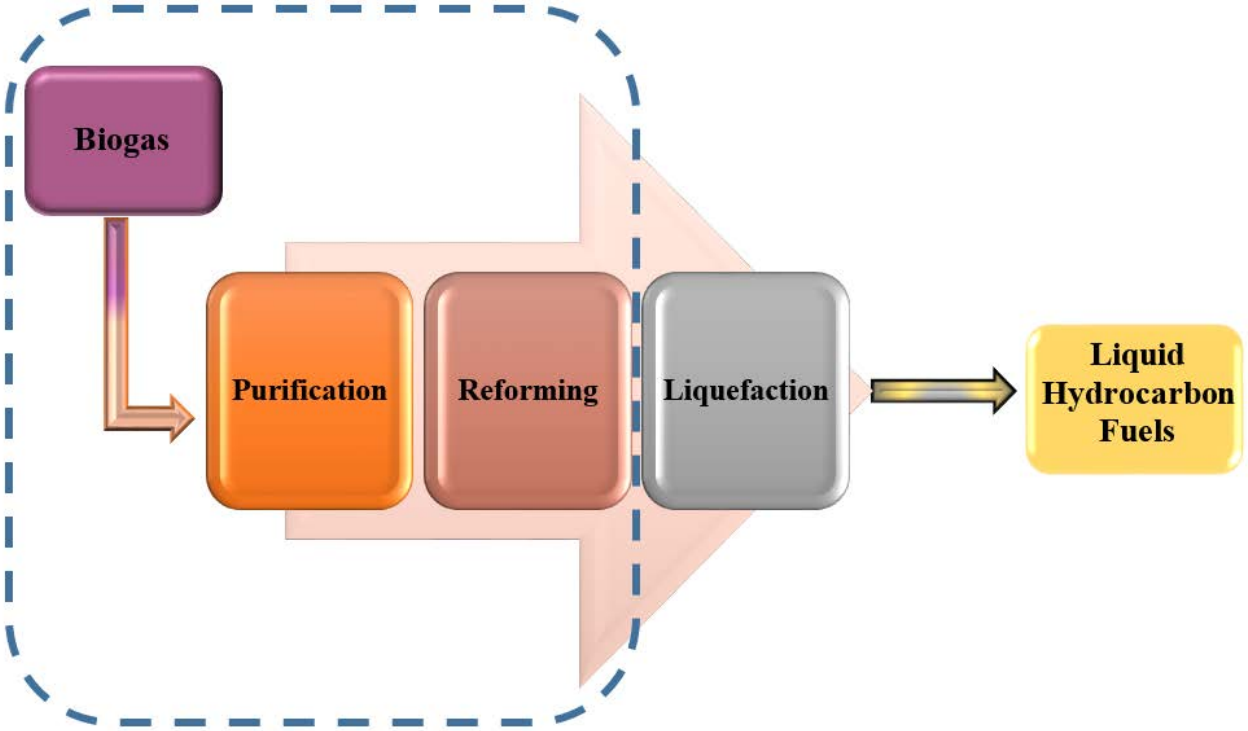

Figure 1.1: Objectives of this research effort (denoted by dashed lines) and place in overall WTE process.

Table 1.1: Biomass conversion to second generation biofuels: Overview, advantages and disadvantages of various technologies/ processes.

Method	Conversion Method	Biomass Source	Potential Fuel Output	Strengths	Weakness	Source
Anaerobic Digestion	Bio-chemical	Landfills, wastewater, agricultural waste	CH_4/CO_2 (Biogas)-medium Btu gas	• Environmental • Carbon neutral • No water input • Reduction of unpleasant odors • Reduction of GHG emissions • Low temperature process (T~35°C)	• Long process (20-30 days) but can be accelerated • For landfills, extraction systems are necessary. • Accumulation of heavy metals in sludge	[57-59]
Pyrolysis	Thermo-chemical	Agricultural, wood	Bio-oil Electricity	• Can be tuned (through temperature) to produce low-medium value gas or aerosols.	• High temperature required (300-700°C) • Coke residue	[60, 61]
Gasification	Thermo-chemical	Agricultural waste, municipal solid waste, wood	Low-Medium Btu gas ($CO/H_2/CO_2$)	• Produces electricity and mechanical energy • Air can/should be present	• Lots of undesired bi-products (pollutants) • Lots of energy loss (combustion) • Requires high temper-atures (T>1000K) • Tar formation • Requires low water content	[60]

CHAPTER 2: LOW TEMPERATURE DRY REFORMING OF METHANE OVER PT-NI-MG/CERIA-ZIRCONIA CATALYSTS[1]

2.1 Introduction

Fossil fuels are a finite resource and the world's energy demands are constantly increasing. Alternative fuel sources are no longer optional, but are now a necessity. Dry reforming of methane (DRM) has been extensively studied in recent years [3, 18, 19, 21, 62, 63]. The process can produce syngas at a H_2:CO ratio of 2:1 which is ideal for Fischer Tropsch Synthesis (FTS) and methanol synthesis, when combined with other reactions such as steam reforming [7, 18, 50] or the water-gas shift (WGS). As a greenhouse gas, methane is 20 times more powerful at trapping heat than carbon dioxide, which makes it considerably harmful to the atmosphere. According to the EPA [15], 29% of methane emissions come from natural gas and petroleum, whereas enteric fermentation (25%), and landfills (18%) also account substantially. The remaining 28% are emitted through various processes such as coal mining and wastewater treatment. These are also under-used sources of methane, which either contain or could be combined with carbon dioxide and other oxidants for conversion processes. For example, biodegradable municipal waste in landfills produces landfill gas (LFG, comprised of roughly equal amounts of methane and carbon

[1] Reprinted with permission from N. H. Elsayed, N. M. Roberts, B. Joseph, and J. N. Kuhn. Low temperature dry reforming of methane over Pt-Ni-Mg/ceria-zirconia catalysts. *Applied Catalysis B: Environmental 179 (***2015)**, 213-219. Copyright © 2015, Elsevier.

dioxide) and the EPA is currently limiting methane emissions from landfills [10]. In addition, biogas can be generated from the anaerobic digestion of biomass and syngas can also be obtained using natural gas in combination with flue gas from fossil fuels. The underlying theme of these approaches is dry reforming.

The dry reforming process utilizes carbon dioxide to help reform methane and obtain hydrogen and carbon monoxide as products through the following reaction (2.1):

$CH_4+CO_2 \rightarrow 2H_2+2CO$ $\Delta H° = 247.3\ {}^{kJ}/_{mol}$ (2.1)

The produced syngas can then be utilized for fuel synthesis of hydrocarbon and oxygenate fuels and chemicals when combined with steam reforming or the WGS reaction. The endothermic dry reforming reaction readily occurs at high temperatures [21]. However, that also adds to the overall cost of the process on an industrial scale, as methane is often parasitically combusted to generate the heat. The DRM reaction is thermodynamically predicted to not occur at temperatures below 350°C with coking being the only possible pathway at such low temperatures[7, 22]. Low temperature dry reforming of methane could reduce the cost making it industrially more viable. This work demonstrates low temperature reforming activity, stability, and the components required for an active catalyst.

The reforming temperature is affected by both the support and the catalyst used. Many supports have been investigated for dry reforming of methane including silica, alumina, $(Ce,Zr)O_2$ and perovskites [19, 30, 31]. For this work, a mixed ceria-zirconia oxide support $(Ce_{0.6}Zr_{0.4})O_2$ was chosen for a variety of reasons. Literature shows that ceria has a high oxygen storage capacity (OSC) which is useful for the reaction in enhancing the reducibility within the fluorite lattice [41]. The ratio chosen for this work was also shown to have the highest catalyst activity and stability versus other compositions [1, 31]. Adding zirconia which has a smaller ionic size, helps create a

lattice strain which in turn causes high oxygen mobility that help improve the redox properties [42, 43]. In addition, $(Ce,Zr)O_2$ is thermally stable at high temperatures [31, 41]. The addition of zirconia to ceria also helps to shift the oxygen vacancies to the more stable surfaces (111) and (110). This oxygen shift aids in moving the reduction equilibrium to the right by utilizing bulk oxygen which in turn significantly favors bulk reduction [44].

Nickel-based catalysts have been widely investigated for dry reforming of methane due to the abundance of nickel, high activity and the economically feasible cost [3, 7, 27, 48, 49]. However, they have a major disadvantage of rapid deactivation and coke formation especially in biomass feedstock due to the presence of sulfur-containing impurities [7, 49, 51]. Adding a small amount of noble metal such as platinum can help decrease coking and enhance catalytic stability and activity [31, 42, 64]. Adding platinum also helps reduce ceria to Ce^{3+} and create oxygen vacancies [65]. Moreover, Pt, even in low loadings, could provide active sites for the conversion. In addition, adding MgO can help to increase the Lewis basicity of the support [7, 66]. This solid solution enhances CO_2 adsorption by adding stability to the Ni crystallites which can reduce carbon deposition from CO disproportionation [2, 7].

The main goal of this work was to examine the effects of different platinum loadings on structure, properties, and dry reforming performance of metal based catalysts immobilized onto a ceria-zirconia support. The addition of a precious metal in low loadings to a Ni-based catalyst is a viable way to achieve low temperature reforming catalysis. The support was synthesized via co-precipitation and metals were loaded via wetness impregnation. Reduction experiments (TPR) showed that adding Pt onto the catalyst favorably decreased the reduction temperature but the impact became less prominent with increasing Pt loading. In addition, CO_2 temperature-programmed desorption (TPD) studies showed that the addition of Ni and Mg increased catalyst

basicity, but the further addition of Pt led to a slight decrease in basic sites. The results of this study demonstrate that the balance between reducibility and basic sites are the influential factors in enhancing the low temperature dry reforming activity in this catalyst system and lead to high activity. The study also demonstrates improvements beyond both the control catalysts that do not contain either Ni and Mg or Pt. The catalysts in this study has among the highest activity for low-temperature (compared at T=450°C) dry reforming in the literature for catalysts not containing Rh or Ir.

2.2 Experimental

2.2.1 Materials and Synthesis

Ceria-Zirconia was prepared via the co-precipitation method as reported by Rossignol et al. [67] in a ratio of 0.6:0.4. The $(Ce_{0.6}Zr_{0.4})O_2$ support was made in batches of 12 grams by weighing 8.7 grams of the cerium precursor $Ce(NO_3)_3$ x $6H_2O$-(99.5% pure; Alfa Aesar) and 3.3 grams of zirconium precursor $ZrO(NO_3)_2$ x H_2O-(99.9% pure; Alfa Aesar). The precursors were then dissolved in 150 mL of deionized water in a large beaker. About 75 ml of ammonium hydroxide (27% w/w NH_3; Mallinckrodt Chemicals) was added to the beaker in 10 mL increments to precipitate the precursors until a clear liquid layer was visible on top of the beaker indicating complete precipitation. The mixture was vacuum filtered and then re-dissolved in 0.25M NH_4OH solution. The solution was vacuum filtered a second time. The filtrate was dried in an oven at 60°C for 1 hr, then 120°C for 12 hr. Finally, the powder was calcined at 800°C for 4 hr.

Nickel (1.34% by mass), magnesium (1.00% by mass), and platinum were loaded on the support via incipient wetness impregnation. Platinum was loaded at 0.07%, 0.16%, 0.33% and 0.64% by mass ratio. The nickel precursor $Ni(NO_3)_2$ x $6H_2O$ (99.9985% pure; Alfa Aesar), the magnesium precursor $Mg(NO_3)_2$ x H_2O (99.999% pure; Alfa Aesar) and the platinum precursor

H_2PtCl_6 x $6H_2O$ (Sigma-Aldrich) were used for the metal loadings. The desired amount of each metal was weighed and all of the precursors were dissolved in an appropriate amount of deionized water (1-2 mL) in one beaker. The solution was then added drop wise onto the support until incipient wetness. The powder was then dried in an oven for 2 hr at 120°C to remove any volatile components and evaporate the water. The process was repeated until all the solution was added. After the final drying, the powder was calcined at 600^{o}C for 3 hr. A control sample that contained no nickel and magnesium was synthesized the same way as mentioned above.

2.2.2 Catalyst Characterization

The synthesized catalyst was characterized using TPR, XRD, N_2 physisorption, and CO_2-TPD. Temperature-programmed reduction (TPR) was done using a Cirrus MKS mass spectrometer (MS) connected in-line with the reactor containing 50 mg of calcined catalyst. The catalyst was loaded between two layers of quartz wool. The reactor was then positioned inside a Thermoscientific Thermolyne tube furnace and high temperature glass wool was added to insulate the top of the furnace. Feed gases were controlled using Alicat Scientific mass flow controllers. All of the gas feed and outlet were wrapped in heating tape to prevent condensation prior to entering the MS. The furnace temperature was controlled using a Eurotherm 3110 PID controller. Each catalyst sample was pretreated under an ultra-high purity (UHP, Airgas) helium flowrate of 50 sccm at 110°C for 30 min using a ramp rate of 10°/min. The sample was then allowed to cool to 50°C and then the gas flow was switched to 5% H_2/He (50 sccm). The sample was then heated at a ramp rate of 10°/min to 900°C and held for 30 min. For the data analysis, calibration curves were measured to calculate the ionization factors.

X-ray diffraction (XRD) was done to determine the crystal structure using a Bruker AXS operating with a Cu Kα source at 40 kV and 40 mA. The data were obtained using a (2θ) angular range of 15-80°. The step size was 0.02° and the dwell time was 3 sec for each step.

BET surface areas and pore volumes were obtained using a Quantachrome Autosorb-IQ. Each experiment was done using 50 mg of catalyst. The sample was first pretreated at 120°C for 2 hr. The sample was then loaded in a small-bulb 6 mm quartz cell. Then, the sample was backfilled with He and outgassed under vacuum for 1 hr. The surface area values were obtained by fitting the data to BET isotherm in the P/P_0 range of 0.05-0.33 using N_2. The pore volume is reported at P/P_0 of ~1. The BJH method was used to determine the average pore size.

CO_2 temperature-programmed desorption (CO_2-TPD) studies were done to determine the catalyst basicity using the same system already described in the TPR section. The catalyst (75.5 mg) was initially reduced at a temperature of 300°C in a 5% H_2 in He gas mixture and held at the reduction temperature for 1 hr. The catalyst was then cooled under He only until a temperature of 50°C was reached. After the temperature stabilized, a 10% CO_2 in He was introduced to the catalyst and flown for 30 min. The catalyst was then purged by flowing He only for another 30 min. The temperature was then increased to 800°C at a ramp rate of 10°C/min and held for 10 min.

2.2.3 Catalytic Testing

Reactions experiments were done in a quartz u-tube microreactor with an internal diameter of 4 mm. All reactions were done at atmospheric pressure using 75.4-75.7 mg of catalyst. The same system described in the TPR section was utilized. The catalyst was first reduced at a temperature of 300°C in a 5% H_2 /He for 1 hr. For the temperature-programmed reactions (TP-rxns), the temperature was then decreased in He (50 sccm) to 200°C and then reforming gas mixture was introduced once this temperature was reached. Methane and carbon dioxide, (both

99.999% pure from Airgas), were introduced in a 1:1 ratio with a total composition of 14% reactants in He gas (44 sccm total flow). The temperature was then increased to 900°C at a 10°C/min ramp rate and held there for 30 min. The gas hourly space velocity (GHSV) was maintained constant at 68,000h^{-1} for all reactions unless otherwise stated. Methane and carbon dioxide conversions were calculated using the following formulas (2.2 and 2.3):

$$CH_4 \text{ conversion} = 1 - \frac{(mol\ out)}{(mol\ in)} \quad (2.2)$$

$$CO_2 \text{ conversion} = 1 - \frac{(mol\ out)}{(mol\ in)} \quad (2.3)$$

Steady-state data were collected using a similar procedure. After the reduction and cooling to 200°C in He, the reforming gas mixture was introduced and the temperature was raised to 470°C. Once steady-state was reached, the temperature was decreased by 10°C and this was repeated until 430°C. TOFs were calculated from the steady-state CO_2 conversion at the various temperatures, using the amount of CO_2 desorbed from the CO_2 TPD to estimate the number of sites. The Weisz-Prater criterion was calculated to be ~10^{-3} which is <<1 indicating that there were no internal diffusion limitations. External mass transfer limitations were determined to be negligible at the GHSV used (determined by testing a series of GHSVs). Regardless of GHSV for the 0.16Pt catalyst, the H_2:CO ratio was largely independent of it at T = 450°C and was ~ 0.27 to 0.30, as determined by a separate set of experiments. In a final experiment for the 0.16Pt catalyst, its stability was tested during an extended time-on-stream (TOS) of 100.5 hr.

A temperature-programmed oxidation study was done following each of the TP-rxn experiments and selected steady-state experiments to quantify the presence of carbon deposits. After reaction experiments, the catalyst was rapidly cooled to 60°C under He (50 sccm). A 10% oxygen in He gas mixture (50 sccm total) was then introduced to the catalyst. The temperature was

then increased to 900°C using a 10°C/min ramp rate and held for 1 hr. No coke formation was detected from any of the samples.

2.3 Results and Discussion

For this work, a series of catalysts were synthesized on a $Ce_{0.6}Zr_{0.4}O_2$ support. The synthesized catalysts were 1.34%Ni1.00%Mg-$Ce_{0.6}Zr_{0.4}O_2$ (0Pt), 0.16%Pt-$Ce_{0.6}Zr_{0.4}O_2$ (0.16Pt/CeZr), 0.07%Pt-1.34Ni1.00Mg-$Ce_{0.6}Zr_{0.4}O_2$ (0.07Pt), 0.16%Pt-1.34Ni1.00Mg-$Ce_{0.6}Zr_{0.4}O_2$ (0.16Pt), 0.33%Pt-1.34Ni1.00Mg-$Ce_{0.6}Zr_{0.4}O_2$ (0.33Pt), 0.64%Pt-1.34Ni1.00Mg-$Ce_{0.6}Zr_{0.4}O_2$ (0.64Pt). The baseline sample (Ni and Mg, but not Pt) was used for tri-reforming by our group in a previous study [1], which optimized the Ni and Mg loadings and the Ce:Zr ratio for activity and stability purposes. The notation used for each catalyst from this point forward is included in Table 2.1.

2.3.1 Characterization

The effect of metal immobilization on the surface area of the support and the pore volumes was examined by N_2-physisorption and is reported in Table 2.1. The synthesis method and ceria to zirconia ratio have a large effect on the surface area of the support which is the reason the literature values range from 35 to149 m^2/g [1, 18, 31, 68, 69]. Previously published studies have shown that high ceria content has been identified to cause pore blockage of the zirconia and decrease the overall surface area [18, 67, 70].

For this work, the oxide support had the highest surface area of 146 m^2/g which is similar to reported values in literature [31]. The surface areas decreased as the metals were loaded as well as the measured pore volumes as reported in Table 2.1. A similar decrease upon metal loading was observed in literature and it was attributed to the pore blockage and sintering by the loaded metals [1, 71, 72]. The decrease in the pore diameters upon loading also contributed to the decrease in

pore volume. The BJH pore size distribution curves for all samples is included in Figure 2.1. Whereas the main pore diameter decreases its width upon loading, the smaller pores tended to be completely blocked. This result is in agreement with the change in surface areas and pore volumes between the support alone and the supported catalysts.

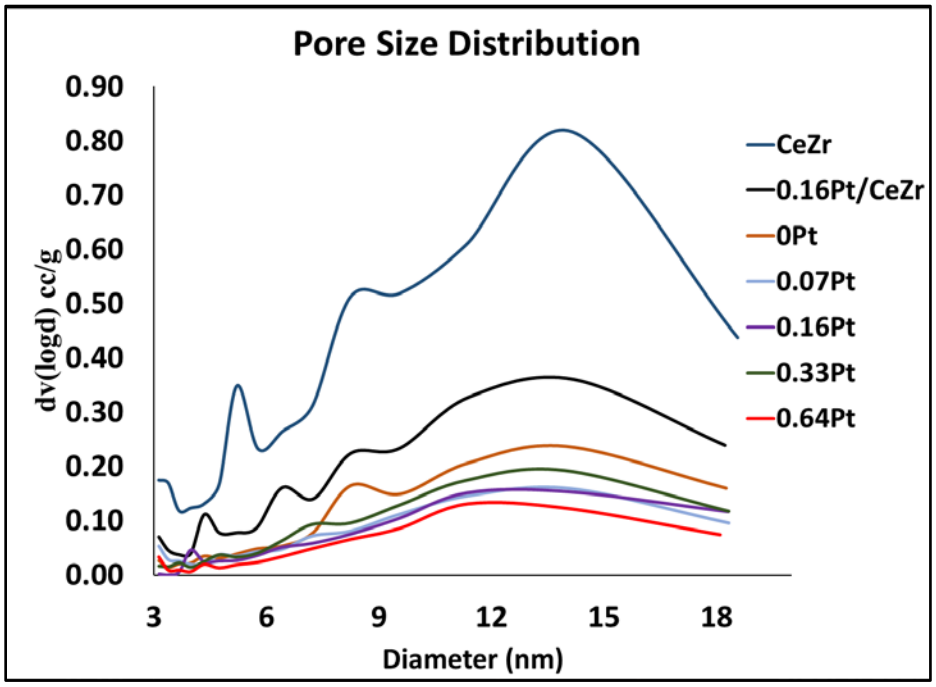

Figure 2.1: BJH pore size distribution of all samples. The support (CeZr) had the most pores and the largest pore size. The pore size decreased with increasing metal loading.

XRD was conducted to ensure that the support is correctly synthesized and the metals are loaded onto the surface. The results are shown in Figure 2.2. The $(Ce_{0.6}Zr_{0.4})O_2$ pattern showed no evidence for the monoclinic phase which are characteristic of ZrO_2. However, the pattern is consistent with a cubic fluorite structure as is previously reported in literature [1, 39, 68]. This finding suggested that the ZrO_2 is incorporated into the CeO_2 lattice. As reported previously,[73] the asymmetry of the diffraction lines also suggested the presence of multiple ceria-zirconia solid solution phases of various compositions. The third diffraction pattern (0Pt) showed the support with only nickel and magnesium loaded. NiO and MgO diffraction lines can be seen around a 2θ

of 42-44° proving that the metals are deposited onto the support. The diffraction patterns of the catalysts with different platinum loadings are also shown in Figure 2.2. Since the platinum content is low and is most likely highly dispersed on the support, no significant diffraction lines related to platinum are observed in the diffraction patterns. This result agreed with other groups who have made similar observations [72]. It is unclear whether the Pt is evenly distributed across the surface or is preferentially adsorbed the support or the $(Ni,Mg)O_2$ phase. In addition, post-reaction and post-reduction XRD patterns were obtained on select catalysts and there were not any observable diffraction shifts or changes.

Table 2.1: Surface, bulk properties, reduction temperatures, and CO_2 adsorption data.

Sample	**Notation**	**S_{BET} (m^2/g)**	**Pore Volume (cc/g)**	**Pore Diameter (nm)**	**Reduction Temperature (°C)**	**Amount CO_2-desorbed (µmole/g.cat) (Temp 50-400°C)**
$Ce_{0.6}\ Zr_{0.4}\ O_2$	CeZr	152[a]	0.35 [a]	14.1[a]	618	0.38
0.16%Pt- $Ce_{0.6}\ Zr_{0.4}\ O_2$	0.16Pt/ CeZr	70	0.16	11.4	196-480	0.71
$Ce_{0.6}\ Zr_{0.4}\ O_2$ - 1.34Ni1.00Mg	0Pt	40	0.10	11.4	382	1.40
0.07%Pt- $Ce_{0.6}\ Zr_{0.4}\ O_2$ - 1.34Ni1.00Mg	0.07Pt	30	0.08	11.4	283	1.29
0.16%Pt- $Ce_{0.6}\ Zr_{0.4}\ O_2$ - 1.34Ni1.00Mg	0.16Pt	31 [a]	0.07 [a]	11.6 [a]	248 [a]	1.30
0.33%Pt- $Ce_{0.6}\ Zr_{0.4}\ O_2$ - 1.34Ni1.00Mg	0.33Pt	34 [a]	0.09 [a]	11.3 [a]	247 [a]	1.07
0.64%Pt- $Ce_{0.6}\ Zr_{0.4}\ O_2$ - 1.34Ni1.00Mg	0.64Pt	22	0.05	11.4	242	0.98

[a] The average of two different samples is reported.

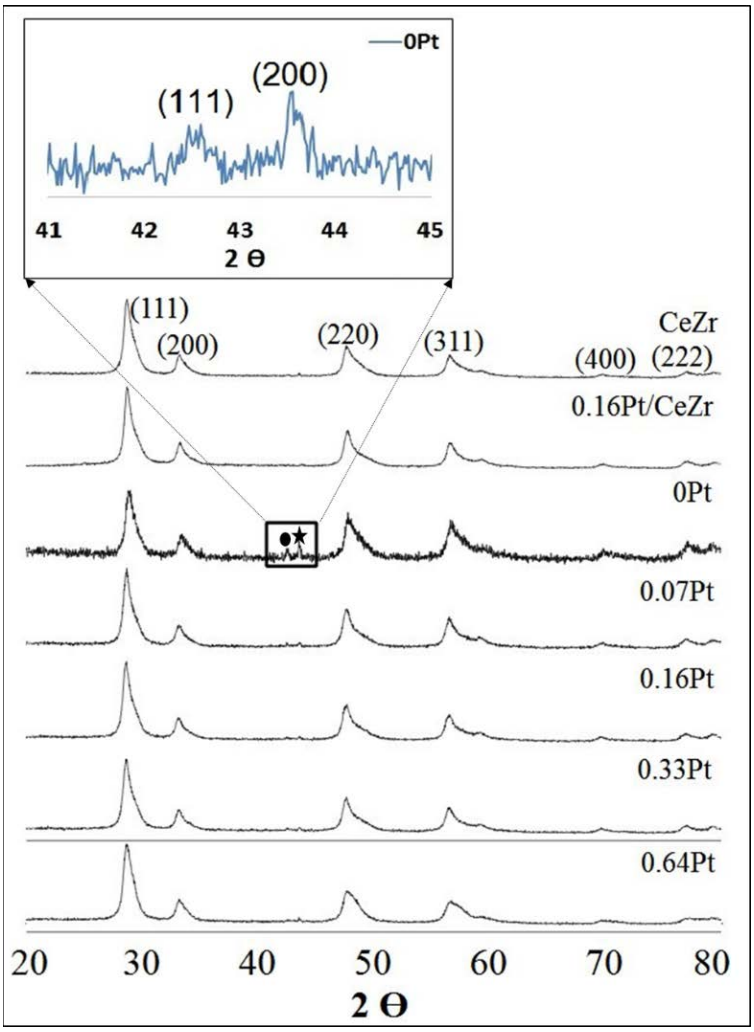

Figure 2.2: XRD pattern of catalysts. The (★) represents the (111) and (●) represents the (200) NiO and MgO diffraction lines as shown in the insert for the 0Pt sample. The Miller indices refer to the cubic fluorite (Ce,Zr)O_2 phase (except for the insert).

TPR was utilized to characterize the catalyst's reducibility. In addition, it also shows how different species within the catalyst interact with each other [1, 74]. The results of the temperature-programmed reduction experiments on the calcined materials can be seen in Figure 2.3 and are summarized in Table 2.1. The support alone had a reduction peak at 618°C, which was consistent [75] with previous findings. Adding Ni and Mg shifted the reduction peak to 382°C. This result agreed literature that nickel helps the ceria to become more reducible by producing mobile oxygen [39]. However, the nickel-based catalyst without any platinum content reduced at a much higher

temperature than catalysts with platinum. The addition of platinum helped further decrease the reduction temperature significantly at first with smaller shifts in reduction as Pt content increased. The catalyst that did not have any nickel or magnesium but had platinum displayed a small but very wide reduction peak that ranged from 196°C to 490°C. This implies that the platinum interaction with the support has a significant effect on increasing the reducibility of the ceria support as well [76-78]. Platinum helps reduce the oxide phases through its affinity to facilitate dissociative hydrogen adsorption. Hydrogen has been identified to adsorb and dissociate on the surface of the platinum whereby it spills over to the entire surface of the ceria [77]. The impact of Pt becoming less prominent with increasing Pt loading likely occurred because the dispersion of the Pt crystallites probably increased with loading.

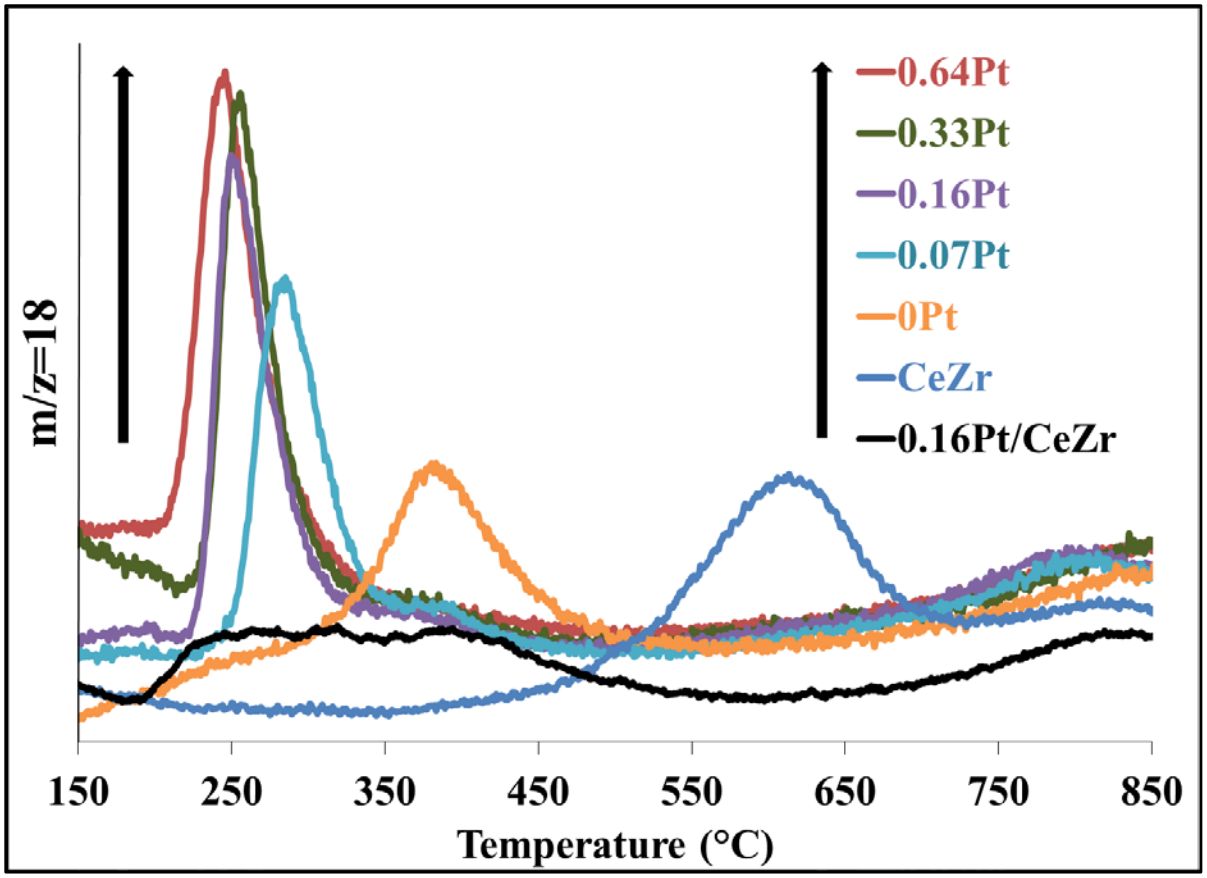

Figure 2.3: TPR profiles of catalysts. Indicative arrows show signal to legend trend of the curves.

There is no general consensus in literature as to which species contributes to each of the two main reduction peaks whether it is as a result of the support or NiO. Kumar et al., Walker et al., and Diskin et al. [1, 31, 79] agreed that the low temperature reduction peak (600°C and below) is attributed to the NiO species. Escritori et al. and Roh and Dong et al. [27, 39, 68] attributed the low temperature reduction peak to the surface region of cerium oxide that is promoted by weakly bound loaded nickel, whereas the higher temperature reduction peak (800 to 900°C) was attributed to the bulk ceria promoted by strongly bound NiO species. Literature has shown unsupported NiO to have a first early reduction peak in the 400-430°C range [39, 68]. For this work, it was determined that the initial reduction temperature is most likely as a result of the weakly bound NiO species. The second reduction peak is most likely attributed to the NiO species with strong interaction with the support [27, 39, 68].

From the reduction profile of $(CeZr)O_2$, it is clear that the support was reduced in agreement with others [18, 65, 80]. Addition of NiO onto the support caused a decrease in the reduction temperature to 382°C which is below the previously reported NiO reduction temperature of 405°C [39]. Addition of platinum further decreased the reduction temperature, which corroborated with literature [18, 65, 81]. Based on the trend and the width of the peaks in the reduction profiles, it is believed that the support is what is mainly getting reduced. However, the metal oxide materials also get reduced which is evident by the sharpness of the reduction peaks for the metal loaded samples. As a result of the metal interaction with the support, they help lower the reduction temperature of the support [72, 81]. This increase in the supports' reducibility occurs as a result of increasing the mobile oxygen.

Temperature-programmed desorption of CO_2 experiments done on the reduced catalysts are provided in Figure 2.4 and the results are summarized in Table 2.1. All metal supported

catalysts displayed a strong initial peak in the range <200°C and had a large profile that extended to about 400°C. The support alone only had a double peak from 100-200°C. This result is consistent with findings in literature [39] which suggest that ceria adds medium basic sites as a result of its large OSC which aids in capturing and releasing oxygen. Adding NiO and MgO improved the basicity of the support as the amount of CO_2 adsorbed increased from 0.38 µmole/g.cat in the support only sample to 1.40 µmole/g.cat in the catalyst with nickel and magnesium [7]. This finding was expected because Mg was anticipated to add surface basicity. This effect was greater than the effect of adding platinum alone to the support which only yielded an adsorbed amount of 0.71µmole/g.cat. This decrease in adsorbed CO_2 amount with Pt loading is correlated to the surface area and pore volume decreases reported in Table 2.1. Literature attributes the lower CO_2 desorption for the platinum catalysts to the dense nature of the oxygen vacancies [82].

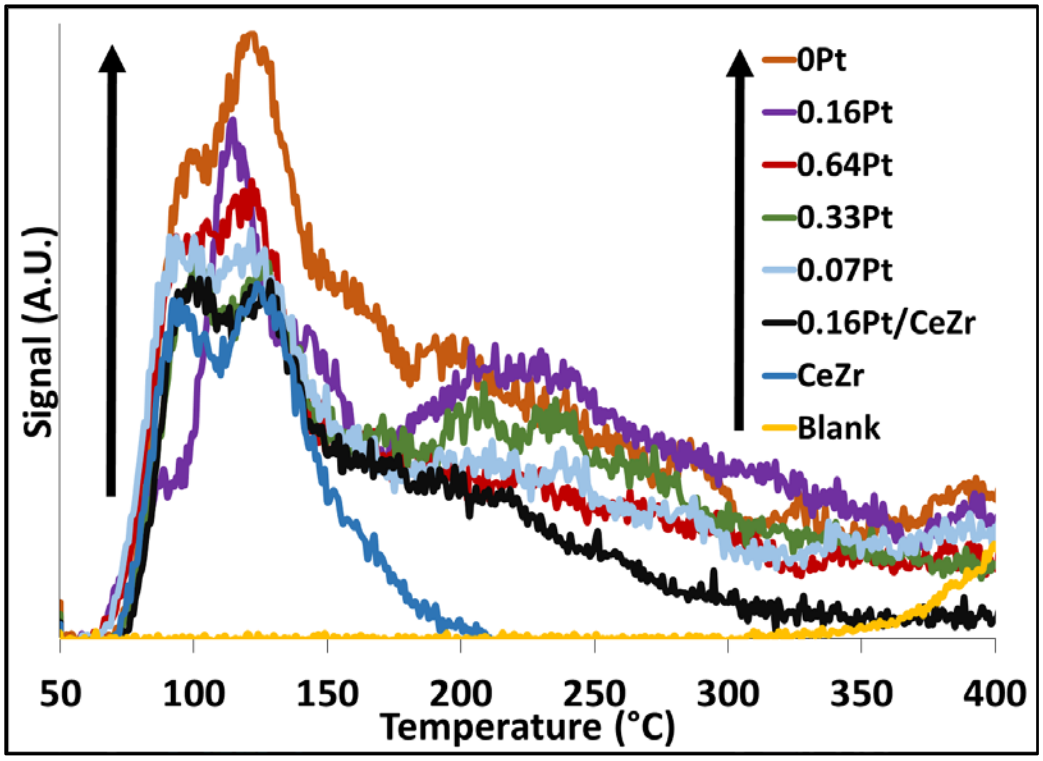

Figure 2.4: TPD-CO_2 of reduced catalysts. Arrows indicate the signal to legend trend.

2.3.2 TP-Rxn Results

Both 10% conversion and 50% conversion temperatures of CH_4 and CO_2 are reported in Table 2.2 as X_{10} and X_{50}, respectively. Results showed 10% methane conversion was achieved at 828°C using only the ceria-zirconia support. In addition, 10% carbon dioxide conversion was achieved at 787°C. Adding nickel and magnesium effectively lowered the conversion temperature to 762°C and 742°C for methane and carbon dioxide, respectively. The addition of platinum further decreased the conversion temperature. Adding Pt alone to the support without Ni and Mg significantly decreased the X_{10} and X_{50} temperatures. However, adding Pt along with Ni and Mg gave the lowest X_{10} and X_{50} temperatures as reported in Table 2.2. The 0.16Pt catalyst showed the most desirable results with an X_{10} for methane at 454°C and for carbon dioxide at 437°C. The equilibrium carbon dioxide conversion, in the absence of coke formation, of 10% would occur at approximately 400°C [22]. High carbon dioxide conversions, relative to methane conversions for a given sample, occurred due to the reverse WGS (rWGS).

The H_2: CO ratio was highest in the catalysts with 0.07Pt and 0.16Pt as reported in Table 2.2. From the trend, it is evident that the H_2: CO ratio decreases with increasing platinum content. This trend is likely a result of decreased platinum dispersion as the amount of platinum increases. In addition, H_2:CO was not close to the desired 1:1 ratio. The low H_2: CO ratio is attributed to the rWGS simultaneously occurring at the low temperatures used for this work. This is further proved by a visible water signal in the MS output data and consistent with other published works [18] and with the thermodynamics. Other published works have shown a H_2: CO ratio of 0.05-0.3 for low temperature dry reforming of methane as well [62]. In the post-reaction TPOs, carbon dioxide produced from coke combustion was not detected in any experiment. This finding is consistent with that the base catalyst (0Pt) was optimized (in terms of Ni and Mg loading and Ce:Zr ratio) for

anti-coking behavior in a previous study [15] and the water formation from the rWGS because water would be better at oxidizing coke deposits than CO_2.

Table 2.2: Temperature-programmed reaction results for the various catalysts.

Sample	X_{10} CH_4 Temperature (°C)	X_{50} CH_4 Temperature (°C)	X_{10} CO_2 Temperature (°C)	X_{50} CO_2 Temperature (°C)	H_2:CO (@450°C)
CeZr	828	n/a	787	n/a	n/a
0.16Pt/CeZr	504	641	488	625	0.23
0Pt	762	848	742	813	n/a
0.07Pt	464	611	450	586	0.35
0.16Pt	454	603	432	578	0.30
0.33Pt[a]	479	608	467	590	0.21
0.64Pt	493	613	479	595	0.22

[a] Reporting the average values of two samples.

The activity trends as a function of two descriptors (peak reduction temperature and number of basic sites) for all catalysts examined in this study is shown in Figure 2.5. The relative activity correlates to the marker size, with larger markers indicating more activity (as defined as inversely proportional to the X_{10} temperature, Table 2.2). Compared to the catalyst without Pt (0Pt), the decrease both in the amount of basic sites and peak reduction temperatures correlated to increasing Pt amounts. Thus, one of the intermediate Pt loadings (i.e., the 0.16Pt sample) yielded the highest dry reforming activity. Since the optimal Pt loading was low, the high platinum dispersion also likely aided in the high activity. High Pt dispersion has been identified to help improve dry reforming activity [18, 72, 83].

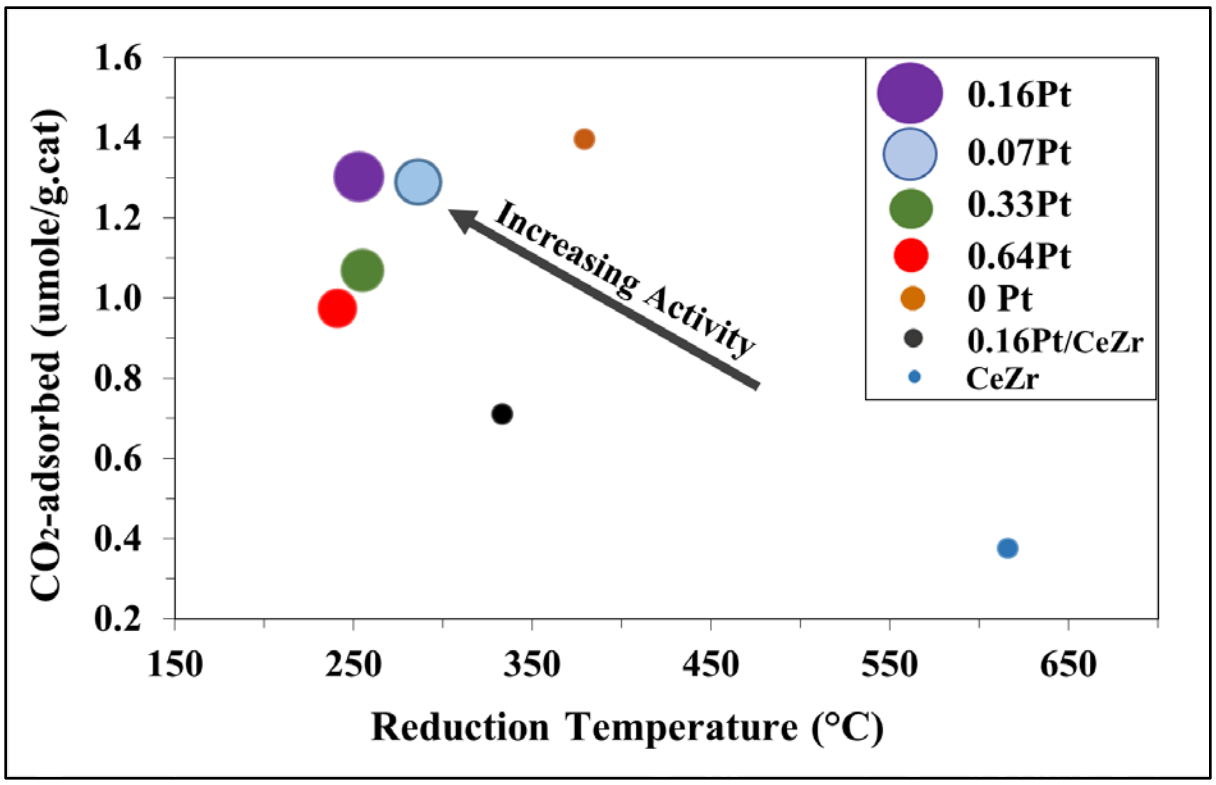

Figure 2.5: Dry reforming activity trends. Adding Pt increased the number of basic sites leading to higher activity for dry reforming. Note that the size of the circles is directly proportional to the activity.

2.3.3 Steady-State Reaction Results

Steady-state experiments were conducted using the 0.16Pt catalyst, with the same feed and space velocity as the TPRxns. First, an isothermal (T = 450°C) stability (TOS = 100.5 hr) test is described. During the initial heating in the presence of reactants, results showed methane (X_{10}) conversion at 444°C (10°C different than shown in Table 2.2) and carbon dioxide (X_{10}) conversion at 430°C (2°C different than shown in Table 2.2). At T = 450°C, the catalyst showed slight deactivation (CH_4 conversion only) over the course of the 100.5 hr on stream (Figure 2.6). The average H_2:CO ratio during this TOS was 0.32 and this result agreed with the temperature-programmed value (0.30) for this sample (Table 2.2). Despite the lengthy TOS, this catalyst showed no coking as measured by a post-reaction TPO (Figure 2.6 insert).

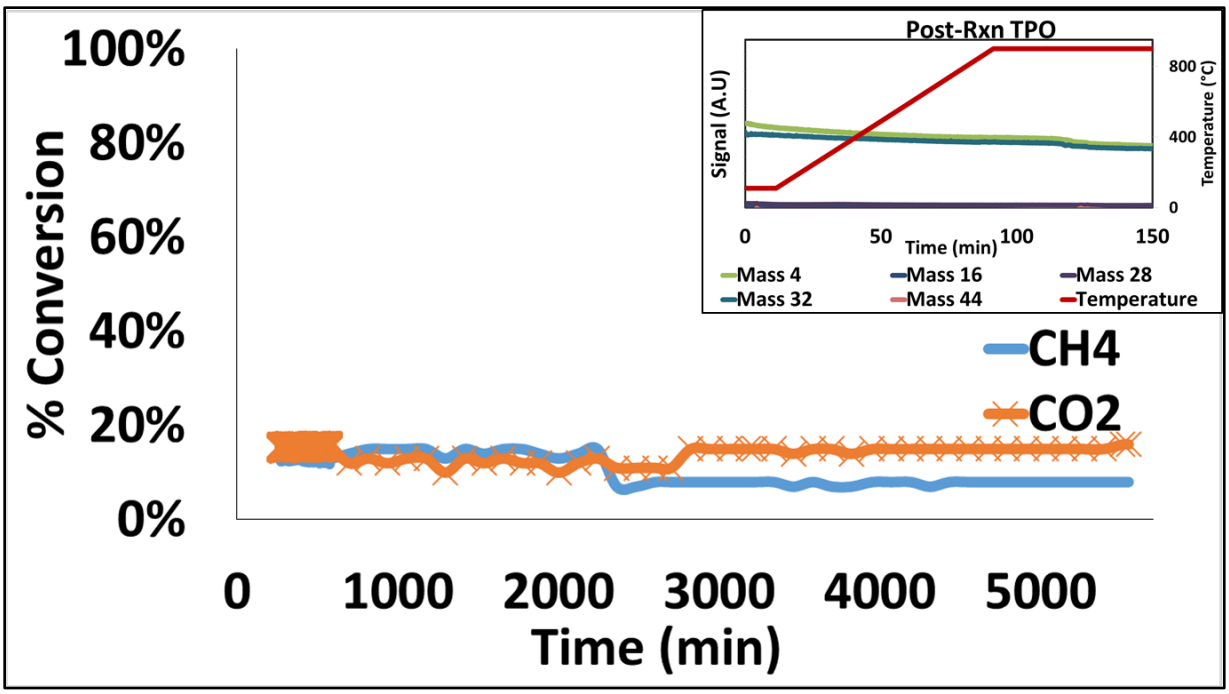

Figure 2.6: CH_4 and CO_2 conversion from 100.5 hr stability test. Insert shows post-test TPO with no coking present.

In a separate experiment, turnover frequencies (TOFs) were obtained for the steady-state CO_2 conversion (normalized by the total CO_2 amount desorbed) of the same, most active sample (0.16Pt) in the temperature range of 430-470°C. At the lowest temperature (430°C), the TOF was $2.69s^{-1}$. The TOF increased with increasing temperature with values of $3.17s^{-1}$, $3.50s^{-1}$, $4.22s^{-1}$, and $4.74s^{-1}$ at respective temperatures of 440°C, 450°C, 460°C, and 470°C. Literature reported comparable TOF for 3.8% Rh/SiO_2 catalyst where the values were between 1.5-$3.6s^{-1}$ at 450°C and 0.1MPa depending on the space [22] velocity. The TOFs were calculated from the CO_2 conversion using TPD site density (assuming 1:1 CO_2:site). Since it was assumed constant, the rate of CO_2 conversion is TOF*site density. The methane rates would be slightly lower since the methane conversion was lower than CO_2 conversion, due to the reverse water-gas shift reaction.

The apparent activation energies were calculated to be 18.5 and 14.8 Kcal/mol from the respective CH_4 and CO_2 conversion data and these value were consistent with the literature (Tables

2.3 and 2.4). A comparison of different catalysts and their respectively reported activation energies is included in Table 2.3. Qualitatively, lower apparent activation energies for CO_2 as compared to CH_4 makes sense since multiple pathways (dry reforming and rWGS) are more likely to exist and corroborated with the results of Table 2.3.

Table 2.3: Activation energies of different metal-based catalysts.

Catalyst	**Apparent Activation Energy (Kcal/mol)**		**Conditions** [a]	**Reference**
	CH_4	**CO_2**		
0.16Pt	18.5	14.8	430-470 °C	This study
5%Ni/CaO-Al_2O_3	25.5	23.6	620-690 °C	[3]
Ni/γ-Al_2O_3	12.2	13.4	500-700 °C	[49]
CeO_2-ZrO_2	24.1	n/c	400-630 °C	[69]
Ni(100)	17.7±2.4	n/c	171-253 °C P= 4.4 mbar	[84]
Ni/CZ	16-18.9	n/c	550-840 °C	[85]
Pt/ZrO_2	n/c	19.8	600 °C P=25kPa	[86]
0.2Pt-15Ni/ CaO-Al_2O_3	26.6	16.9	580-620 °C	[87]

[a] Pressure is 1 atm unless otherwise noted.
n/c refers to not calculated

Activation energies and turnover frequencies from a number of studies are compared as shown in Table 2.4. Ni and Pt are included since they are used in the current study and Rh and Ir are included because they are the most active. Since SiO_2 in general is an inert supports, its use in supported catalysts are included as well as the support which yields the most active catalyst for each immobilized metal. The various activation energies and original conversion studies are available as the reference column. The actual TOF values are the corrected values published by Bradford et al [7]. In general, the TOF values were corrected using the reported activation energies

and concentration dependencies (as described in the footnotes of Table 2.4) to conditions of their studies (T = 450°C, $P_{CO2} = P_{CH4}$ = 195 torr).

In this compilation of TOFs, most of the original studies have estimated the value based on methane conversion and the number of available metal sites from H_2 or CO chemisorption. Since methane is activated by the metal sites, it is a good assumption that the sites for methane activation at least correlate to the available metal surface area that can chemisorb these probe molecules even if it is not exactly matching. Whereas this approach is common, there is also generally a desire to use a reactant molecule to determine the number of actives sites. Since, in this study, both metallic Ni and Pt sites may activate methane (as seen in dry reforming activity for the control catalysts), basic sites that are able to adsorb acidic CO_2 was selected to determine the number of active sites for normalization of the CO_2 conversion rate. Thus, differences in TOFs could be embedded in the choice of quantifying the active sites and the selection of CO_2 or CH_4 conversion rates, though the latter is expected to be minimal because these would be equal when there are no side reactions.

The CO_2 TOF value from the present study was corrected to these conditions using the correction factors of 0.5 order for CH_4 and 0.25 order for CO_2. These are the same correction factors as used for the Ni/La_2O_3, [36, 40] which is the most active sample from the literature not containing Ir or Rh. It should be noted that the present study was performed at the same temperature as the comparison whereas the Ni/La_2O_3, [36, 40] was used in dry reforming at T > 450°C and corrected to the same conditions used by Bradford et al. [7] for comparison purposes. From Table 2.4, it is evident that the catalyst used for the current study had one of the highest TOF surpassed only by Rh/SiO_2 and Ir/TiO_2.

Table 2.4: Literature comparison of apparent activation energies and turnover frequencies (TOFs) at T= 450 °C for selected catalysts.

Metal	Catalyst	Apparent Activation Energy (Kcal/mol)[a]			TOF (s^{-1}) [a]	Reference [b]
		CH_4	CO_2	CO		
Pt	0.16Pt	18.5	14.8	n/c	9.6 [c]	This study
	Pt/SiO_2	n/c	19	n/c	0.85	[88, 89]
	Pt/TiO_2	n/c	19	n/c	4.4	[88, 89]
Ni	Ni/SiO_2	13	n/c	n/c	0.61	[90]
	Ni/La_2O_3	n/c	n/c	15	9.2	[36, 40]
Rh	Rh/SiO_2	n/c	23	n/c	0.14	[91]
	Rh/TiO_2	n/c	18	n/c	25	[89]
Ir	Ir/SiO_2	n/c	n/c	42	0.04	[92]
	Ir/TiO_2	n/c	18	n/c	22	[89]

[a] Activation energies and TOFs as reported by Bradford et al. [7]. TOFs have been corrected to their standard conditions
[b] Original references for the reported values
[c] TOF of 3.5 s^{-1} corrected to higher partial pressures of CH_4 and CO_2 using approach of Bradford et al. [7], which is 0.5 order for CH_4 and 0.25 order for CO_2
n/c refers to not calculated

2.4 Conclusion

Low temperature (430 to 470°C) dry reforming of methane was studied over different metal based catalysts on a ceria-zirconia oxide support. The combination of Pt with $NiMg/(Ce,Zr)O_2$ catalysts increased the low temperature dry reforming activity compared to the control catalysts without Ni and Mg and Pt. The activity increase is attributed to the high dispersion and synergistic effects between the platinum and oxide phases, which is correlated to the reduction temperature and the number of basic sites. The study proposed a complex catalyst system in which a conventional reforming catalyst ($NiMg/(Ce,Zr)O_2$) is modified by a precious metal to balance the

conversion of both reactants. As a result, high conversions were achieved at low temperatures, which is also evident in the comparison of TOFs to the literature values. Minimal deactivation occurred for the long-term testing. Further research is needed to examine the active site requirements for both CO_2 and CH_4, as well as increasing the H_2:CO ratio through the addition of steam (bi-reforming) to the feed to decrease the driving force for the rWGS reaction.

CHAPTER 3: COMPARISON OF PD-NI-MG/CERIA-ZIRCONIA AND PT-NI-MG/CERIA-ZIRCONIA CATALYSTS FOR SYNGAS PRODUCTION VIA LOW TEMPERATURE REFORMING OF MODEL BIOGAS[2]

3.1 Introduction

Biomass-derived syngas (H_2 and CO) can be used as a feedstock for Fischer Tropsch Synthesis (FTS) to produce diesel and jet fuel. Biomass is considered as an alternative fuel as it offers many advantages and can be obtained from a variety of sources. Biogas produced from biomass is derived from agricultural crops, animal wastes, sludge digesters and municipal solid waste (MSW). For instance, biogas derived from anaerobic MSW digestion, known as landfill gas (LFG) which accounts for 18% of all methane emissions [15], can be used as a renewable feedstock. In addition, it has the potential to have a zero carbon footprint as well as decreased emissions of methane and carbon dioxide, the two most abundant greenhouse gases, into the atmosphere. Dry reforming of methane (reaction 3.1) which only utilizes carbon dioxide as the oxidant has been shown to give H_2:CO ratios ($\leq$1) [18-20] as can be seen in the following reactions where dry methane is coupled with the water-gas shift (reaction 3.2):

[2] Reprinted with permission from N. H. Elsayed, N. M. Roberts, B. Joseph, and J. N. Kuhn. Comparison of Pd-Ni-Mg/ceria-zirconia and Pt-Ni-Mg/ceria-zirconia catalysts for syngas production via low temperature reforming of model biogas. *Topics in Catalysis* 59.1 (**2016**): 138-146. Copyright © 2016, Springer.

$CH_4+CO_2 \rightarrow 2H_2+2CO$ $\Delta H° = 247.3\ {}^{kJ}/_{mol}$ (3.1)

$CO+H_2O \rightarrow CO_2+ H_2$ $\Delta H° = -41\ {}^{kJ}/_{mol}$ (3.2)

A desired H_2:CO of 2:1 is necessary for FTS to produce longer chain hydrocarbons (C10+) [23-25], though lower values are desirable for alcohols, acetic acid, and alkenes [26]. Coupling dry reforming with steam reforming (bi-reforming, reactions 3.1 and 3.3) and/or partial oxidation of methane (tri-reforming, reactions 3.1, 3.3, and 3.4) can improve the H_2:CO ratio [1, 28, 29] as shown in the following reactions:

$CH_4+H_2O \rightarrow 3H_2+CO$ $\Delta H° = 206.3\ {}^{kJ}/_{mol}$ (3.3)

$CH_4 + {}^{1}/_{2}\ O_2 \rightarrow CO + 2H_2$ $\Delta H° = -35.6\ {}^{kJ}/_{mol}$ (3.4)

The reforming reaction is thermodynamically not predicted to occur at temperatures below 350°C but readily occurs at temperatures greater than 600°C [1, 7, 93]. Using noble metal catalysts can help drive the reaction to lower temperatures making it more economically feasible and also open possibilities for intensified processes. Coupling low temperature (T<600°C) dry reforming with heat from solar energy as an example can help reduce or eliminate the need for heating by natural gas combustion [32]. The current work focuses on low temperature dry reforming of methane, as a model of biogas, using Pt or Pd doped nickel magnesium catalysts.

Many supports have been investigated for dry reforming, bi-reforming and tri-reforming of methane. Studied supports have included different silicates, ceria, alumina, zirconia, lanthanum oxide, perovskites and magnesium oxide [19, 30, 31, 36-38]. The support used for this study was a (Ce, Zr)O_2. The ratio chosen for the support, $Ce_{0.6}Zr_{0.4}$, was determined to be the best ratio in terms of activity and surface area by previous studies done in this group [1].

Nickel has been widely studied as a methane reforming catalyst [2-6]. Alone, nickel atoms are prone to carbon deposition especially during methane decomposition. The length between Ni-Ni bonds increases as carbon atoms adsorb thereby allowing deeper penetration until more layers of graphitic carbon form eventually deactivating the catalyst [7]. However, coupling NiO with MgO helps to reduce carbon deposition by reducing agglomeration of Ni crystallites, thereby improving catalyst lifetime [2, 7]. Furthermore, addition of noble metals such as Pt and Pd helps the catalyst to reduce at lower temperatures [20, 53, 56]. This is due to noble metals' high affinity for hydrogen atoms which in turn reduces the amount of carbon deposits. In addition, noble metals affect the basicity of the catalyst thereby changing the amount of carbon dioxide adsorbed. This effect is caused by a shift in surface coverage that allows for more stability to intermediates formed after methane decomposition and CO disproportionation [7, 20].

The goal of this study is to compare the catalyst properties of Pt or Pd doped Ni-Mg ceria-zirconia catalysts for low temperature (below 500°C) dry reforming of methane. Nickel catalysts are well known as reforming catalysts but suffer from rapid deactivation via coke formation. Addition of MgO helps to increase the Lewis basicity and adds stability to the Ni crystallites [7, 66]. Furthermore, addition of small quantities of noble metals have the ability to decrease the reduction temperature as TPR studies proved. Noble metals can also improve catalyst activity as reaction studies have shown.

3.2 Experimental Section

3.2.1 Synthesis and Materials

The ceria-zirconia support was synthesized in a 0.6:0.4 ratio respectively using the co-precipitation method described elsewhere [67]. Each batch of support was synthesized by weighing 8.7 grams of the cerium precursor $Ce(NO_3)_3 \times 6H_2O$-(99.5% pure; Alfa Aesar) and 3.3 grams of

zirconium precursor $ZrO(NO_3)_2$ x H_2O-(99.9% pure; Alfa Aesar). Both precursors were dissolved together in 150 mL of deionized water in a large beaker. Then, ammonium hydroxide (75 mL; 28% w/w NH_3; Sigma Aldrich) was added to the beaker slowly to precipitate the precursors until a clear liquid layer was visible on top of the beaker indicating complete precipitation. The mixture was then stirred and vacuum filtered until it was visibly dry. The filtrate was then re-dissolved in 0.25M NH_4OH solution and vacuum filtered a second time. The filtrate was dried in an oven at 60°C for 1 hr, then 120°C for 12 hr. Finally, the powder was calcined at 800ºC for 4 hr.

Incipient wetness impregnation was used to load the metals, nickel (1.37-1.39% by mass), magnesium (1.00% by mass), platinum (0-0.64% by mass), and palladium (0-0.51% by mass) onto the support. The nickel precursor $Ni(NO_3)_2$ x $6H_2O$ (99.9985% pure; Alfa Aesar), the magnesium precursor $Mg(NO_3)_2$ x H_2O (99.999% pure; Alfa Aesar), the platinum precursor H_2PtCl_6 x $6H_2O$ (≥37.5% metal basis, Sigma-Aldrich), and the palladium precursor $(NH_4)_2PdCl_6$ (99.99%, Sigma Aldrich). After weighing the desired amount of precursors, deionized water (2 mL) were used to dissolve them. The solution was then added drop wise onto the support until incipient wetness. The resulting wet powder was then dried in an oven for 2 hr at 120°C to remove any volatile components and evaporate the water. This process was repeated until all the solution was added. Immediately following the final drying, the powder was calcined at 600ºC for 3 hr. Two control samples that contained no nickel and magnesium but only Pt or Pd were synthesized the same way as mentioned above.

3.2.2 Catalyst Characterization

The catalysts were characterized using temperature-programmed reduction (TPR), X-ray diffraction (XRD), N_2 physisorption (BET) and CO_2 desorption (TPD-CO_2). A Cirrus MKS mass spectrometer (MS) connected in-line with a u-tube reactor containing 50-75.5 mg of catalyst was

used for the TPR and TPD-CO_2 studies. Two layers of quartz wool surrounded the catalyst on both sides to keep it in place inside the reactor. The reactor was then positioned inside a Thermoscientific Thermolyne tube furnace and high temperature glass wool was added to insulate the top of the furnace. Alicat Scientific mass flow controllers were used to control the feed gases. In addition, all of the gas feeds and outlets were wrapped in heating tape to prevent condensation prior to entering the MS. The furnace temperature was controlled using a Eurotherm 3110 PID controller. For TPR studies, catalysts were pretreated under 50 sccm of helium (UHP, Airgas) for 30 min at 110°C. Catalysts were then cooled to 50°C where the gas flow was switched to 5% H_2/He (50 sccm). The sample was then heated at a ramp rate of 10°/min to 900°C and held for 30 min. Ionization factors were calculated using calibration curves prior to data analysis.

A Bruker AXS diffractometer using a Cu Kα source at 40 kV and 40 mA was used for the XRD. The data were obtained using a (2θ) angular range of 20-80°. The step size was 0.02° and the dwell time was 3 sec for each step.

A Quantachrome Autosorb-IQ was used for obtaining BET surface areas as well as BJH pore volumes and pore diameters. Each experiment was done using 50-55 mg of catalyst. Each sample was initially pretreated at 120°C for 2 hr prior to loading to remove any moisture. The sample was then loaded in a small-bulb 6 mm quartz cell. Helium was used to backfill the sample where it was then outgassed under vacuum for approximately 1 hr. The surface area values were obtained by fitting the data to a BET isotherm in the P/P_0 range of 0.05-0.33 using N_2. The pore volume is reported at P/P_0 of ~1.

CO_2 temperature-programmed desorption (CO_2-TPD) studies were done to determine the catalyst basicity using the same system already described previously in the TPR section. The catalyst (75.5 mg) was initially reduced at a temperature of 300°C and held at that reduction

temperature for 1 hr in a 5% H_2 in He gas mixture. After reduction, only He (50 sccm) was flown to cool the catalyst until a temperature of 50°C was reached. Once the temperature stabilized at 50°C, a 10% CO_2 in He was introduced to the catalyst and flown for 30 min at a constant GHSV of 68,000h^{-1}. The catalyst was then purged by once again flowing He only (50 sccm) for another 30 min. The temperature was then increased to 800°C at a ramp rate of 10°C/min and held for 10 min.

3.2.3 Catalytic Testing

For the dry reforming reaction experiments, after the reduction step, the catalyst was cooled to 200°C in He flowing at 50 sccm. Dry reforming reaction experiments were conducted at a constant space velocity of 68,000 h^{-1} and atmospheric pressure. The reactants, methane and carbon dioxide (both 99.999% pure from Airgas) were then introduced in a 1:1 ratio (7% concentration of *each* reactant in He, 44 sccm total flowrate) to the catalyst. After the reactant flow was stable, the temperature was increased to 900°C using a 10°C/min ramp rate and held for 30 min. Steady-state reaction experiments were also conducted on select Pt and Pd catalysts. The catalyst is reduced in a similar manner as described above. After cooling to 200°C, the temperature is ramped to 470°C using a 10°C/min ramp rate and held for 30 min or until the MS signals were very steady. The temperature is then reduced to 440°C, left to stabilize then held for 30 min. The process is repeated until a temperature of 430°C is reached. Temperature-programmed oxidation studies were done on selected post-reaction catalysts and following steady-state experiments. The catalyst was cooled to 60°C under inert He (50 sccm) and held until the temperature stabilized. Oxygen in helium was then introduced in a 0.1:0.9 ratio respectively with a total flow rate of 50 sccm at a constant GHSV. The temperature was then increased to 900°C using the same ramp rate of 10°C/min and held for one hour. The oxidation studies showed no presence of surface coke on any of the tested catalysts.

The amount of CO_2 adsorbed in the temperature-programmed desorption studies was used was an estimate of active sites to determine the turnover frequencies (TOFs) from the steady state conversions of CO_2. Through a previous study of testing different GHSV, it was determined that external mass transfer limitations were insignificant for this catalyst system and that there were no internal diffusion limitations as confirmed by the Weisz-Prater criterion [20].

3.3 Results and Discussion

Four different catalysts 0.13%Pd-1.39wt%Ni1.0wt%Mg (0.13Pd), 0.51%Pd-1.37wt%Ni1.0wt%Mg/$Ce_{0.6}Zr_{0.4}O_2$ (0.51Pd), 0.16%Pt-1.34wt%Ni1.0wt%Mg/$Ce_{0.6}Zr_{0.4}O_2$ (0.16Pt), 0.64%Pt-1.34wt%Ni1.0wt%Mg/$Ce_{0.6}Zr_{0.4}O_2$ (0.64Pt), as well as two controls 0.15%Pd/$Ce_{0.6}Zr_{0.4}O_2$ (0.15Pd/CeZr) and 0.16%Pt/$Ce_{0.6}Zr_{0.4}O_2$ (0.16Pt/CeZr) were synthesized and studied for low temperature dry reforming of methane. The simplified notation for each catalyst is included in Table 3.1 and will be used from now onward. The catalysts were characterized using TPR, XRD, N_2-Physiorption, TPD-CO_2. Temperature-programmed dry reforming experiments were done and were directly followed by temperature-programmed oxidation studies. Steady-state reaction experiments were done on the two most promising catalysts (0.13Pd and 0.16Pt). Post-reaction steady-state characterizations (TPO, XRD, N_2-physisorption) were also done on those catalysts.

3.3.1 Characterization

Temperature-programmed reduction experiments were done on all catalysts to determine the reducibility of the catalyst. The results are presented in Figure 3.1, with the peak reduction temperature also in Table 3.1. Pd catalysts had lower reduction temperatures overall compared to Pt catalysts. It has been well documented in the literature that the presence of metals influence CeO_2 by increasing its reducibility [47, 68, 76, 81]. Both the 0.13Pd and 0.51Pd catalysts had the

lowest initial reduction temperatures of 135°C and 170 °C. However, the 0.13Pd sample displayed a very prominent reduction peak compared to the other samples. In addition, the 0.15Pd/CeZr control catalyst had a reduction temperature of 145°C unlike the 0.16Pt/CeZr control which did not have a single peak but rather a broad distributed one from 196-480°C.

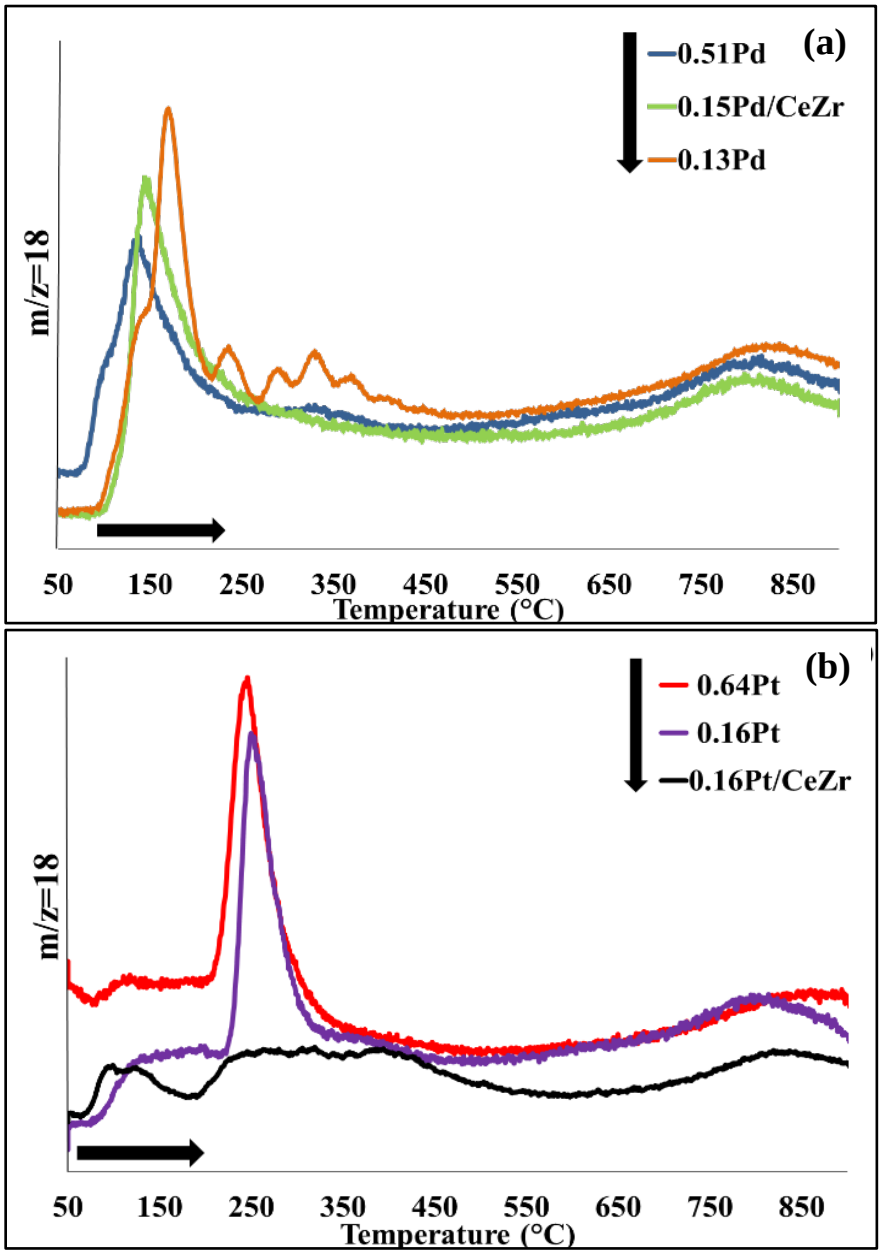

Figure 3.1: Temperature-programmed reduction (TPR) profiles as represented by water formation (m/z 18). (a) TPR of Pd catalysts, (b) TPR of Pt catalysts. Legend arrows indicative of increasing reduction temperature.

Table 3.1: Surface area, pore properties, CO_2 desorption data and reduction temperature.

Sample	Notation	S_{BET} (m^2/g)		Pore Volume (cc/g)		Pore Diameter (nm)		Amount CO_2-desorbed (µmole/g.cat) (Temp 70-550°C)	Peak Reduction Temperature (°C)
0.13%Pd- $Ce_{0.6}Zr_{0.4}O_2$ - 1.39Ni1.0Mg	0.13Pd	28	30.8[b]	0.06	0.06[b]	9.55	9.57[b]	1.23	169
0.15%Pd- $Ce_{0.6}Zr_{0.4}O_2$	0.15Pd/ CeZr	43		0.08		4.33		0.93	147
0.51%Pd- $Ce_{0.6}Zr_{0.4}O_2$ - 1.37Ni1.0Mg	0.51Pd	52		0.11		9.56		2.91	137
0.16%Pt- $Ce_{0.6}Zr_{0.4}O_2$ - 1.34Ni1.0Mg[a]	0.16Pt	31 *	21.5[b]	0.07 *	0.06[b]	11.6 *	11.3[b]	1.53	248 *
0.16%Pt- $Ce_{0.6}Zr_{0.4}O_2$[a]	0.16Pt/ CeZr	70		0.16		11.4		0.71	196-480
0.64%Pt- $Ce_{0.6}Zr_{0.4}O_2$ - 1.34Ni1.0Mg[a]	0.64Pt	22		0.05		11.4		1.01	242

*Indicates the average of two experiments reported

[a] Data obtained from a previous study [20]

[b] Post-reaction characterization

All reduction profiles had an initial intense reduction peak and a second less prominent reduction peak at a higher temperature although this was more evident in the Pt-doped catalysts versus the Pd-doped catalysts. The initial reduction peak can be attributed to the surface cerium oxide and weakly bound metals whereas the higher temperature reduction is attributed to removal of oxygen in the bulk ceria strongly bound to NiO [27, 68, 74, 94]. Noble metals helped reduce ceria to Ce^{3+} and create oxygen vacancies [65]. Hydrogen likely activated on the metal and migrated to the support. In the presence of Pt or Pd, reduction likely occurred as a result of hydrogen spillover since noble metals are known to dissociatively adsorb hydrogen [56, 77, 94, 95].

N_2-physisorption was done to examine the effects of metal addition on the surface and bulk properties of the support. BJH pore size distribution curves are provided in Figure 3.2 and the results are reported in Table 3.1. For the Pt catalysts, the surface area and pore volume decreased with increasing Pt amounts. These findings are consistent with previously published works [1, 71, 72] and is likely the result of Pt blocking some of the pores and becoming less dispersed with increasing amounts. The Pd catalysts exhibited a similar decrease in surface area and pore volume with metal loading.

X-ray diffraction patterns for the Pd and Pt catalysts are shown as Figure 3.3(a) and Figure 3.3(b), respectively. All the major diffraction lines were consistent with a cubic fluorite structure characteristic of CeO_2. This result indicated that the ZrO_2 in the support is incorporated into the CeO_2 crystal lattice consistent with previously published literature [1, 39, 56]. Furthermore, the asymmetric nature of the diffraction lines suggests the existence of multiple phases for the ceria zirconia solid solution [73]. There were no visible diffraction lines associated with Pd or Pt as expected due to the low content and expected high dispersion of the metals. These results are

consistent with the literature [56, 72]. On the other hand, MgO and NiO diffraction lines are seen at a 2θ between 42-44° on all samples but are more prominent especially in the 0.64Pt catalyst, indicating NiO and MgO deposition onto the support**.**

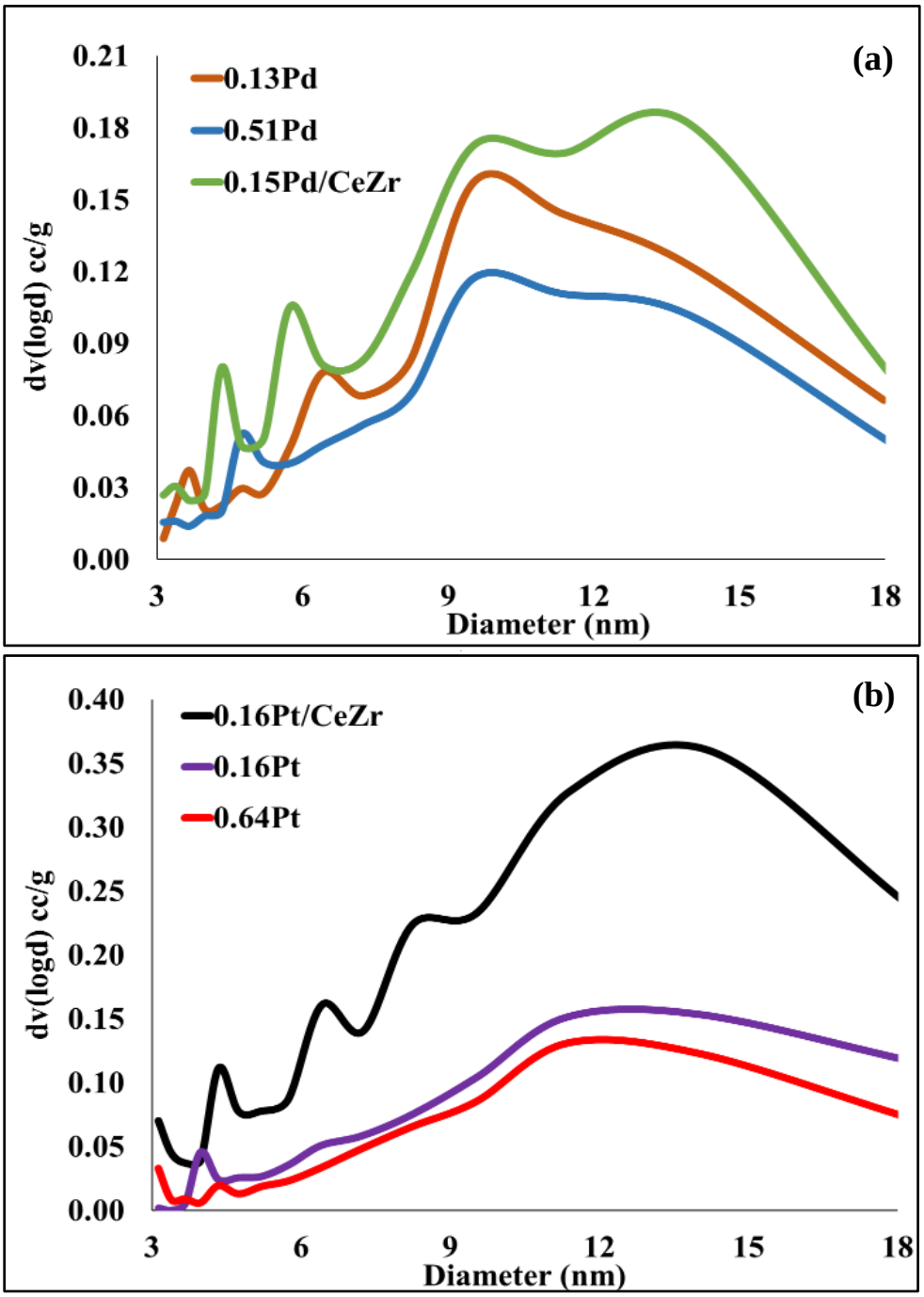

Figure 3.2: BJH pore size distribution curves. (a) Pd and (b) Pt catalysts.

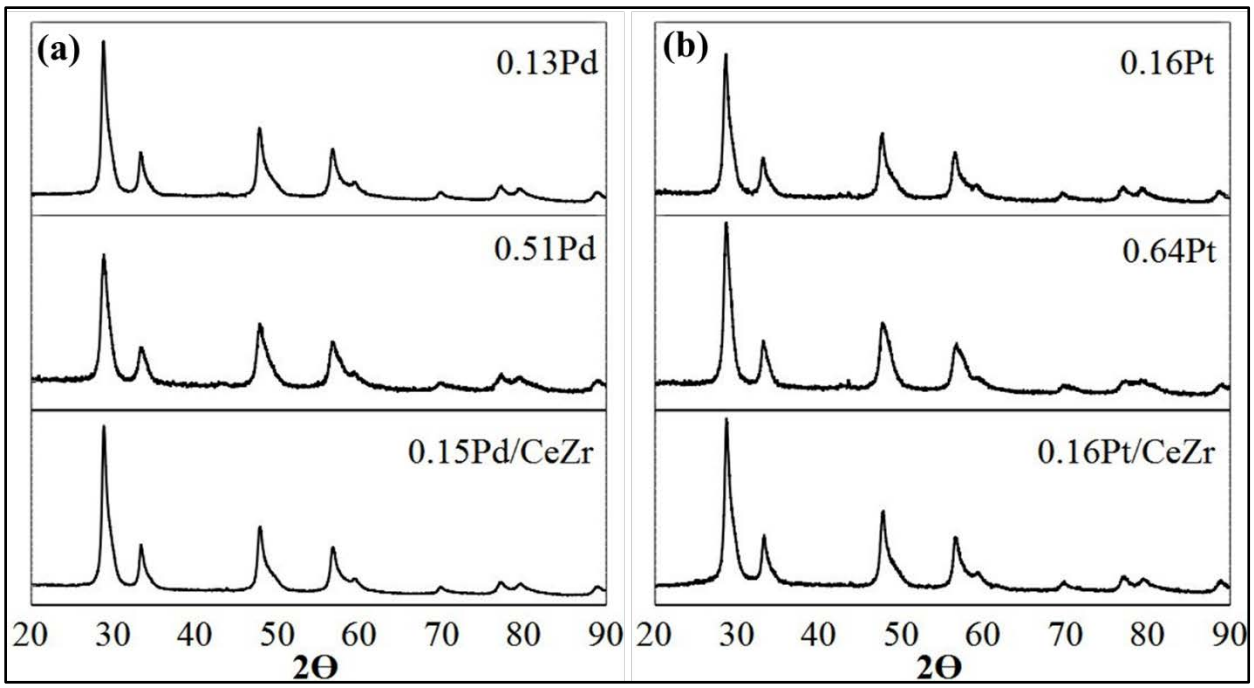

Figure 3.3: X-ray diffraction patterns of Pd (A) and Pt (B) catalysts. (200) and (111) NiO and MgO diffraction lines are highlighted in the 0.64Pt sample with the dotted box and represented by (*) and (°).

Catalyst basicity was determined using temperature-programmed desorption studies of carbon dioxide. The results are shown in Figure 3.4 and are summarized in Table 3.1. The amount of carbon dioxide desorbed varied between 0.93 to 2.91 µmole/g for the Pd catalysts where the 0.51Pd catalyst had the highest amount of CO_2 desorbed of 2.91 µmole/g.

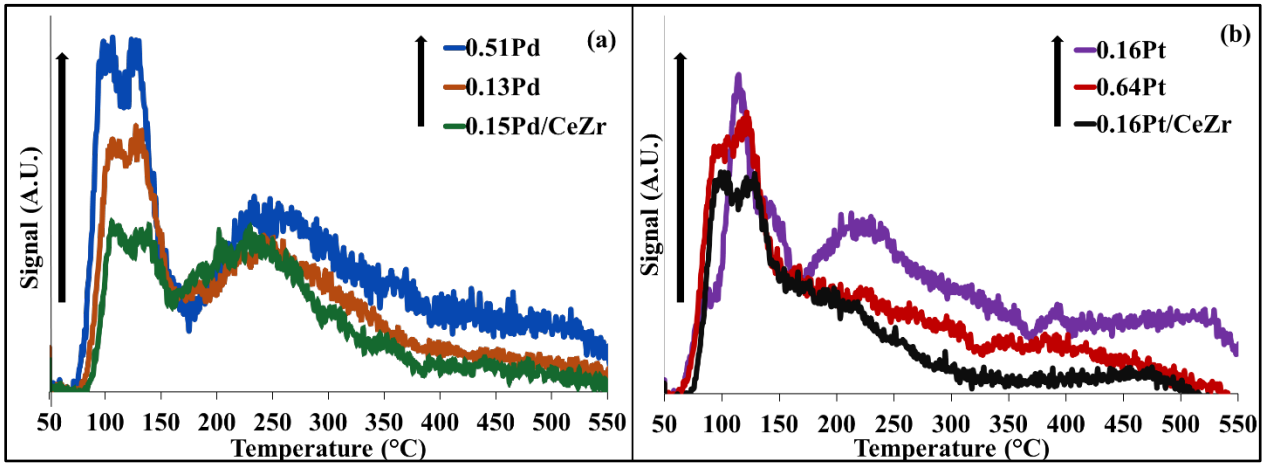

Figure 3.4: TPD-CO_2 (m/z = 44) of reduced Pd (A) and Pt (B) catalysts. Arrows correspond to legend order.

The Pt catalyst had a lower amount of carbon dioxide desorbed overall between 0.71 for the control sample without any nickel and magnesium to a high of 1.53 for the 0.16Pt catalyst. A more basic catalyst as indicated by the higher amount of CO_2 adsorbed is preferable since it can reduce carbon deposition by shifting equilibrium concentrations from CO disproportionation [7].

3.3.2 TP-Dry Reforming

CO and H_2 production as a function of temperature from the dry reforming reaction studies are presented for all catalysts in Figure 3.5. Conversion temperatures (of 10% and 50%) of both reactants as well as syngas ratios were calculated for all catalysts and are summarized in Table 3.2. Overall, Pd catalysts had lower 10% conversion temperatures for both methane and carbon dioxide versus Pt catalysts. The 0.13Pd catalyst had the lowest 10% methane conversion temperature of 383°C followed by the 0.16Pt at 454°C. The 0.51Pd sample had a 10% methane conversion temperature of 457°C which was lower than the 0.64Pt temperature of 493°C. Both control samples (0.15Pd/CeZr and 0.16Pt/CeZr) had higher 10% methane conversion temperatures, 517°C for 0.15Pd/CeZr and 504°C for 0.16Pt/CeZr. The H_2:CO ratio for all catalysts however was between 0.22-0.41 with Pd catalysts having slightly higher syngas ratios compared to Pt ones. The 0.13Pd and 0.51Pd had the highest H_2:CO ratio for all catalysts however was between 0.22-0.41 with Pd catalysts having slightly higher syngas ratios compared to Pt ones. Both 0.13Pd and 0.51Pd had the highest H_2:CO ratio of 0.39 and 0.41, respectively. The lower than stoichiometric syngas ratio is attributed to the RWGS reaction simultaneously occurring as a side reaction under the low temperatures employed for this study and is consistent with previous works done in this group and other groups [18, 20, 38, 55, 62]. In general, both Pd and Pt catalysts had comparable results which is consistent with findings from other studies that concluded that Ru and Rh were among the most

active catalysts for methane reforming followed by Ir and finally Pt and Pd with comparable activities [96].

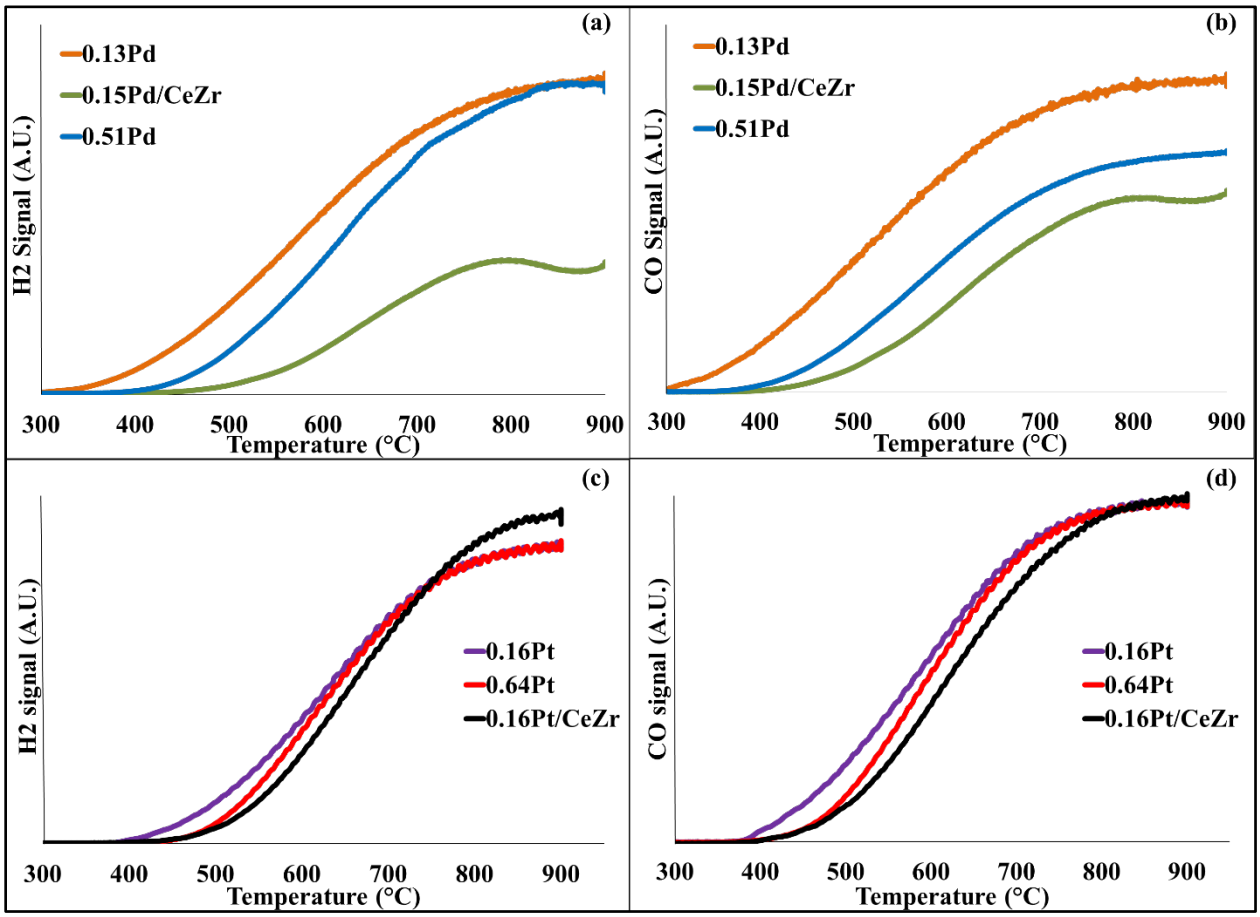

Figure 3.5: Hydrogen and carbon monoxide formation over 0.13Pd (a/b) and 0.16Pt (c/d) with respect to temperature.

3.3.3 Steady-State Dry Reforming (470-430°C)

Steady-state studies were done on the two most active samples (0.13Pd and 0.16Pt) in the temperature range 430°C-470°C. The turnover frequencies (TOFs), rates, and activation energies were calculated based on CO_2 conversion for the Pd catalysts and compared to those of the Pt catalysts done in a previous study by this group [20]. The results are summarized in Table 3.3. The rates and turnover frequencies for Pt catalysts were slightly higher than those for Pd catalysts. At the lowest tested temperature of 430°C, 0.13Pd had a TOF of $2.4s^{-1}$ whereas 0.16Pt had a TOF of

2.69s^{-1}. Overall Pt displayed higher rates compared to Pd and had a similar increasing rate trend with increasing temperature. Apparent activation energies were also calculated for the reactants for each catalyst and are summarized in Table 3.3. The activation energies of CH_4 were comparable for both 0.13Pd and 0.16Pt which had an E_a of 18.2 kcal/mol and 18.5kcal/mol respectively. However, 0.16Pt had a marginally lower CO_2 activation energy of 14.8kcal/mol compared to 16.9kcal/mol for 0.13Pd. Both catalysts had activation energies within the general range of previously published works. For Ni/CZ at temperatures between 550-840°C, it was found that the E_a was 16-18.9kcal/mol for CH_4 [85], whereas for 0.2Pt-15Ni/CaO-Al_2O_3, the E_a for CO_2 was 16.9kcal/mol at temperatures between 580-620°C [87].

Table 3.2: Dry reforming 10% and 50% conversion temperatures and H_2:CO ratio at T=450°C.

Catalyst	**10% CH_4 Conversion T (°C)**	**50% CH_4 Conversion T (°C)**	**10% CO_2 Conversion T (°C)**	**50% CO_2 Conversion T (°C)**	**H_2:CO @T=450 °C**	**Reference**
0.13Pd	383	542	366	521	0.39	This Study
0.51Pd	458	597	441	577	0.41	This Study
0.15Pd/ CeZr	517	708	499	664	0.24	This Study
0.16Pt	454	603	432	578	0.30	[20]
0.64Pt	493	613	479	595	0.22	[20]
0.16Pt/ CeZr	504	641	488	625	0.23	[20]

Table 3.3: Turnover frequencies, rates, and apparent activation energies of select catalysts (at given temperatures and P=1atm). TOFs and rates based on CO_2 conversion.

Temperature (°C)	TOF (s^{-1})		Rate (mol/hr/g.cat)*10^2		Apparent activation Energy (kcal/mol)			
					0.13Pd[a]		0.16Pt[b]	
	0.13Pd[a]	0.16Pt[b]	0.13Pd[a]	0.16Pt[b]	CH_4	CO_2	CH_4	CO_2
430	2.40	2.69	1.06	1.26				
440	2.84	3.17	1.26	1.48				
450	3.37	3.50	1.49	1.73	18.2	16.9	18.5	14.8
460	3.93	4.22	1.74	1.98				
470	4.58	4.74	2.03	2.22				

[a] This study
[b] Reference [20]

3.3.4 Post-Reaction Characterization

Post steady-state experiment characterization was done using TPO, XRD, and N_2 physisorption on 0.13Pd and 0.16Pt catalysts. In a separate set of steady-state experiments, post-reaction temperature-programmed oxidation (TPO) studies were also done immediately after cooling following the steady-state experiment and showed no surface coke present. XRD patterns of both spent catalysts did not display any shifts. Surface areas of the 0.13Pd sample was 28 m^2/g pre-reaction and 30.8 m^2/g post-reaction, which is within experimental error given the small amount of sample tested (<75mg) resulting from sample loss due to transfer from the U-tube reactor to the N_2-physisorption cell. Both pore volume and pore diameter were the same pre- and post-reaction at 0.06 cc/g and 9.57 nm, respectively. For the 0.16Pt sample, the surface area decreased slightly and went from an average of 31 m^2/g pre-reaction to 22 m^2/g post-reaction as

summarized in Table 3.1. On the other hand, the 0.16Pt pore volume decreased from 0.07 cc/g to 0.062 cc/g and the pore diameter decreased from 11.6 nm to 11.3 nm as well.

3.4 Conclusion

This study compared low temperature dry reforming of methane using Pt and Pd doped Ni/Mg catalysts on a ceria zirconia oxide support. TPR studies showed Pd doped catalysts having lower reduction temperatures than Pt doped catalysts. Carbon dioxide desorption studies confirmed that Pd catalysts had more basic sites as more carbon dioxide was adsorbed. On the other hand, reaction studies showed that both catalysts were comparable in terms of 10% methane conversion with Pd having slightly lower conversion temperatures. Reaction experiments showed that 0.13Pd had a 10% methane conversion of 383°C with conversion decreasing with decreasing temperature. Pt catalysts had a similar decrease in conversion with reduced temperatures and a 10% methane conversion at 454°C. Post-reaction oxidation studies showed no surface coke present on any of the tested catalysts. The surface areas, pore volumes as well as pore diameters showed negligible changes following the reaction. Post-reaction XRD did not show shifts. Although both Pd and Pt catalysts had comparable reaction results, Pt catalysts had marginally higher TOF's (2.69-4.74 s^{-1}) compared to Pd catalysts (2.40-4.58 s^{-1}). On the other hand, Pd catalysts had lower reduction as well as reaction temperatures, were more basic further reducing the possibility of coke formation and had slightly higher H_2:CO ratios. For those reasons, the negligible change in the pore properties in the spent catalysts, and because of the more economical cost of Pd compared to Pt, it would be more feasible to use Pd catalysts for industrial applications.

CHAPTER 4: EFFECT OF SILICON POISONING ON CATALYTIC DRY REFORMING OF SIMULATED BIOGAS[3]

4.1 Introduction

Many potential sources of biogas are possible including landfills that produce undesired landfill gas (LFG) from anaerobic digestion of municipal solid waste (MSW). LFG, which accounts for 20 % (in 2014) of all U.S. methane emissions [97] and is subject to more stringent regulations, can be used as a renewable feedstock. A promising route is utilizing the biogas to produce H_2 and CO known as syngas through methane reforming. The syngas can then be used as a feedstock for Fischer- Tropsch synthesis to produce liquid hydrocarbons or the hydrogen can be used on its own as an alternative fuel. This route is especially encouraging given that biogas was recently added as an advanced biofuel under the EPA's Renewable Fuel Standard released in 2014. Reforming of methane is typically facilitated at temperatures greater than 600°C through the use of nickel catalysts due to their high activity and low costs. Using precious metal doped catalysts can decrease the reforming temperature significantly as previously demonstrated by this group [20, 98]. Unfortunately, biogas also contains various impurities that can adversely affect the reforming catalyst and the processing equipment. Volatile methyl siloxanes (VMS; generally addressed as siloxanes) are among the leading impurities present in LFG that cause equipment damage. Siloxanes are compounds comprised of silicon, oxygen as well as methyl groups and can be linear

[3] This chapter is currently in review as part of a manuscript to a scientific journal.

or cyclic molecules (see Table 4.1). Siloxanes are harmful because they irreversibly decompose to silica [99-103], which then deposits and coats the equipment [34, 104] leading to equipment failure and shortened lifetime. As concerns grow over the harmful effect of siloxane decomposition to the landfill processing equipment, manufacturers have begun setting allowable limits of siloxanes in the feed for the equipment to continue functional operation. Engine manufacturers have set the allowable limit of siloxane concentration in the feed gas to 2.8 mg/m^3 according to McBean [33]. Concentrations of siloxanes in LFG vary significantly depending on the location, age, source as well as contents of the landfill and have been estimated in the literature to be anywhere from 0.005-15 mg/m^3 [102, 105, 106]. These values are also important to solid oxide fuel cells (SOFCs) since they typically employ Ni anodes which only 10 ppbv siloxanes (~0.15 mg/m^3) caused a decrease in performance [107, 108] and a general tolerance of a few ppm is stated [109].

The need to determine the effect of these siloxanes is becoming pressing and can be seen through the steady increase in related research in the last decade or so not only on equipment effects but on all stages of LFG processing. Many studies have looked at siloxanes removal technologies and/or other impurities for the purpose of gas cleanup and preserving the equipment used such as engines and turbines to recover the LFG [34, 105, 110-113]. However very little literature looks at the siloxane poisoning influence on reforming catalysts. The objective of this initial study is to compare the effects of silicon poisoning for high temperature reforming catalyst (1.3 wt% Ni-1.0 wt % $Mg/Ce_{0.6}Zr_{0.4}O_2$) and the low temperature catalyst (0.16 wt % Pt-1.3 wt% Ni-1.0 wt% $Mg/Ce_{0.6}Zr_{0.4}O_2$) to literature studies on biogas conversion processes. The low and high temperature catalyst systems have already respectively been proven to be effective at dry reforming of methane at low temperatures (≤450 °C) [20, 98] and dry [20, 98] and tri-reforming [114] of methane at typical temperatures (~800 °C). For simplicity, dry reforming was selected in

this study as the model reforming reaction. The effects of silica deposits between these catalysts and engine and fuel cell applications may be altered due to composition and operation/condition differences. Different silicon poisoning amounts equivalent to 1 week of exposure, 1 month, and 6 months (assuming a 24/7 plant operation; see Appendix B for calculation details; Table B1) were selected for the accelerated catalyst poisoning. These amounts were chosen to study the effects of various exposure amounts and determine if and when the catalysts begins deactivation. The catalysts were directly poisoned via deposition wetness of a silicon containing solution assuming a worst case scenario where all the VMS in the raw gas decompose to silica and deposit onto the catalyst. Previous groups have studied the effects of poisoning in a similar ex situ accelerated approach for rhodium-based reforming catalysts [115, 116]. This approach was chosen over flowing siloxanes in the feed for safety purposes so as to not clog the capillary tubes of the online analytical system and to permit the accelerated deactivation approach. In addition to possible equipment damage that could occur, the vapor pressures of siloxanes are rather high compared to the typical contaminant levels in LFG and, even with further dilution, it is not possible to achieve even the high end of siloxane concentration levels in LFG. Thus, any direct introduction of siloxanes would also result in accelerated deactivation studies. Other groups have shown that VMS such as hexamethylcyclotrisiloxane (D3) decompose to SiO_2 at temperatures as low as 200 °C on silica [117] and 250 °C on alumina [102], which are much lower than even the low temperature reforming temperature. Siloxane decomposition to silica occurs even under reducing conditions as noted by silica formation in anodic chambers of SOFCs [103] and wet biogas [102, 117].

Table 4.1: Properties of selected volatile methyl siloxanes[a].

Compound: [Common Name]	Molecular Structure	Formula	Molar Mass (g/mol)	Density (g/L) at 20°C (liquid)
Hexamethyldisiloxane: [L2]	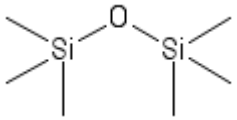	$C_6H_{18}OSi_2$	162	753
Octamethyltrisiloxane: [L3]	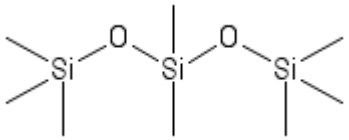	$C_8H_{24}O_2Si_3$	236	817
Decamthyltetrasiloxane: [L4]	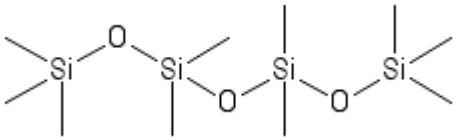	$C_{10}H_{30}O_3Si_4$	310	853
Octamethylcyclotetrasiloxane: [D4]	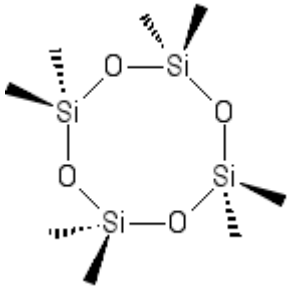	$C_4H_{24}O_4Si_4$	297	953

a: adapted from [34]

4.2 Experimental Procedure

4.2.1 Synthesis and Materials

The ceria-zirconia support was synthesized in a 0.6:0.4 ratio respectively using the co-precipitation method described elsewhere [67]. Each batch of support was synthesized by weighing 8.7 grams of the cerium precursor $Ce(NO_3)_3$ x $6H_2O$-(99.5 % pure; Alfa Aesar) and 3.3 grams of zirconium precursor $ZrO(NO_3)_2$ x H_2O-(99.9 % pure; Alfa Aesar). Both precursors were dissolved together in 150 mL of deionized water in a large beaker. Then, ammonium hydroxide (75 mL; 28 % w/w NH_3; Sigma Aldrich) was added to the beaker slowly to precipitate the precursors until a clear liquid layer was visible on top of the beaker indicating complete precipitation. The mixture was then stirred and vacuum filtered until it was visibly dry. The filtrate was then re-dissolved in 0.25 M NH_4OH solution and vacuum filtered a second time. The filtrate was dried in an oven at 60 °C for 1 h, then 120 °C for 12 h. Finally, the powder was calcined at 800 °C for 4 h.

Incipient wetness impregnation was used to load the metals, nickel (1.3 % by mass), magnesium (1.0 % by mass), and platinum (0.16 % by mass) onto the support. The nickel precursor $Ni(NO_3)_2$ x $6H_2O$ (99.9985 % pure; Alfa Aesar), the magnesium precursor $Mg(NO_3)_2$ x H_2O (99.999 % pure; Alfa Aesar), and the platinum precursor H_2PtCl_6 x 6 H_2O (≥37.5 % metal basis, Sigma-Aldrich). The desired amount of precursors were then dissolved in deionized water (2 mL). The solution was then added dropwise onto the support until incipient wetness. The resulting wet powder dried in an oven for 2 h at 120 ˚C to remove volatile components and evaporate the water. This process was repeated until all the solution was added. Immediately following the final drying, the powder was calcined at 600 ˚C for 3 h. Wetness impregnation was also used to introduce the silicon. The desired mass of catalyst is weighed in a ceramic boat. The necessary amount of Ludox® which is a colloidal silica suspension (40 wt% suspension in water, Sigma-Aldrich) is

weighed in a vial and DI water is added to thin the Ludox® (about 1.5 mL for every gram of Ludox®). The Ludox® solution is then added dropwise unto the catalyst until incipient wetness. The catalyst is then placed in a heated oven at 350 °C for 15 min. The process is repeated until all the Ludox® solution is used up. Upon final drying, the catalyst is then calcined at 600 °C for 4 h. A second batch of the NiMg only catalyst was done using the same method described, but was calcined at 800 °C to determine if a change in surface area and/or bulk properties would occur for the high temperature catalyst based on calcination temperature.

4.2.2 Catalyst Characterization

The catalysts were characterized using temperature-programmed reduction (TPR), X-ray diffraction (XRD), N_2 physisorption (BET), scanning electron microscopy coupled with energy dispersive spectroscopy (SEM/EDS), and Fourier transform infrared spectroscopy (FTIR). A Cirrus MKS mass spectrometer (MS) connected in-line with a u-tube reactor containing 75.5 – 75.9 mg of catalyst was used for the TPR studies. Prior to running the studies, MS calibration curves were used to obtain ionization factors. The catalyst was placed between two layers of quartz wool to keep it in place inside the reactor. The reactor was then placed inside a Thermoscientific Thermolyne tube furnace and insulated with high temperature glass wool at the top. Alicat Scientific mass flow controllers controlled the feed gas flowrates. Condensation was prevented by wrapping all of the gas feeds and outlets in heating tape prior to entering the MS. The furnace temperature was controlled using a Eurotherm 3110 PID controller. For the TPR studies, catalysts were pretreated under 50 $Scm^3\ min^{-1}$ of He (UHP, Airgas) for 30 min at 110 °C. Catalysts were then cooled to 50 °C where the gas flow was switched to 5% H_2/He (50 $Scm^3\ min^{-1}$). The sample was then heated at a ramp rate of 10 °C/min to 900 °C and held for 30 min.

X-ray diffraction patterns were obtained using a Bruker AXS diffractometer using a Cu Kα source at 40 kV and 40 mA. The data were obtained using a (2θ) angular range of 20-80 °. The step size was 0.02 ° and the dwell time was 3 sec for each step.

Brunaur Emmett and Teller (BET) surface area as well as BJH pore volumes and pore diameters were obtained using a Quantachrome Autosorb-IQ. Approximately 55-56 mg of catalyst was used for each experiment. Each sample was pretreated by placing it in an oven at 120 °C for 2 h prior to loading to remove any moisture. The catalyst was then loaded in a small-bulb 6 mm quartz cell. The sample was backfilled using He where it was then outgassed under vacuum for approximately 6 h. The surface area values were obtained by fitting the data to a BET isotherm in the P/P_0 range of 0.05-0.33 using N_2. The pore volume is reported at P/P_0 of ~1.

A Hitachi S-800 scanning electron microscope equipped with energy dispersive spectroscopy (SEM/EDS) was used to obtain the catalyst images. All images were taken at 16.0 kV and 3000x magnification.

A Fischer Thermoscientific Nicolet iS50 FT-IR/DRIFTS with multibounce ATR was used to obtain infrared spectra of the catalysts.

4.2.3 Catalytic Testing

The catalyst (similar amount as stated for TPR) was reduced in a 5 % H_2/He mixture at 300°C for 1 h prior to running the dry reforming reaction experiments. After reduction, the catalyst cooled to 200 °C under a constant flow of 50 Scm^3 min^{-1} of inert He. After temperature stabilization, carbon dioxide and methane were introduced (both 99.999 % pure from Airgas) were then introduced in a 1:1 ratio to the catalyst in inert He (20% reactants in 50 Scm^3 min^{-1} total flow rate). The gas hourly space velocity was maintained constant at 68,000 h^{-1}. The temperature was then ramped at 10 °C/min to 900 °C and held for 30 min.

4.3 Results and Discussion

Two different reforming catalysts, a high temperature one with 1.3 %Ni and 1.0% Mg and a low temperature one with 0.16 % Pt added to the Ni and Mg were synthesized on ceria zirconia mixed oxide support ($Ce_{0.6}Zr_{0.4}O_2$). Ludox®, a silica colloidal suspension, was selected for silicon introduction, as the methodology to simulate, accelerated way, the long-term effects of siloxane decomposition to silica. This approach is employed because siloxanes irreversibly decompose to silica [99-103]. Previous studies have shown that VMS (even cyclic molecules) can decompose at temperatures as low as 200 °C [102, 117] with some molecules such as trimethylsilanol having a boiling point as low as 90 °C [106]. Therefore, although the siloxanes are the starting compounds, the damage actually results from the silica [34, 104]. For this initial study, reactions were tested at temperatures up to 900 °C and a worst case scenario was assumed where all of the VMS decompose to silica on the catalyst.

Three different poisoning amounts were chosen, 1 week, 1 month, and 6 months to study the effects of accelerated deactivation. The amounts were chosen based on several assumptions (see appendix B) including a plant that operates on a 24/7 basis with a flowrate of 4250 $Sm^3\,h^{-1}$. The density of the catalyst was taken to be 1700 kg/m^3. A survey of available literature showed a varying range of approximations from 0.005-15 mg/m^3 for the amount of siloxanes present in LFG since it depends on size and content of waste in the landfill [102, 105, 118]. With that in mind, the concentration of siloxanes in the feed was assumed to be 5 mg/m^3 ultimately equivalent to ~2 mg Si/m^3 which is in the mid-range of the literature values. This Si amount would then result in an equivalent SiO_2 amount of ~4 mg SiO_2/m^3. A gas hourly space velocity (GHSV) remained the same (68,000 h^{-1}) as used for the lab experiments. Sample calculations for silica % weight gain

based on the assumptions is provided in appendix B (Table B1). The results along with the nomenclature that will be used for the poisoned catalysts is provided in Table 4.2.

Table 4.2: Mass gain of silica.

Catalyst Composition (Fresh)	Sample	Nomenclature	Mass Gain SiO_2
1.3wt%Ni-1.0wt%Mg/$Ce_{0.6}Zr_{0.4}O_2$	1 week NiMg	1W-NiMg	1.5%
	1 month NiMg	1M-NiMg	12%
	6 month NiMg	6M-NiMg	66%
0.16wt%Pt-1.3wt%Ni-1.0wt%Mg/$Ce_{0.6}Zr_{0.4}O_2$	1 week Pt	1W-Pt	1.1%
	1 month Pt	1M-Pt	11%
	6 month Pt	6M-Pt	62%

4.3.1 Characterization

4.3.1.1 Temperature-Programmed Reduction (TPR)

The reducibility of the catalyst, as shown in Figure 4.1, was determined through temperature-programmed reduction experiments (TPR). Catalyst reduction is measured by tracking the formation of water shown by mass to charge ratio (m/z=18) from the output of the mass spectrometer. Reduction temperature has been identified to be directly related to activity with lower temperatures indicating higher activity as previously reported in these catalyst systems [20]. All catalysts had a similar reduction profile with an initial peak indicating the formation of water then a tail (Figure 4.1). Overall, the Pt catalysts (fresh and poisoned) had lower reduction temperatures compared with the NiMg only catalysts. The fresh Pt catalyst displayed a reduction temperature of 248 °C [20]. Addition of silica caused an increase in reduction temperature where

1W-Pt had a reduction temperature of 304 °C. The 1M-Pt had a reduction temperature of 311 °C. The trend continued where 6M-Pt reached a high reduction temperature of 315 °C. The same trend was present in the NiMg only catalyst. Increasing the poisoning caused an increase in the reduction temperature from 382 °C for the fresh catalyst to a high of 546 °C for the 6M-NiMg catalyst.

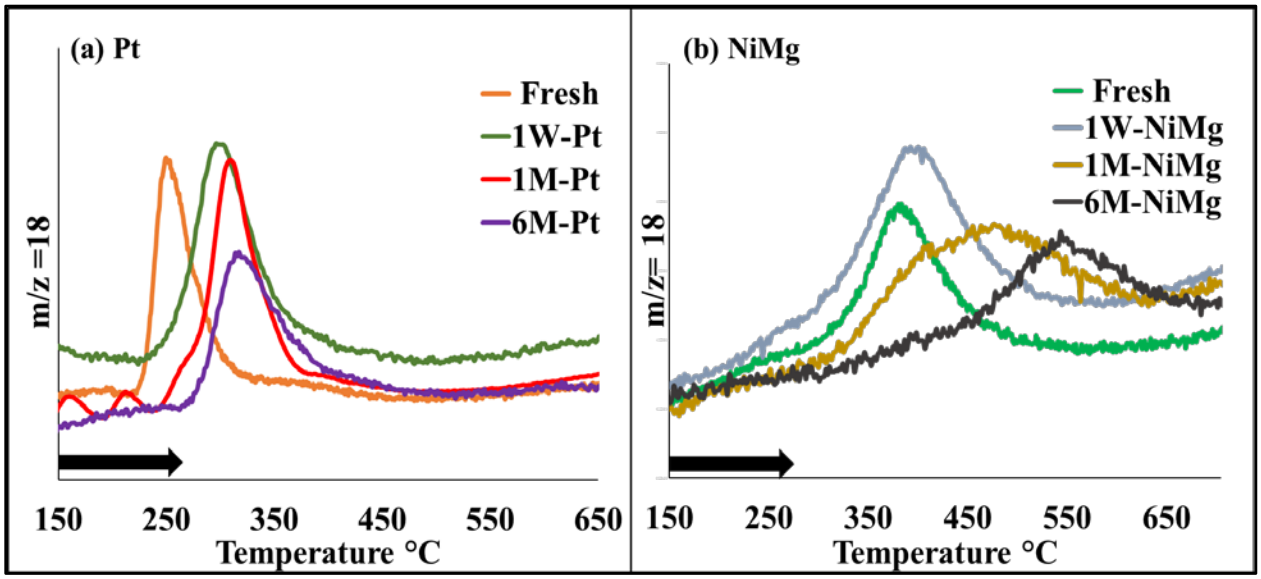

Figure 4.1: Temperature-programmed reduction (TPR) profiles as represented by water formation (m/z 18). (a) TPR of Pt catalysts (b) TPR of NiMg only catalysts. Legend arrows indicative of increasing reduction temperature.

4.3.1.2 N_2 Physisorption Analyses

Brunauer-Emmett-Teller (BET) surface areas, pore volumes, and pore diameters are presented in Table 4.3. Due to the commercial silicon agent (Ludox®) having a higher specific surface area than the unpoisoned catalysts, the total specific surface area actually increased with increasing silica deposits. The effect silica deposits was more readily observed through decreases in the average pore diameter. There was little impact on the total pore volume with silica deposits. Most likely, the porous silica coated the supports' mesopores causing a decrease in peak pore diameter. Results presented and interpreted are also in agreement and suggested that initially a monolayer forms, which is unselective to specific surfaces.

Table 4.3: Specific surface areas (SSA)[a] and bulk properties.

	SSA (m^2/g)	PV (cc/g)	PD (nm)
Fresh Pt [b]	31	0.07	11.6
1W-Pt	31.5	0.07	9.5
1M-Pt	34.4	0.08	7.2
6M-Pt	59.1	0.1	6.4
NiMg only Calcined at 600°C			
Fresh NiMg	40.0	0.1	11.4
1W-NiMg	27.0	0.06	11.4
1M-NiMg	36.3	0.09	11.4
6M-NiMg	73.8	0.1	5.2
NiMg only Calcined at 800°C			
Fresh NiMg [b]	40.0	0.1	11.4
1W-NiMg	35.0	0.1	11.3
1M-NiMg	28.9	0.07	7.2
6M-NiMg	22.9/33.5	0.06/0.08	8.2/8.2

[a] Ludox® SSA: ~220m^2/g
[b] From a previous study [98]

To verify these interpretations, the high temperature catalyst was calcined at a higher temperature (800 °C rather than 600 °C) more indicative of its operation temperature. The calcination temperature had a significant effect on the specific surface area and pore properties of the high temperature catalyst. The decreases in specific surface area, pore volume, and pore diameter with silica loading indicated pore shrinkage and surface blockage, which would be

anticipated to adversely impact the catalyst activity. Reaction results discussed in the next section indicated that the catalyst deactivated even at the smallest poisoning amount which rendered the need to explore the possibility that some of the silica may agglomerate and leave the system as small particles unnecessary.

4.3.1.3 Scanning Electron Microscopy Coupled With Energy Dispersive Spectroscopy (SEM/EDS)

Visual differences between the fresh and poisoned catalysts, as well as to confirm the elements present in the catalyst system, were examined by SEM-EDS as shown in Figure 4.2. For the fresh 0.16Pt catalyst, no silica was observed, as anticipated, on the surface of the catalyst (Figure 4.2(a)).

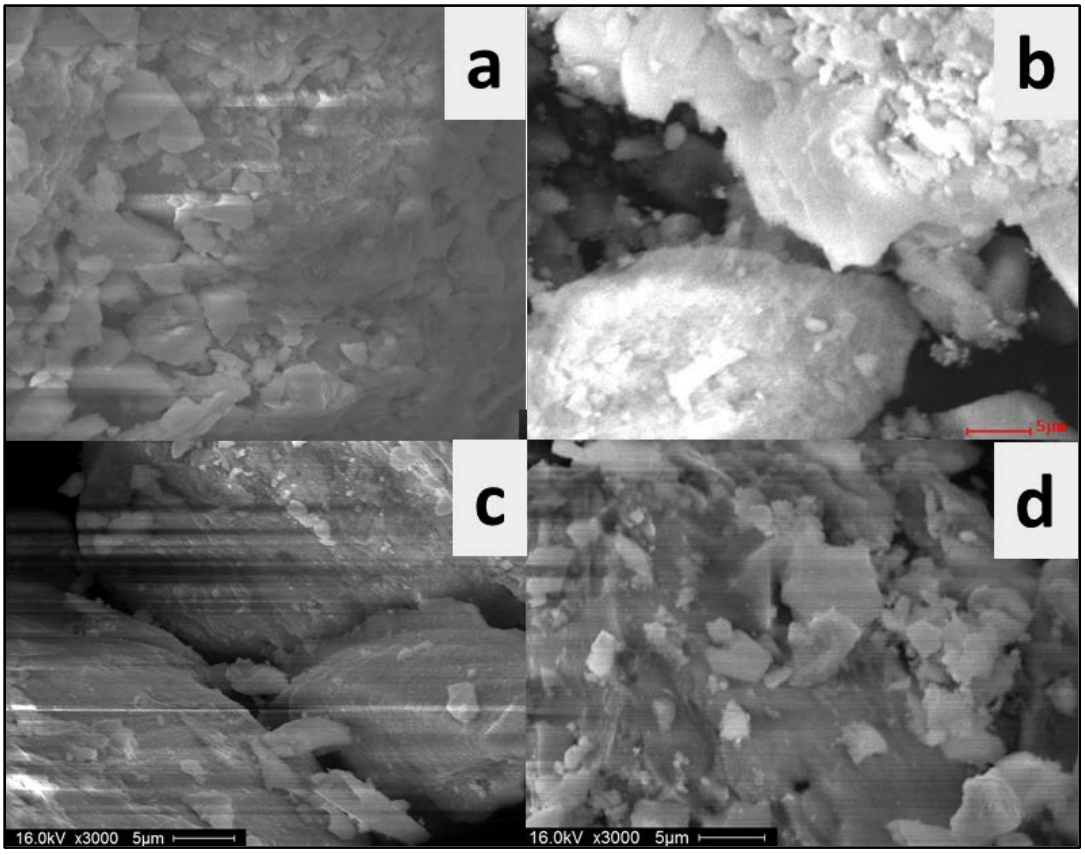

Figure 4.2: SEM images of fresh vs. 6M catalysts. (a) SEM image of fresh 0.16Pt catalyst (b) SEM image of 6M-Pt catalyst (c) SEM image of fresh NiMg catalyst (d) SEM image of 6M-NiMg catalyst.

Alternatively, the 6M-Pt catalyst indicated the presence of silica as evidenced by the bright white regions (Figure 4.2(b)) compared to the fresh catalyst. A similar observation was seen in the fresh NiMg (Figure 4.2(c)) compared to the 6M-NiMg sample (Figure 4.2(d)) where the evidence of silica was prominent. EDS studies showed the presence of Pt, Ce, Zr, Ni and Mg in the fresh catalyst with percentages within experimental error. As summarized in Table 4.4, silicon was present both for NiMg and 0.16Pt poisoned catalysts. This finding indicated the physical presence of silicon and further proves that it has a direct effect in the decreased catalyst activity as will be discussed in the reaction section. Silicon was present in much higher concentrations (40 wt%) in the tested 6M sample compared to 7.9 wt% in the 1M sample (not shown; ratio nearly ~6), with no presence in the fresh catalyst as expected.

Table 4.4: EDS quantitative data (in Wt%, carbon-free basis) for fresh 0.16Pt and NiMg catalysts compared to the 6M- Pt and 6M-NiMg catalysts.

Element / Sample	Fresh Pt	6M-Pt	Fresh NiMg	6M-NiMg
O	16	34	12	24
Mg	0.6	nd	0.4	0.40
Si	nd	40	nd	32
Pt	nd	5.2	nd	nd
Ce	62	nd	67	34
Ni	5.7	nd	3.3	9.2
Zr	15	nd	18	nd

nd= not detected

4.3.1.4 FT-IR Spectroscopy

Potential structural changes caused by poisoning was monitored by Fourier Transform infrared spectroscopy (FT-IR; Figure 4.3). The addition of silica has changed the peaks in the 700-1250 cm^{-1} range for both the 0.16Pt (Figure 4.3a) and the NiMg only (Figure 4.3 b) catalysts. Both crystalline and amorphous silica have peaks in the same range. This result indicated that the catalysts have been contaminated with silica. Peaks in the lower range of 950-1100 cm^{-1} are indicative of stretching vibration of Si-O-Si bonds [119]. These findings are similar to previous findings obtained by Rasmussen et al. [120] who concluded that the catalyst was likely poisoned through a bond formation of a partially oxidized siloxane atom to an active Pt site. Similar absorbance peaks were visible for the NiMg only catalyst, indicating the presence of silica for the poisoned catalyst that were absent in the unpoisoned catalyst.

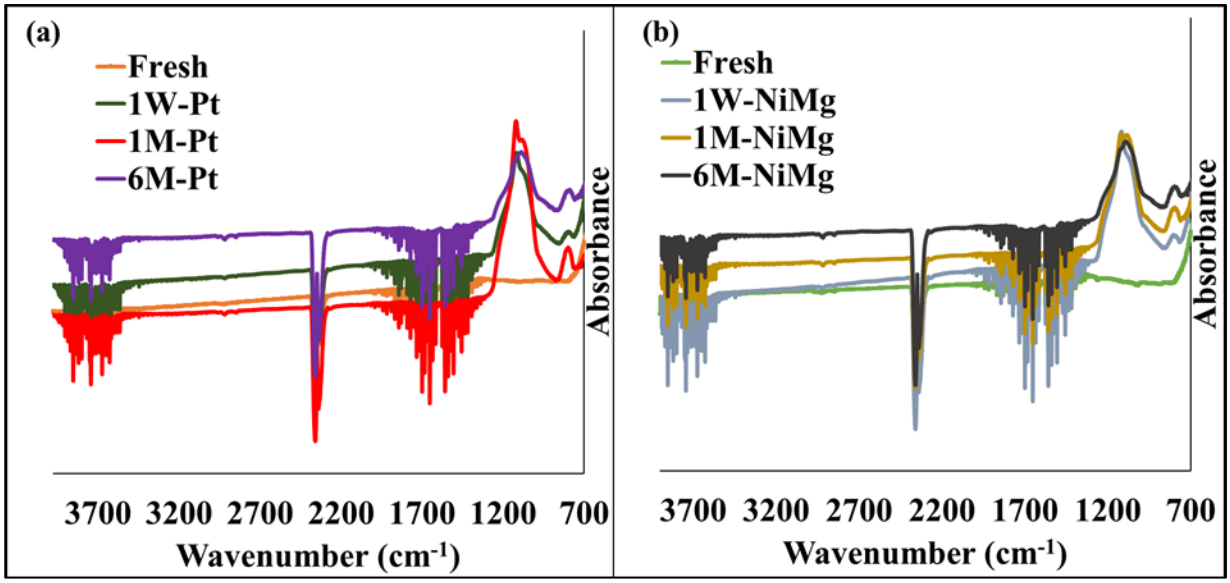

Figure 4.3: IR spectra of Pt and NiMg catalysts. (a) Pt catalysts both poisoned and fresh (b) NiMg catalysts both poisoned and fresh

4.3.1.5 XRD

X-ray diffraction (XRD) patterns (Figure 4.4) showed that silica has been deposited onto the catalyst even at the smallest amount used. This conclusion can be seen by the change in the

diffraction pattern at the lower 2theta (20-25°) values as indicated by the arrows showing the broad peak consistent with silica [121]. The first diffraction pattern at the very top showed a fresh, un-poisoned catalyst and indicated that the Miller indices of the cubic ceria-zirconia solid solution are primary crystalline phase. The poisoning process had minimal impact on its crystalline features.

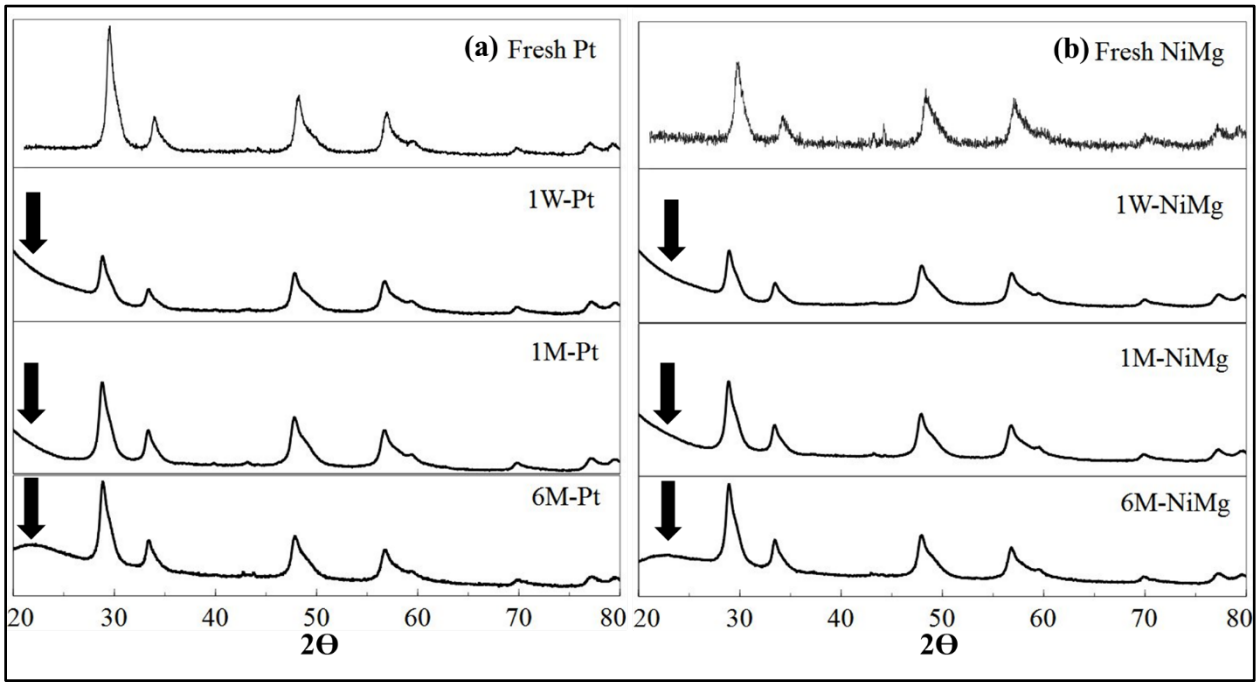

Figure 4.4: X-ray diffraction patterns of 0.16Pt and NiMg catalysts. (a) 0.16Pt catalysts both fresh and with different poisoning amounts (b) NiMg catalysts both fresh and with different poisoning amounts.

4.3.2 Dry Reforming

Hydrogen and carbon monoxide production as a function of temperature are shown in Figure 4.5. The fresh catalysts (0.16Pt and NiMg) were able to reform methane to produce both H_2 and CO at lower temperatures compared to the poisoned catalysts. Catalytic activity decreased with increased poison amount as evident by the increased temperature at which H_2 and CO were produced. The results of temperatures where 10 % (X_{10}) and 50 % (X_{50}) of both CH_4 and CO_2 were converted to syngas are summarized in Table 4.5. Addition of even minute amounts of silica, as seen in the 1W-Pt catalyst, increased the temperatures from 454 °C to 518 °C for X_{10} CH_4

conversion and from 402 °C to 503 °C for X_{10} CO_2 conversion. Higher poisoning amounts have successively increased the conversion temperature to reach a maximum of 587 °C for X_{10} CH_4 conversion for the 6M-Pt catalyst and 566 °C for X_{10} CO_2 conversion for the same catalyst. This trend fits with the literature.

Table 4.5: Methane and carbon dioxide 10% (X_{10}) and 50% (X_{50}) conversion temperatures.

Pt Catalysts	**CH_4 Conversion Temperature °C**		**CO_2 Conversion Temperature °C**		**H_2:CO (@450°C)**
	X_{10}	**X_{50}**	**X_{10}**	**X_{50}**	
Fresh*	454	603	432	578	0.30
1W-Pt	518	630	503	613	0.22
1M-Pt	535	675	510	657	0.20
6M-Pt	587	752	566	726	0.11
NiMg Catalysts	**CH_4 Conversion Temperature °C**		**CO_2 Conversion Temperature °C**		**H_2:CO (@800°C)**
	X_{10}	**X_{50}**	**X_{10}**	**X_{50}**	
Fresh*	762	848	742	813	0.31
1W-NiMg	810	900	790	875	0.13
1M-NiMg	842	nr	827	900	0.09
6M-NiMg	nr	nr	900	nr	n/a

*From a previous study [20]
-nr: Not reached
n/a: not applicable since there was no reactant conversion

Rasmussen et al. studied the catalytic activity over Pt catalysts for CO conversion using raw flue gas and the X_{50} conversion temperature increased from 199 °C for the fresh catalyst to 251 °C for the poisoned catalyst [120].The H_2:CO ratio (at 450 °C) also suffered with the addition of poison. For the low temperature catalyst, 0.16Pt, the ratio decreased from 0.30 for the fresh

catalyst to 0.22 for 1W-Pt sample and continued to decrease ultimately reaching 0.11 for 6M-Pt catalyst. Ideally, higher H_2:CO ratios near 2:1 at a minimum are required for chemical processes such as methanol synthesis and Fischer Tropsch (FT). Similar observations were seen for the NiMg only catalyst where the temperature increased from 762 °C to 810 °C for the X_{10} of CH_4 for the 1W-NiMg catalyst and reached 842 °C for 1M-NiMg. Furthermore, addition of silica has caused the 50 % methane (X_{50}) conversion and in the case of 6M-NiMg, the X_{10} conversion to be unreached thereby making the catalyst essentially unusable in this operational window. The H_2:CO ratios also decreased with increased poisoning amounts as observed in the low temperature catalyst. At 800°C, the fresh catalyst had a H_2:CO ratio of 0.31 which decreased to 0.13 for the 1W-NiMg catalyst and reaching 0.09 for 1M-NiMg sample. There was no detectable H_2 or CO produced at 6M-NiMg catalyst which correlates to the lack of reactant conversion.

Based on previous results on these catalyst systems [20, 98] and others using Ni supported on rare earth oxides [122, 123] in which a bifunctional mechanism (active support) has been proposed, the change in temperatures was comparable for both CH_4 and CO_2 conversion. This comparison suggested that silica adsorption was unselective to different surfaces. Furthermore, the addition of small amounts of silica in the 1W-Pt and 1W-NiMg samples indicated that the effect is more substantial, on a silica amount basis, at low poisoning. This non-linearity in conversion temperature with increased poisoning would be consistent with an initial monolayer formation occurring before multilayer formation. This speculation is consistent with findings [117] from examination of metal oxides for siloxane adsorption. From the N_2 physisorption and TPR results, the role of active site blocking seemed more prevalent than pore blockage. In other words, substantial activity loss occurred even though specific surface areas and total pore volumes increased with silica addition.

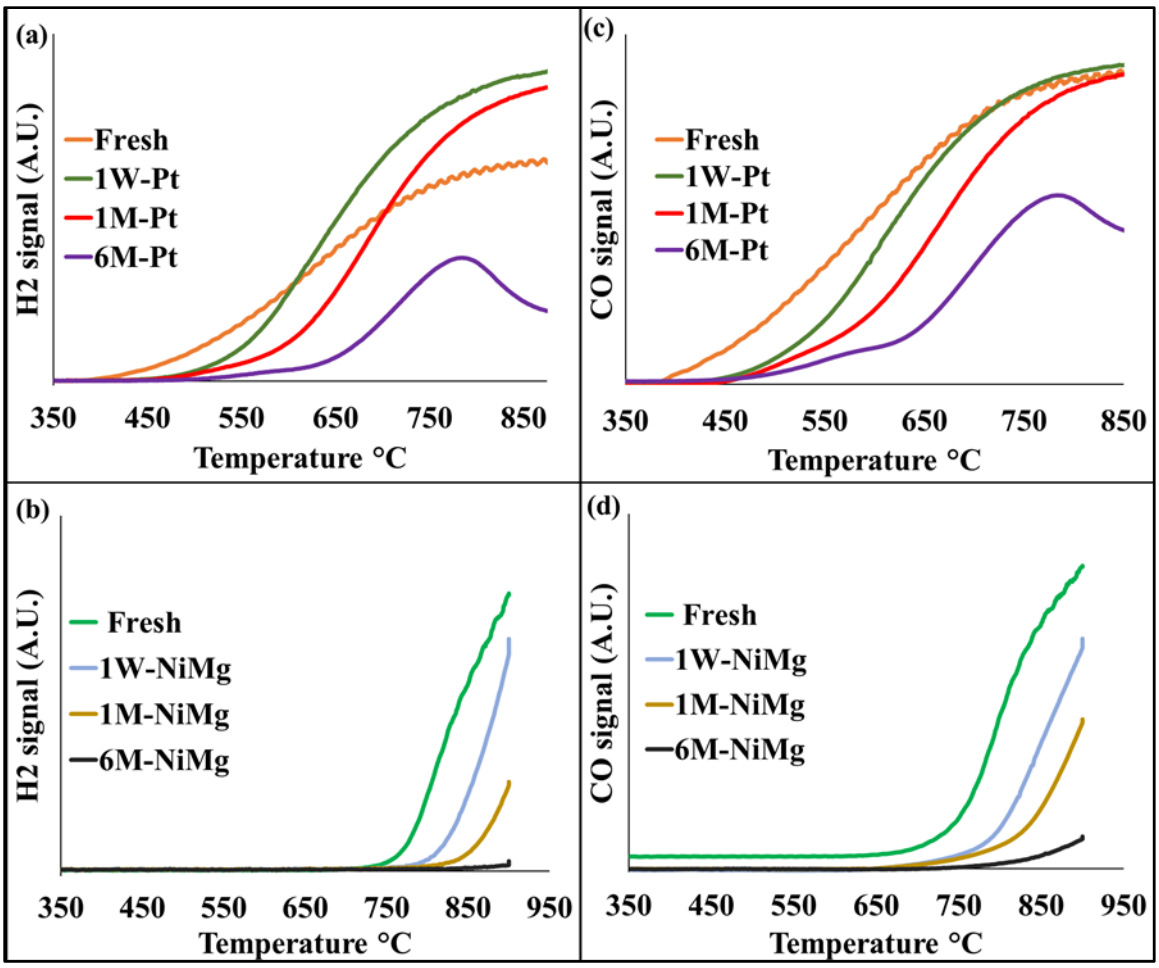

Figure 4.5: Hydrogen and carbon monoxide formation with respect to temperature. Formation over 0.16Pt catalyst (a/c). Formation over NiMg catalysts (b/d).

As presented in Figure 4.6, the NiMg catalyst calcined at 800 °C had a higher reduction temperature compared to its 600 °C-calcined catalyst counterpart. This comparison indicated that the catalyst calcined at higher temperature would be less active. Therefore, reaction data was determined to be unnecessary for the higher temperature calcined catalyst since the loss of activity was already high. Since the sample calcined at higher temperature had lower specific surface area and total pore volume than its counterpart calcined at low temperature, the role of pore blocking would likely increase since the amount of silicon was constant and the silica would likely become more crystalline.

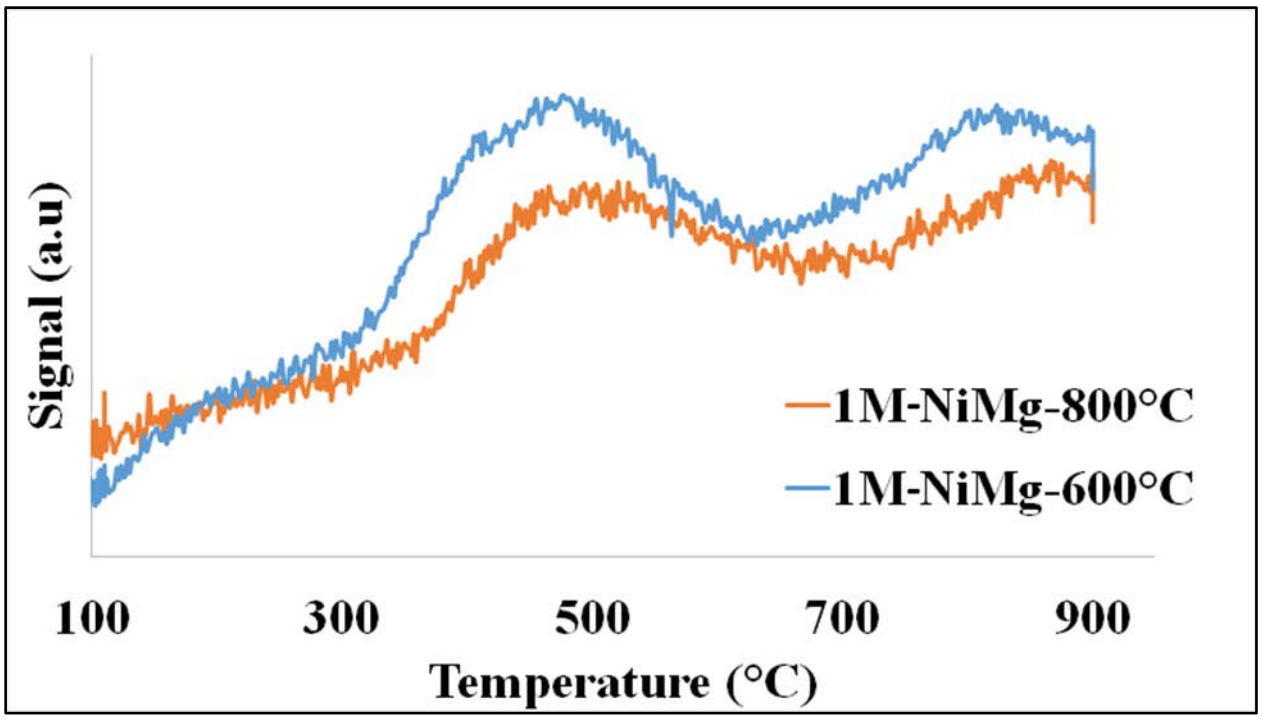

Figure 4.6: TPR profiles of 1M-NiMg catalysts at 600°C calcination and 800°C calcination.

If the siloxane decomposition could be controlled to decompose into a stable, porous (i.e., crystalline) silica phase initially rather, it may be possible to prevent substantial coverages of the active catalyst surface. That is, direct poisoning of the catalyst would not occur. To achieve size selectivity in reforming catalysis, this has been achieved by our group during the synthesis of zeolite coatings [124, 125]. However, even if the siloxane decomposition to silica resulted in a porous outer layer that did not cover the active catalyst surface, pressure issues and/or transport limitations over extended time-on-stream.

Finally, based on the strong poisoning effects of the 1W-Pt and 1W-NiMg samples, the results of this study suggested that at least ~ 96 % (1-1/26) of siloxanes would need to be removed prior to the reformer for a catalyst to achieve stable operation over 6 months. Based on the assumptions used in the base case for the calculations (see appendix B), the mass concentration of siloxanes would need to be lower than ~0.16 mg/m^3. Deeper purification may also be needed as

catalyst poisoning by siloxane decomposition appears irreversible. Advances for efficient and economical siloxanes removal techniques are thus required for biogas resources to contribute to future synthetic fuel production.

4.4 Summary and Conclusion

Silica addition has been demonstrated to have adverse impacts on reforming catalysts, which is typical scenario from the decomposition of siloxanes present in biogas. Both catalyst systems indicated decreases in methane and carbon dioxide conversions with increasing deposited silica amounts, with the effect becoming less prominent at increasing silica amounts as shown in Figure 4.7.

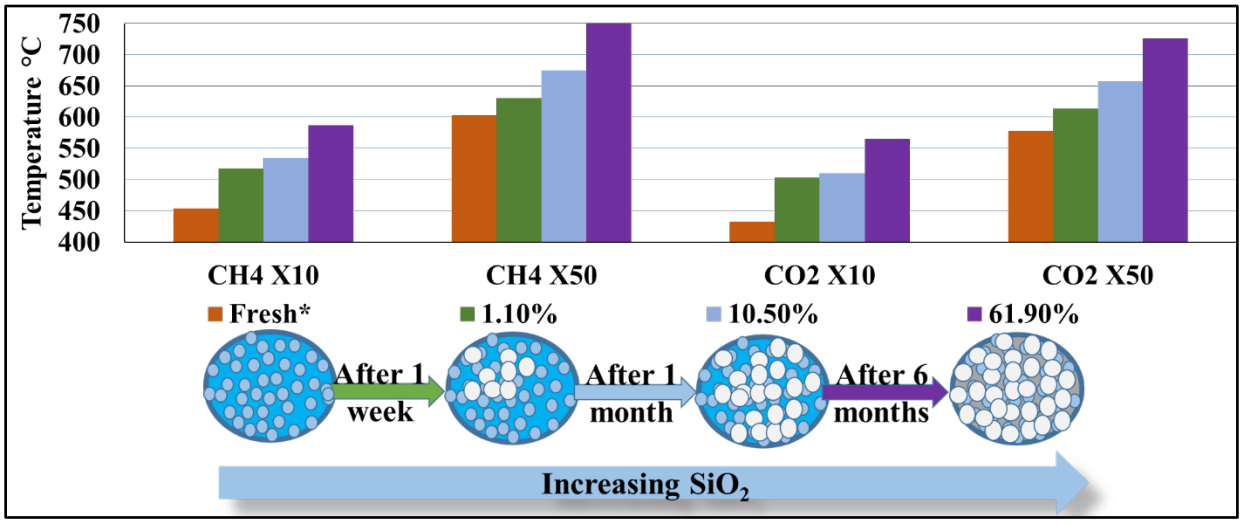

Figure 4.7: Effect of silica addition on CH_4 and CO_2 conversion.

This is in agreement with previous results that showed reduction temperature was a key indicator of activity [20], peak reduction peaks increased in correlation with the with increasing deposited silica amounts. Regardless of which catalyst system is selected, the results of this study have shown that siloxanes are harmful to the reforming catalysts' performances. The catalyst systems showed signs of deactivation even at low amounts of poisoning as shown. Therefore, it is

imperative that the biogas be scrubbed from siloxanes, as well as the sulfides, as their presence would result in catalysts having to be replaced more frequently.

CHAPTER 5: SYNGAS PRODUCTION AND REACTANT CONVERSION USING PT-NI-MG/CERIA-ZIRCONIA AND PD-NI-MG/CERIA-ZIRCONIA CATALYSTS AND EFFECT OF GHSV ON LOW TEMPERATURE BI-REFORMING OF MODEL BIOGAS[4]

5.1 Introduction

Growing energy demands coupled with the inevitable eventual depletion of the finite fossil fuels necessitate the need for alternative fuels. Biogas conversion to liquid hydrocarbon fuels is one promising alternative. Much of the biogas as well as natural gas produced through the petrochemical industry, enteric fermentation, municipal solid wastes and other processes is underutilized. Combusting the stranded natural gas can provide enough carbon dioxide and water to act as an oxidant for the endothermic reaction and is comparable to biogas. For instance, North Dakota in recent years, has increased oil production from Bakken formations by 40 fold to reach 1,130,000 bpd causing a surge in associated natural gas formation according to the EIA. However, more than 30% of that stranded gas equivalent to 375 million cu. ft/day ultimately gets flared and never reaches the market [126].

Biodegradable municipal waste dumped in landfills generate a type of biogas called landfill gas (LFG) that is composed mainly of methane and carbon dioxide. Biogas is produced by the anaerobic digestion of MSW or other biodegradable waste, which can be used as a future source

[4] This chapter is currently in review as part of a manuscript to a scientific journal.

of methane and carbon dioxide. Both methane and carbon dioxide are significant greenhouse gases. According to the EPA [15], 18% of methane anthropogenic emissions come from landfills. The EPA estimates that the US generates more than 250 million tons of municipal solid waste (MSW) per year which mostly go to landfills [10]. Biogas, the biodegradable component of MSW accounts for about 215 billion cu.ft.

Biogas, including landfill gas (LFG) has excellent potential to become a carbon-neutral energy source; presently, only 15% is utilized for energy. In addition, it can possibly reduce the potential emission of methane and carbon dioxide into the atmosphere. As a greenhouse gas, methane is 20 times more powerful at trapping heat than carbon dioxide which makes it considerably harmful to the atmosphere. Currently, LFG is flared, burned for electricity and the methane is condensed.

Methane reforming produces syngas, a mixture of hydrogen and carbon monoxide that can be further used as a feedstock for important industrial processes like methanol synthesis and Fischer Tropsch synthesis (FTS) to make long chain hydrocarbons such as diesel fuel. Reforming of methane is done several different ways including tri-reforming which utilizes carbon dioxide, steam and oxygen [1, 50, 127] shown as reactions (5.1-5.3).

$$CH_4 + CO_2 = 2CO + 2H_2 \qquad \Delta H° = 247.3\ {}^{kJ}/_{mol} \tag{5.1}$$

$$CH_4 + H_2O = CO + 3H_2 \qquad \Delta H° = 206.3\ {}^{kJ}/_{mol} \tag{5.2}$$

$$CH_4 + {}^{1}/_{2}\,O_2 = CO + 2H_2 \qquad \Delta H° = -35.6\ {}^{kJ}/_{mol} \tag{5.3}$$

Another method is dry reforming (DRM) shown in reaction (5.1) where only carbon dioxide and methane are in the feed, and finally there is also steam reforming of methane (SRM) described by reaction (5.2) where the feed consists of steam along with methane. Both DRM and

SRM have been extensively studied in recent years [3, 5, 18, 19, 21, 29, 41, 62, 63, 128]. Each of the mentioned reforming methods has advantages and disadvantages.

Tri-reforming has been shown to produce syngas ratios between 1.5-2.3 with high methane conversion rates of more than 90% on nickel catalysts as reported in the literature [1, 50, 129]. However, tri-reforming can be very costly on an industrial level since it requires addition of oxygen in the feed. Dry reforming of methane requires no added oxygen in the feed; however, this endothermic reaction readily occurs only at high temperatures (T>600°C) and requires an external source of heating [21]. Thermodynamically the reforming of methane is not possible below 350°C [7, 93]. Unfortunately, DRM also suffers from very low syngas ratios (≤1) making it inefficient for processes requiring higher H_2:CO ratios. Steam reforming of methane can produce syngas ratios of up to 3:1. However because steam needs to be added in the feed, the costs become very high and thus not feasible on an industrial scale especially for small to mid-sized plants. Previous studies in this group had focused on reducing the reforming temperature of methane for DRM using a nickel magnesium catalyst doped with platinum and/or palladium on a ceria zirconia oxide support [20, 98]. Although the reforming temperature for 10% conversion was brought down significantly (T=454°C), the syngas ratios were nowhere near stoichiometric with a maximum ratio of 0.41 for a 0.51wt% Pd-1.37wt%Ni 1.0wt%Mg/$Ce_{0.6}Zr_{0.4}$ catalyst [98]. The desire to improve the low syngas ratios previously obtained while maintaining low reforming temperatures served as the motivation behind this work. The combined dry and steam reforming processes (reactions 5.1 and 5.2) known as bi-reforming which is the focus of this study can reduce the cost making it more viable on a large scale as well as produce syngas at a ratio of 2:1 which is ideal for Fischer Tropsch Synthesis (FTS) and other industrial processes [7, 18, 50, 130]. Some catalysts that have been specifically investigated for bi-reforming included Ni doped onto $La_2Zr_2O_7$

pyrochlore [131], NiO/MgO and CoO/MgO [37, 132]. Nickel is a commonly used reforming catalyst because it is inexpensive and readily available. However nickel suffers from rapid deactivation and coke formation leading to several studies that added various precious metal dopants to circumvent these drawbacks associated with nickel-only catalysts by stabilizing the nickel and enhancing its activity [31, 42, 56].

The goal of this study is to compare the properties of two catalysts Pt or Pd doped Ni-Mg supported on ceria zirconia to obtain a syngas ratio close to 2:1 for low temperature ($T \leq 500°C$) bi-reforming of methane. It is known that steam reforming of methane produces more H_2 versus dry reforming of methane alone [29, 50, 128, 133]. Driving the reaction to lower temperatures opens avenues for intensification processes which can utilize solar energy through parabolic troughs [32, 134, 135]. Furthermore, complete conversion of methane is not required for electricity generation and doesn't require a particular syngas ratio [134].

However, at the desired lower temperatures, a challenge arises since reaction kinetics dominate over thermodynamics for DRM where RWGS reaction is more prevalent causing less H_2 production [128]. Determining the optimum amount of steam to improve the H_2:CO ratio while still allowing the DRM reaction to occur and maintaining a low operating temperature can be very challenging. Ideally, using lower steam to carbon ratios ($S/C<2.5$) allows for easier implementation on an industrial scale. The lower ratio reduces equipment size by decreasing overall mass flow [21]. For this study different feed compositions were tested as well as different gas hourly space velocities (GHSV) to optimize and determine the effect on syngas ratio if any.

5.2 Experimental

5.2.1 Materials and Synthesis

The support consisting of ceria-zirconia in a molar ratio of 0.6:0.4 was synthesized using the co-precipitation method described elsewhere in literature [67]. Each batch of support was synthesized by weighing 8.7 grams of the cerium precursor $Ce(NO_3)_3$ x $6H_2O$-(99.5% pure; Alfa Aesar) and 3.3 grams of zirconium precursor $ZrO(NO_3)_2$ x H_2O-(99.9% pure; Alfa Aesar). Both precursors were dissolved together in 150 mL of deionized water in a large beaker. Then, the precursor was precipitated using ammonium hydroxide (75 mL; 28% w/w NH_3; Sigma Aldrich) that was added to the beaker slowly until a clear liquid layer was visible on top of the beaker indicating complete precipitation. The mixture was then thoroughly stirred to completely dissolve and vacuum filtered until it was visibly dry. The filtrate was then re-dissolved in 0.25M NH_4OH solution and vacuum filtered a second time. The filtrate was dried in an oven at 60°C for 1 hr, then 120°C for 12 hr. Finally, the powder was calcined at 800ºC for 4 hr.

Incipient wetness impregnation was used to load the metals, nickel (1.37-1.39% by mass), magnesium (1.00% by mass), platinum (0.16% by mass), and palladium (0.13% by mass) onto the support. The nickel precursor $Ni(NO_3)_2$ x $6H_2O$ (99.9985% pure; Alfa Aesar), the magnesium precursor $Mg(NO_3)_2$ x H_2O (99.999% pure; Alfa Aesar), the platinum precursor H_2PtCl_6 x $6H_2O$ (≥37.5% metal basis, Sigma-Aldrich), and the palladium precursor $(NH_4)_2PdCl_6$ (99.99%, Sigma Aldrich) were all used to prepare the catalyst. The desired amount of metal precursors were dissolved in 2 mL of deionized water. The solution was then added drop wise onto the support until incipient wetness. The resulting wet powder was then dried in an oven for 2 hr at 120°C to remove any volatile components and evaporate the water. This process was repeated until all the

solution was successfully added. Immediately following the final drying, the powder was calcined at 600^{o}C for 3 hr.

5.2.2 Catalyst Characterization

The catalysts were extensively characterized using X-ray diffraction (XRD) to determine the crystal structure, temperature programmed reduction (TPR) to determine the reducibility of the catalyst, N_2 physisorption (BET) to obtain surface areas as well as pore volumes, and temperature programmed desorption studies (TPD-CO_2) for the catalysts' basicity and results were previously published [20, 98]. Temperature programmed oxidation (TPO) studies were done on post reaction on the long term study to combust any present surface coke that may have formed during the reaction.

For the XRD studies, a Bruker AXS diffractometer using a Cu Kα source at 40 kV and 40 mA was used. A (2θ) angular range of 20-80° was used to obtain the data. A step size of 0.02° with a 3 sec dwell time for each step was used.

A Cirrus MKS mass spectrometer (MS) was used for the TPR, TP-RXN, TPD-CO_2 to determine catalyst basicity and post reaction TPO studies. The desired amount of catalyst (37.7-150.6 mg) was loaded in u-tube microreactor and sandwiched between two layers of inert quartz wool on either side to hold it in place. The loaded reactor was then connected to MS in-line feed gases using ultratorr fittings. It was then placed in a Thermolyne tube furnace manufactured by Thermo scientific and more high temperature quartz wool was added to insulate the top of the furnace. The temperature of the furnace was controlled by a Eurotherm 3110 PID controller. Feed gases were controlled using Alicat Scientific mass flow controllers. For TPR studies, catalysts were pretreated under 50 sccm of helium (UHP, Airgas) for 30 min at 110°C. The Catalysts were then cooled to 50°C. Once the temperature stabilized, the gas flow was switched to 5% H_2/He (50

sccm). The sample was then heated at a ramp rate of 10°/min to 900°C and held for 30 min. Ionization factors were calculated using calibration curves prior to data analysis.

BET surface areas, BJH pore volumes and pore diameters were all obtained using a Quantachrome Autosorb-IQ. Each experiment was done using 50-55 mg of catalyst. Prior to analyzing, each sample was initially pretreated at 120°C for 2 hr to remove any moisture. The sample was then loaded in a small-bulb 6 mm quartz cell. Helium was used as the backfill gas for the sample which was then outgassed under vacuum for approximately 1 hr. The surface area values were obtained by fitting the data to a BET isotherm in the P/P_0 range of 0.05-0.33 using N_2. The pore volume is reported at P/P_0 of ~1.

Diffuse Reflectance Infrared Fourier Transform Spectroscopy (DRIFTS) was performed on the catalysts to probe the surface adsorbed species under different feed conditions and temperatures. A Nicolet IS50 spectrometer from Thermo Scientific equipped with a MCTA detector was used. The catalyst was loaded in a high pressure/ high temperature-resistant reactor cell from Harrick Scientific with two ZnSe windows and one quartz window. The gas inlet and outlet ports of the reactor cell were used to feed and drain the gases. The inlet lines were insulated and temperature controlled with heating tape. Argon (AIRGAS, AR-UHP300, 100%), carbon dioxide (AIRGAS UN1013, 99.999% purity) were used for the feed. A water bubbler attached to an Argon source was used for the water feed. The samples were loaded in the DRIFTS cell and initially activated under Ar flow (40 sccm) for 2 hrs, while heating the sample to 250 ^oC with a ramp rate of 2.5 ^oC/min. Once the sample was cooled down post activation, gases were flown as desired. Two different gas flow patterns were executed. In the first case (referred to as $CO_2 + H_2O$) CO_2 (8 sccm CO_2 with 25 sccm Ar) was initially flown for 10 minutes with subsequent flushing of the cell with Ar (40 sccm) for 30 minutes. Then H_2O was flown (through a water bubbler with

2.5 sccm Ar flown at 40°C) for 20 mins and subsequently flushed with Ar for 30 minutes. In the second case (referred as $H_2O + CO_2$), the feed was reversed with water being flown first, then Ar flushing followed by CO_2 flow and a second Ar flushing step. Once, CO_2 and H_2O have been flown for both of the cases, a temperature programmed desorption (TPD) experiment was conducted. Spectra were taken at 30 ^oC, 100 ^oC and 200 ^oC. All the TPD spectra were composed of 150 scans with a resolution of 2Å (0.241 cm^{-1}).

For the post reaction temperature programmed oxidation study (TPO), immediately following the long term reaction study, the catalyst was cooled under 50 sccm He until it reached room temperature. Then a 10% O_2 in He (50 sccm total flow) was introduced to the catalyst at a constant GHSV. Finally, the temperature was then increased to 900°C at a ramp rate of 10°C/min and held for 30 min.

5.2.3 Catalytic Testing

For the bi-reforming reaction experiments, the catalyst was reduced in 5%H_2 in He for 1 h. After the reduction step, the catalyst was cooled to 200°C in He flowing at 50 sccm. Bi-reforming reaction experiments were conducted at three different space velocities of 86,700 h^{-1}, 136,000 h^{-1} and 272,000 h^{-1} at atmospheric pressure. The reactants, methane, carbon dioxide (both 99.999% pure from Airgas) and water were then introduced in a 3:1:2 ratio, respectively (error $\leq$ 8%; total reactant concentration $\leq$ 1%) to the catalyst with a total flow rate of 100 sccm. A feed analysis was done prior to the start of the reaction, after the reactant flow was stable, the temperature was increased to 600°C using a 10°C/min ramp rate and held for a minimum of 20 min or until signals became very stable in the MS. The temperature was then decreased to 550°C and held for another 20 min. The process was repeated by decreasing the temperature in 50°C increments and holding for 20 min until 400°C.

5.3 Results and Discussion

5.3.1 Equilibrium Conversions

A simulation of equilibrium conversions at the operating conditions utilized experimentally was done using Aspen Plus V7.3 software. The feed ratio was 3:1:2 for CH_4:CO_2:H_2O respectively.

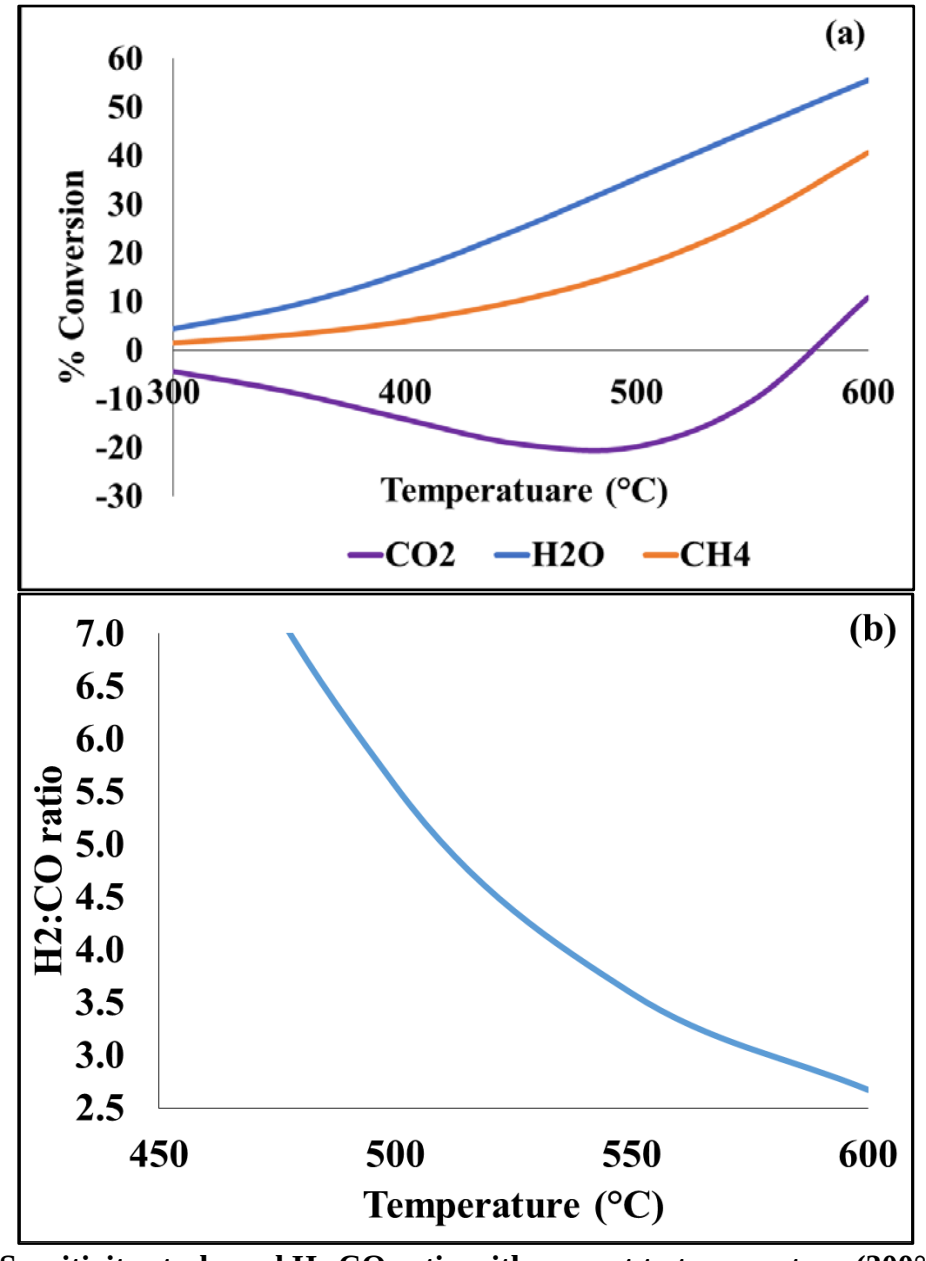

Figure 5.1: Sensitivity study and H_2:CO ratio with respect to temperature (300°C-600°C) at 1 atm using a feed composition in Kmol CH_4=3, CO_2=1 and H_2O=2. (a) Sensitivity study shows equilibrium conversion of reactants. (b) Syngas ratio.

The temperature was varied from 300-600°C in increments of 50° while maintaining a constant pressure of 1atm. The only allowable products were H_2, CO, CH_4, CO_2, H_2O. Figure 5.1(a) shows the conversion of the reactants while varying the temperature from 300°C to 600°C. Initially, only H_2O and CH_4 show positive conversion while CO_2 shows negative conversion below 500°C indicating the production of CO_2 as a result of the water-gas shift reaction which is simultaneously occurring with the reforming. At 500°C, the highest conversion possible for CH_4 was 16.9% reaching a maximum of 40.6% at 600°. On the other hand H_2O displayed a conversion of 35.3% at 500°C and reached 55.6% at a temperature of 600°C. CO_2 had a maximum positive conversion of 10.9% at 600°C as a result of its earlier production due to the water gas shift reaction. Syngas ratios are shown in Figure 5.1(b), from the simulation it was evident that very high syngas ratios were possible using the chosen feed composition. The ratios displayed the same trend observed experimentally (as shown in the next section) of decreasing with increasing temperatures as expected, at 500°C, the syngas ratio was 5.6 whereas it went down to 2.7 at a temperature of 600°C.

5.3.2 Experimental Results

Two catalysts 0.16%Pt-1.34 wt%Ni 1.0 wt%Mg/$Ce_{0.6}Zr_{0.4}$ and 0.13%Pt-1.39 wt%Ni 1.0 wt%Mg/$Ce_{0.6}Zr_{0.4}$ were synthesized and studied for bi-reforming of methane. Simplified notation that will be used from now on for each catalyst is included in Table 5.1. The catalysts were characterized using XRD, N_2-Physisorption, TPR, and TPD-CO_2. Steady-state bi-reforming experiments were done on the catalysts in the range of (600°C-400°C). A long term study was done on the most promising catalyst (0.16Pt). In addition, post reaction characterization (XRD, BET, TPO) was also done on the catalyst.

X-ray diffraction patterns for the Pd and Pt catalysts were reported in a previous study [98]. Both the diffraction pattern for 0.13Pd and 0.16Pt was consistent with a cubic fluorite structure characteristic of CeO_2. This is consistent with previously published studies of $CeZrO_2$ supports suggesting that the ZrO_2 in the support is incorporated into the CeO_2 crystal lattice [1, 39, 56]. It is important to also point out that the diffraction lines had characteristic asymmetric peaks indicating that several phases of the ceria zirconia solid solution may be present [73]. NiO and MgO peaks were visible at a 2θ between 42-44° for both the 0.13Pd and 0.16Pt. On the other hand, Pt and Pd diffraction lines were not visible as expected because of the very low content and high dispersion in the catalyst system consistent with previous literature [56, 72].

The reducibility of this catalyst system was previously studied through temperature-programmed reduction experiments [20, 98]. The results and peak reduction temperatures are summarized in Table 5.1. Overall, the Pd catalyst displayed a lower and more defined reduction temperature compared to Pt catalysts. Both reduction profiles had two distinct peaks, one at a lower temperature attributed to the weakly bound metals and surface cerium oxide and one at a higher temperature likely resulting from the strongly bound NiO and oxygen in bulk ceria [27, 68, 74, 94]. However regardless, it is important to point out that both the Pd and Pt catalyst reduced at much lower temperatures compared to the support alone. This is not surprising since it has been well documented in the literature that the reducibility of CeO_2 is favorably influenced by the addition of small amounts of metals [31, 47, 68, 76, 81]. In addition, specifically noble metals such as those used for this catalyst system have been shown to help ceria reduce to Ce^{3+} by creating oxygen vacancies[65] since noble metals have an affinity to dissociatively adsorb hydrogen thereby allowing hydrogen spillover [56, 77, 94, 95].

Table 5.1: Physiochemical properties.

Sample	Notation	S_{BET} (m^2/g)		Pore Volume (cc/g)		Pore Diameter (nm)		Amount CO_2-desorbed (µmole/g.cat) (Temp 70-550°C)	Peak Reduction Temperature (°C)
0.13%Pd-$Ce_{0.6}Zr_{0.4}O_2$-1.39Ni1.0Mg[a]	0.13Pd	28	30.8[b]	0.06		9.5		1.23	169
0.16%Pt-$Ce_{0.6}Zr_{0.4}O_2$-1.34Ni1.0Mg[b]	0.16Pt	31 *	17.0[c]	0.07 *	0.05[c]	11.6 *	7.2[c]	1.53	248 *
$Ce_{0.6}Zr_{0.4}O_2$[b]	CeZr	152*		0.35 *		14.1*		0.38	618

*Indicates the average of two experiments reported

[a] Data obtained from previous studies [98]

[b] Data obtained from previous studies [20]

[c] Post-reaction characterization from this study

Surface and bulk property changes of the catalyst system were examined by N_2-physisorption in a previous study [98]. The results are summarized in Table 5.1. In general, the surface areas as well as pore volumes decreased with the addition of metals consistent with previously reported results in the literature [1, 71, 72]. This is likely due to some pore blocking done by the metals.

In a previous study, temperature programmed desorption of carbon dioxide was utilized to determine catalyst basicity [98]. The results are reported in Table 5.1. The 0.13Pd catalyst was more basic as it had 2.91 μmole/g of CO_2 desorbed, whereas the 0.16Pt catalyst had only 1.53 μmole/g over the tested range. A more basic catalyst is desirable because of its ability to shift equilibrium concentrations resulting from CO disproportionation thereby reducing deposition of carbon [7].

Table 5.2: Comparison of steam reforming alone vs. dry reforming alone vs. bi-reforming reaction data at 500°C and 1 atm.

T=500°C	**0.16Pt**			**0.13Pd**		
	H_2:CO	**CH_4 Conv (%)**	**CO_2 Conv (%)**	**H_2:CO**	**CH_4 Conv (%)**	**CO_2 Conv (%)**
Dry Reforming	0.4	20	25	0.4	37	57
Steam Reforming 1:1-CH_4:H_2O	2.5	33	N/A	3.6	51	N/A
Bi-Reforming (1:1:1)	1.2	78	32	2.9	42	10
Bi-Reforming (3:1:2)	1.9	33	36	3.0	25	13

N/A: Not applicable because there was no CO_2 in the feed.

5.3.3 DRIFTS

Figure 5.2 (a and c) shows the DRIFTS spectra of 0.16Pt and 0.13Pd with H_2O flow followed by CO_2 flow respectively. Figure 5.2 (b and d) shows the spectra of the opposite case with CO_2 flown followed by H_2O flow for 0.16Pt and 0.13Pd respectively. Water and OH^- adsorption were visible through bands >3500cm^{-1}[136-138]. Hydroxyl group formation was the most common peak in all the samples at ~3695cm^{-1}[138]. Gas phase water molecules were also evident at ~3745cm^{-1} and an increase in concentration was evident with increasing temperature indicating that more water molecules are desorbing from the catalyst [138]. In all tested samples, carbonates (bridging, bidentate, monodentate, free and out of plane bending modes) as well as some formates (bidentate and bridging modes) were observed. Bidentate carbonates were seen through bands 1580 cm^{-1}, 1553 cm^{-1}, 1560 cm^{-1}, 1295 cm^{-1}, 1045 cm^{-1} consistent with literature [138] whereas monodentate carbonates were observed at 1538 cm^{-1}, 1460 cm^{-1}, 1390 cm^{-1}, 1060 cm^{-1}. Bridging carbonates were seen through bands 1130 cm^{-1}, 1220 cm^{-1}, 1730 cm^{-1}[136-138]. Bands 866 cm^{-1} and 857 cm^{-1} were also observed which indicated the presence of out of plane bending vibrations [139]. Free carbonates and chelating bidentate modes were seen at bands 1434cm^{-1} and 1656cm^{-1} respectively [136].

Both asymmetrical and symmetrical O-C-O stretching were observed through the presence of bands 1585 cm^{-1} and 1375 cm^{-1} respectively [140]. In addition, bidentate C-H stretching was observed at 2845cm^{-1} as well as bridging at 2950cm^{-1}[138]. The ceria-zirconia oxide support (CeZr) showed formation of both carbonates and formats during both cases (CO_2 followed by H_2O) and (H_2O followed by CO_2). Furthermore, peak ~3650cm^{-1} showed the presence of germinal hydroxyl ions over the ceria consisted with literature [138]. However formate peaks decreased for

the metal loaded samples (NiMg, 0.16Pt, 0.13Pd). No C-H vibrations were visible, only bands ~1585cm^{-1} which is often indicative of O-C-O vibrations for formats.

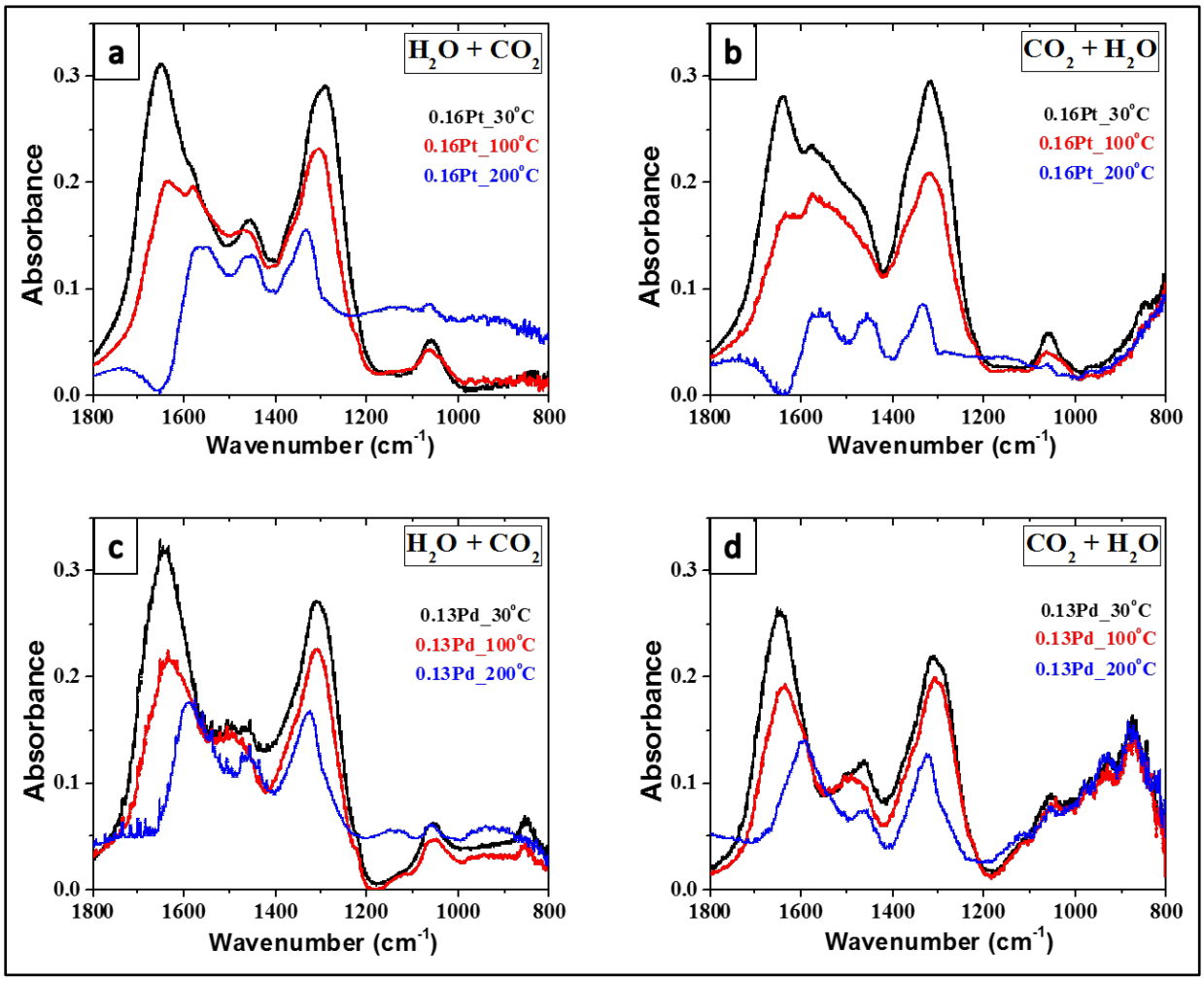

Figure 5.2: DRIFTS spectra of 0.16Pt and 0.13Pd catalysts. (a) 0.16Pt with H_2O then CO_2 flown, (b) 0.16Pt with CO_2 then H_2O flown, (c) 0.13Pd with H_2O then CO_2 flown, (d) 0.16Pt with CO_2 then H_2O flown

This lack of formate bands in the metal loaded catalysts can be attributed to a decrease in Ce-O and/or Zr-O sites where formats are typically formed, resulting from metal loading. This is also consistent with the decrease in surface area with metal loading observed through N_2-physisorption. It is important to note that both 0.16Pt and 0.13Pd samples had prominent carbonate bands. However, the 0.13Pd sample showed stronger carbonate adsorption indicating that CO_2

adsorbs stronger onto the 0.13Pd catalyst compare to the 0.16Pt catalyst. This is consistent with previous TPD-CO_2 studies on this catalyst system which showed more CO_2 desorption on the 0.13Pd catalyst compared to the 0.16Pt catalyst [98].

5.3.4 Steady-State Reaction Studies (600-400°C)

Syngas production as a function of temperature from the steady state studies are presented in Figure 3. In general, both the 0.13Pd and 0.16Pt had a decrease in syngas ratio with increasing temperature regardless of GHSV used. On the other hand, the 0.16Pt catalyst displayed overall higher syngas ratios compared to the 0.13Pd catalyst under the highest and lowest GHSV used. In general 0.16Pt catalyst had much higher reactant conversions compared to the 0.13Pd catalyst. At 500°C, 0.16Pt catalyst had CH_4 conversions of 39%, 33% and 14% at 86,700h^{-1}, 136,000h^{-1}, 272,000h^{-1} respectively. However, 0.13Pd catalyst had 40%, 25% and 8% at 86,700h^{-1}, 136,000h^{-1}, 272,000h^{-1} respectively. Activation energy calculated for CH_4 was 11 Kcal/mol for 0.16Pt catalyst and 11.5 Kcal/mol for 0.13Pd catalyst which are comparable to literature values for tri-reforming and water gas shift using similar catalyst systems [50, 141].

It is important to note that most of the carbon was accounted for by doing a carbon balance on the system at the various temperatures. At the desired 500°C with a GHSV of 272,000h^{-1}, 98% of the carbon was accounted for in the 0.16Pt catalyst; whereas 100% of the carbon was accounted for in the 0.13Pd catalyst. At a GHSV of 136,000h^{-1} and a temperature of 500°C, 93% of the carbon was present in the 0.13Pd catalyst compared to 91% in the 0.16Pt catalyst.

The syngas ratios for both 0.16Pt and 0.13Pd catalysts are shown in Figure 5.3 (a) and (b) respectively. Both catalysts had lower syngas ratios with increasing temperature. However, 0.16Pt catalyst had syngas ratios closer to the desired 2:1 ratio at 500°C. The highest syngas ratio was 9.13 at 450°C at a GHSV of 272,000h^{-1} for 0.16Pt sample and 9.63 at a GHSV of 136,000h^{-1} for

the 0.13Pd catalyst. This is a result of the water-gas shift reaction simultaneously occurring along with the bi-reforming reaction at that temperature.

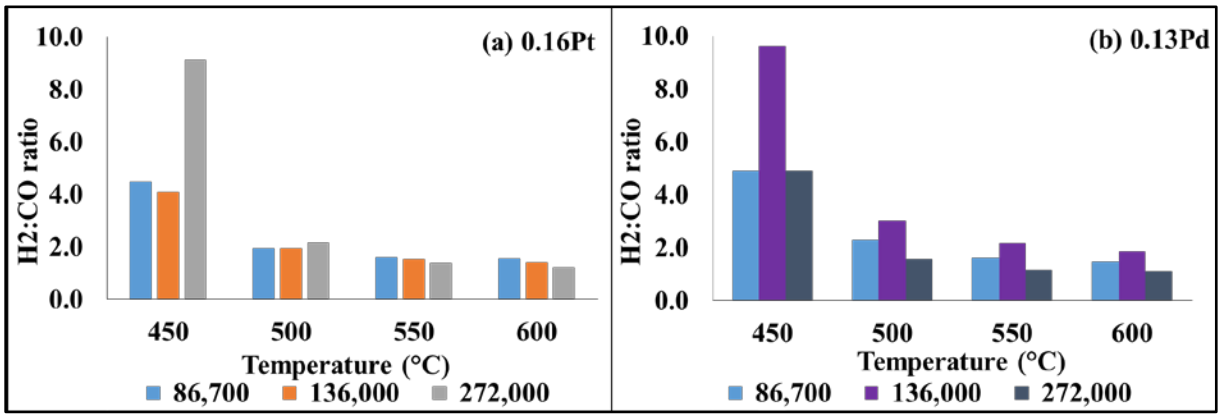

Figure 5.3: H_2:CO ratio with respect to temperature at different GHSV (h^{-1}). (a) H_2:CO ratio of 0.16Pt catalyst, (b) H_2:CO ratio of 0.13Pd catalyst.

At 500°C, the 0.16Pt catalyst had syngas ratios of 1.94, 1.95 and 2.16 for GHSV's of 86,700h^{-1}, 136,000h^{-1}, 272,000h^{-1} respectively. On the other hand, the 0.13Pd catalyst had syngas ratios of 2.29, 3.02 and 1.57 for GHSV's of 86,700h^{-1}, 136,000h^{-1}, 272,000h^{-1} respectively at 500°C. The varying trend in syngas ratio in the 0.13Pd catalyst can be attributed to Pd adsorbing CO_2 more strongly than Pt. This is also consistent with DRIFTS results where more pronounced carbonate peaks were visible on the 0.13Pd catalyst compared to the 0.16Pt catalyst. Previous temperature-programmed desorption of CO_2 studies (TPD-CO_2) done by this group have also shown the 0.13Pd catalyst having more CO_2 desorbed compared to the 0.16Pt catalyst [98]. Nonetheless, the lowest syngas ratio was at 600°C at the highest GHSV of 272,000h^{-1} for both catalysts where 0.16Pt had a ratio of 1.22 and 0.13Pd had a ratio of 1.10.

Conversion of methane at the different GHSV's with respect to temperature is shown in Figure 5.4 for both 0.16Pt and 0.13Pd. Methane conversion increased with increasing temperature as expected and generally decreased with increasing space velocity. The highest conversion of methane was 62% at a GHSV of 86,700h^{-1} for the 0.16Pt catalyst at 600°C. Meanwhile the

conversion of methane reached a maximum of only 59% for the 0.13Pd catalyst at the same GHSV and temperature.

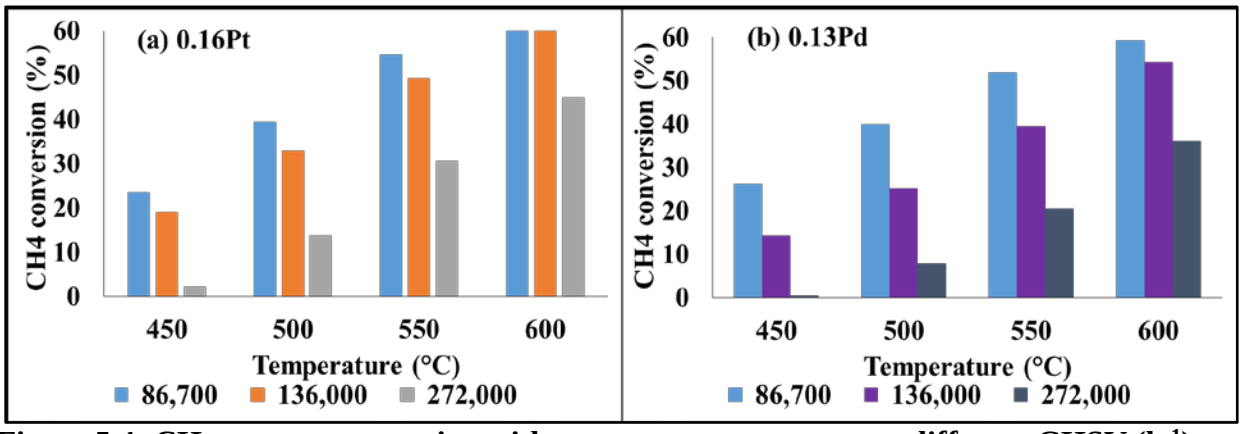

Figure 5.4: CH_4 percent conversion with respect to temperature at different GHSV (h^{-1}). (a) CH_4 percent conversion of 0.16Pt catalyst, (b) CH_4 percent conversion of 0.13Pd catalyst.

At 500°C and a GHSV of 136,000h^{-1}, 0.16Pt had a CH_4 conversion of 33% compared to the 0.13Pd catalyst's 25% conversion under the same conditions. Conversions of CO_2 are shown in Figure 5.5. Overall, CO_2 had higher conversions with increasing temperatures as expected since the water-gas shift reaction where CO_2 can be produced favors lower temperatures (T<500°C). Similarly increasing the GHSV decreased the conversion of CO_2. Conversion of CO_2 was 36% at a GHSV of 136,000h^{-1} for the 0.16Pt catalyst at 500°C, whereas for the 0.13Pd catalyst, the CO_2 conversion was only 13% at the same GHSV and temperature consistent with the higher syngas ratio under those conditions. The maximum CO_2 conversion was 97% for the 0.16Pt catalyst at a GHSV of 86,700h^{-1} compared to 96% for the 0.13Pd catalyst. At 500°C and GHSV of 272,000h^{-1}, the conversion of CO_2 was 11% and 16% for the 0.16Pt and 0.13Pd catalysts respectively.

5.3.5 Conditions (Feed Composition) Effect of Feed

Different bi-reforming feed compositions were tested on both 0.16Pt and 0.13Pd catalysts and compared to both dry reforming as well as steam reforming results. A summary of the results

are shown in Table 5.2. Dry reforming alone had very low syngas ratios of only 0.41 for 0.16Pt catalyst and 0.44 for the 0.13Pd catalyst at 500°C. Steam reforming had higher syngas ratios when the reactant feed was 1:1 for CH_4:H_2O. The syngas ratio was higher for 0.13Pd at 3.55 compared to 2.51 for 0.16Pt for steam reforming alone. Two different feed compositions were tested for bi-reforming. The first composition was 1:1:1 for CH_4:CO_2:H_2O which yielded a syngas ratio of 1.24 for 0.16Pt and 2.87 for 0.13Pd. Methane conversion was 78% for 0.16Pt compared to only 42% for 0.13Pd. Adjusting the feed to 3:1:2 for CH_4:CO_2:H_2O, the syngas ratio increased to 1.94 for 0.16Pt with a CH_4 conversion of 33% and 3.02 for 0.13Pd with a lower conversion of 25% for CH_4.

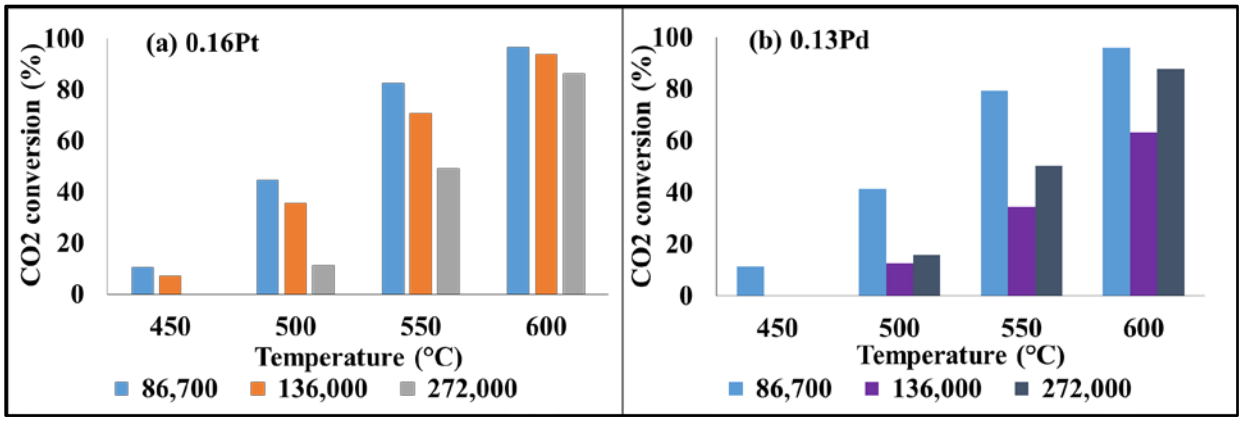

Figure 5.5: CO_2 percent conversion with respect to temperature at different GHSV (h^{-1}). (a) CO_2 percent conversion of 0.16Pt catalyst, (b) CO_2 percent conversion of 0.13Pd catalyst.

5.3.6 Time on Stream Study

A steady state experiment was done on the 0.16Pt catalyst using a GHSV of 136,000h^{-1} at a constant temperature and pressure of 500°C and 1atm, respectively. The feed ratio was 3:1:2 for CH_4:CO_2:H_2O respectively. The catalyst was left on-stream for 3 hours. Figure 5.6 shows the conversion of the reactants with time on stream. Conversion did not decrease with time on stream for any of the reactants indicating that the catalyst remained active even with extended time on stream. Conversions of CH_4 and CO_2 were constant at 37% and 33% respectively.

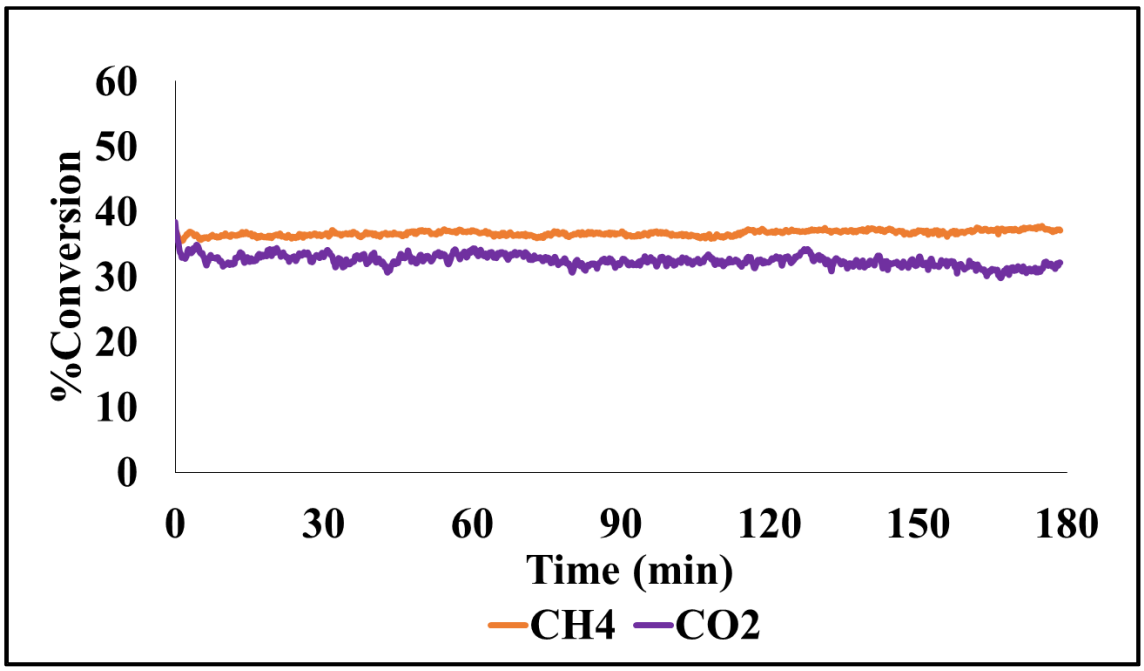

Figure 5.6: Time-on-stream study of 0.16Pt sample at T=500°C and P= 1 atm. Figure shows reactant % conversion with respect to time on stream.

A post reaction temperature programmed oxidation study was done by flowing 10% oxygen in the carrier gas and ramping the temperature to 900°C. No surface coke was visible indicating that the catalyst did not deactivate. Post reaction XRD was also done and no diffraction lines shifts were observed in comparison to the fresh catalyst. Post reaction BET showed minor decreases in surface area, pore volume and pore diameter as reported in Table 5.1.

5.4 Conclusion

This study compared the activity of a Pt and Pd doped Ni/Mg catalyst supported on ceria zirconia oxide for low temperature bi-reforming of methane while maintaining a syngas ratio of 2:1. The optimum feed composition used was 3:1:2 for CH_4:CO_2:H_2O respectively. Three different GHSV were tested to study the effect on conversion and syngas ratio if any. At the lowest GHSV of 86,700h^{-1}, 0.16Pt catalyst produced a H_2:CO ratio of 1.95 with a methane conversion of 39% and carbon dioxide conversion of 45% at 500°C. On the other hand, 0.13Pd had a higher syngas ratio of 2.29 under the same conditions as well as comparable conversions of 40% and 41% for

methane and carbon dioxide respectively. Alternatively at 136,000h^{-1}, 0.16Pt catalyst maintained a syngas ratio of 1.94 with a methane conversion of 33% along with a carbon dioxide conversion of 36%. However 0.13Pd had much lower reactant conversions of 25% for methane and 13% for carbon dioxide although the syngas ratio was higher at 3.02. This is likely a result of the lower dispersion of Pd compared to Pt. At the highest tested GHSV of 272,000h^{-1}, 0.16Pt catalyst produced a syngas ratio of 2.16 with a conversion of 14% for CH_4 and 11% for CO_2. Conversely, at a GHSV of 272,000h^{-1}, 0.13Pd had a syngas ratio of only 1.57 with 8% conversion for CH_4 and 16% conversion for CO_2. DRIFTS spectra suggested that 0.13Pd had higher carbonate adsorption compared to the 0.16Pt catalyst which is consisted with the higher syngas ratios observed over the same catalyst. Overall, 0.16Pt is the optimum catalyst for this study because it had a consistent syngas ratio closer to 2:1 at the desired 500°C temperature compared to 0.13Pd which had syngas ratios that varied from 1.57-3.02 at the different GHSV tested. In addition, 0.16Pt catalyst generally had consistently more desirable higher methane conversions.

CHAPTER 6: CONCLUSIONS AND FUTURE WORK

6.1 Conclusions

This study focused on synthesizing and testing low temperature (T<500°C) reforming of methane catalysts comprised of (0.07-0.64 wt%) Pt and (0.13-0.51 wt%) Pd doped 1.34wt%Ni-1.00wt%Mg on a ceria-zirconia oxide $(Ce_{0.6}Zr_{0.4})O_2$ support. Both dry and bi-reforming of methane were studied over the synthesized catalysts in order to determine the optimum catalyst and conditions for the desired syngas ratio (~2:1). For landfill gas (LFG) applications, the effect of siloxane decomposition to silica was studied over the reforming catalysts using three different amounts (1 week, 1 month and 6 month) to determine the extent of damage to the catalyst.

Different loadings of Pt or Pd were studied to determine the optimum catalyst that would convert at least 10% (X_{10}) of the reactants at temperatures at or lower than 500°C while resisting coking. Initial temperature programmed reduction studies showed that the 0.16wt%Pt-1.34wt%Ni-1.00wt%Mg/$Ce_{0.6}Zr_{0.4}O_2$ catalyst (0.16Pt) had the lowest reduction temperature of 248°C compared to other Pt doped catalysts. In addition, it had one of the highest amounts of CO_2 desorbed at 1.30 μmol/g.cat indicating that it is more basic than other catalysts leading to higher activity. Furthermore, dry reforming reaction results showed that the 0.16Pt catalyst had the lowest CH_4 as well as CO_2 X_{10} conversion temperatures of 454°C and 432°C respectively. This catalyst system was also shown to be very stable when left on stream for more than 100 hours (dry reforming).

A series of Pd doped catalysts were synthesized and also tested for methane reforming to determine which noble metal, Pt or Pd, had superior activity for methane reforming. It was determined that 0.13wt% Pd-1.34wt%Ni-1.00wt%Mg/$Ce_{0.6}Zr_{0.4}O_2$ catalyst (0.13Pd) was the more desirable catalyst in the Pd series. It had a reduction temperature of 169°C with 1.23 µmol/g.cat of CO_2 desorbed. Furthermore, 10% CH_4 conversion was achieved at 383°C while 10% CO_2 conversion occurred at 366°C over this catalyst. At 450°C, the turnover frequency was determined to be $3.37s^{-1}$ compared to $3.50s^{-1}$ for the 0.16Pt catalyst. In addition, the calculated rate was equivalent to $1.49*10^{-2}$ mol/hr/g.cat for the 0.13Pd catalyst compared to $1.73*10^{-2}$ mol/hr/g.cat for the 0.16Pt catalyst.

For biomass derived landfill gas (LFG) applications, the effect of siloxanes on the reforming catalyst was determined using accelerated poisoning studies. Three different poisoning amounts equivalent to deposition from 1 week (1W), 1 month (1M) and 6 month (6M) of continuous LFG flow over the low temperature catalyst (0.16Pt) as well as high temperature catalyst (NiMg) were tested. It was shown that even minimal exposure amount had adverse effects on both catalysts, where 1 week (1W Pt) of poisoning decreased the reforming temperature from 454°C to 518°C for CH_4 X_{10} using 0.16Pt catalyst. The unfavorable trend continued with the X_{10} temperature increasing to 535°C at 1M Pt until reaching a maximum of 587°C for 6M Pt. Similarly for the high temperature reforming NiMg catalyst, at 1 week (1W NiMg) the CH_4 X_{10} increased from 762°C to 810°C and reached 842°C at 1M NiMg whereas there was no conversion of methane detected at 6M for this catalyst up to the maximum tested temperature of 900°C. These results confirmed that siloxanes adversely affect the reforming catalyst and the LFG would require cleanup prior to processing.

Dry reforming studies have shown that both 0.16Pt and 0.13Pd catalysts are capable of reforming methane at temperatures less than 500°C with comparable turnover frequencies and rates. However, the produced syngas ratios were nowhere near the desired ratio of 2:1 with the 0.13Pd catalyst having a syngas ratio of 0.39 compared to 0.16Pt catalyst's 0.30 at 450°C. This is attributed to the reverse water gas shift (rWGS) reaction simultaneously occurring with the reforming reaction at the low operating temperature used. Addition of steam to the feed (bi-reforming) was utilized to improve the H_2:CO ratio. Bi-reforming studies have shown that using a 3:1:2 CH_4:CO_2:H_2O improved the syngas ratio to 1.94 for 0.16Pt catalyst which is very close to the desired 2:1 ratio. However the ratio increased to an undesirable high of 3.02 for 0.13Pd catalyst. Conversion of methane also increased to 33% for the 0.16Pt catalyst and 25% for the 0.13Pd catalyst at 500°C.

6.2 Future Work

6.2.1 Gas Cleanup and Cost Analysis

The future direction of this work should include two main components. The first is to focus on finding an effective scrubbing and cleanup process for the LFG that is inexpensive as well as efficient. The tolerable limits of the process equipment are known and published by the manufacturers. However, limits for minimal catalyst deactivation are still underdeveloped. Therefore, a maximum amount of siloxane removal should be considered in order to minimize catalyst deactivation and increase its lifetime. Removal technologies that can be further developed include adsorption which consists of both a regenerative and non-regenerative type. Adsorption is typically done using either fixed or fluidized adsorption bed [34]. The second type of removal technology is through absorption, which can either be chemical or physical. Finally, contaminants can also be removed via a deep chilling and condensation process [34]. Each of these processes

has both advantages and limitations and should be further evaluated for cost, efficiency and economic feasibility.

6.2.2 FTS Catalyst Components Suitable for Combined Process

The second main area to focus on is combining the reforming catalyst with an FTS catalyst through process intensification. FTS can be operated at low temperatures (LTFT, T<300°C) using cobalt catalysts or high temperatures (HTFT, T>300°C) using iron catalysts on a variety of supports. Low temperature FT is often more selective towards longer hydrocarbons and waxes which need to be further refined into fuel products [142], whereas high temperature FTS is more selective towards lower hydrocarbon chains such as olefins and gasoline [143].

This goal should focus on synthesizing and testing an Fe-based FTS catalyst that is capable of operating at high temperatures (FTHT). In addition, to incorporate both catalysts (the low temperature reforming and FTS) in a single step though a physical mixture and determine effect on activity, selectivity and conversion. The key issue will be to determine the optimal reaction temperature for highest hydrocarbon selectivity.

Previous studies have looked at both cobalt and iron based catalysts for FTS [144-149]. Both metals offer different advantages and disadvantages. For the purposes of this project, an iron-based catalyst is likely the more attractive choice. Iron is readily available, economically feasible and is already used on an industrial level. More importantly, iron catalysts can operate at a wider, higher temperature range which is desirable for the single step component of this project. This is especially useful for the combined process with the dry/steam reforming step which operates at temperatures on the higher end of those for FTS. In addition, iron catalysts are more resistant to oxidation with water under FTS conditions [150] and are less selective towards methane [144].

Finally, iron catalysts are more resistant to sulfur and ammonia present in syngas than Co catalyst; biomass-derived syngas has more sulfur content [147, 150].

REFERENCES

[1] D.M. Walker, S.L. Pettit, J.T. Wolan, J.N. Kuhn, Applied Catalysis A: General 445–446 (2012) 61-68.

[2] M.C.J. Bradford, M.A. Vannice, Applied Catalysis A: General 142 (1996) 73-96.

[3] A.A. Lemonidou, I.A. Vasalos, Applied Catalysis A: General 228 (2002) 227-235.

[4] C. Courson, L. Udron, D. Świerczyński, C. Petit, A. Kiennemann, Catalysis Today 76 (2002) 75-86.

[5] C. Courson, E. Makaga, C. Petit, A. Kiennemann, Catalysis Today 63 (2000) 427-437.

[6] J. Guo, H. Lou, H. Zhao, D. Chai, X. Zheng, Applied Catalysis A: General 273 (2004) 75-82.

[7] M. Bradford, M. Vannice, Catalysis Reviews 41 (1999) 1-42.

[8] International Energy Outlook, EIA, 2014.

[9] C.E. Behrens, C. Glover, G. Whitney, Congressional Research Service 30 (2010).

[10] EPA, http://www.epa.gov/lmop/publications-tools/handbook.html, 2011, Landfill Methane Outreach Program.

[11] National Renewable Energy Laboratory (NREL), http://www.nrel.gov/learning/re_biomass.html, 2014, 8/11/2015, Biomass.

[12] I.E. Agency, http://www.iea.org/publications/freepublications/publication/KeyWorld2016.pdf, 2016, Key world energy statistics.

[13] EPA, https://www.epa.gov/ghgemissions/overview-greenhouse-gases#methane, 2016, Methane Emissions.

[14] EPA, https://www.epa.gov/lmop/accomplishments-landfill-methane-outreach-program, 2016, Accomplishments of the Landfill Methane Outreach Program.

[15] EPA, http://www.epa.gov/climatechange/ghgemissions/gases/ch4.html, 2010, 07 July 2014, Methane Emissions.

[16] LFG Energy Project Development Handbook, Environmental Protection Agency, 2014, pp. 1-16.

[17] NaturalGas.Org, http://naturalgas.org/overview/uses-electrical/, 2013, Electrical Uses.

[18] S. Damyanova, B. Pawelec, K. Arishtirova, M.V.M. Huerta, J.L.G. Fierro, Applied Catalysis B: Environmental 89 (2009) 149-159.

[19] S. Zhang, S. Muratsugu, N. Ishiguro, M. Tada, ACS Catalysis 3 (2013) 1855-1864.

[20] N.H. Elsayed, N.R.M. Roberts, B. Joseph, J.N. Kuhn, Applied Catalysis B: Environmental 179 (2015) 213-219.

[21] J.R. Rostrup-Nielsen, J. Sehested, J.K. Nørskov, Adv. Catal. 47 (2002) 65-139.

[22] D. Pakhare, J. Spivey, Chemical Society Reviews 43 (2014) 7813-7837.

[23] M.E. Dry, in: S. André, D. Mark (Eds.), Fischer-Tropsch Technology: Studies in Surface Science and Catalysis, Elsevier, USA, 2004, pp. 196-257.

[24] M.E. Dry, Catalysis today 71 (2002) 227-241.

[25] J.R. Rostrup-Nielsen, Catalysis Today 63 (2000) 159-164.

[26] P.M. Mortensen, I. Dybkjær, Applied Catalysis A: General 495 (2015) 141-151.

[27] W.-S. Dong, H.-S. Roh, K.-W. Jun, S.-E. Park, Y.-S. Oh, Applied Catalysis A: General 226 (2002) 63-72.

[28] N.A.S. Amin, T.C. Yaw, International Journal of Hydrogen Energy 32 (2007) 1789-1798.

[29] K. Nakagawa, K. Anzai, N. Matsui, N. Ikenaga, T. Suzuki, Y. Teng, T. Kobayashi, M. Haruta, Catal Lett 51 (1998) 163-167.

[30] G. Valderrama, C. Urbina de Navarro, M.R. Goldwasser, Journal of Power Sources 234 (2013) 31-37.

[31] P. Kumar, Y. Sun, R.O. Idem, Energy & Fuels 21 (2007) 3113-3123.

[32] D.S. Simakov, H.Y. Luo, Y. Román-Leshkov, Applied Catalysis B: Environmental (2015).

[33] E.A. McBean, Canadian Journal of Civil Engineering 35 (2008) 431-436.

[34] M. Ajhar, M. Travesset, S. Yüce, T. Melin, Bioresource Technology 101 (2010) 2913-2923.

[35] R. Dewil, L. Appels, J. Baeyens, Energy Conversion and Management 47 (2006) 1711-1722.

[36] Z. Zhang, X.E. Verykios, Applied Catalysis A: General 138 (1996) 109-133.

[37] G.A. Olah, A. Goeppert, M. Czaun, G.K.S. Prakash, Journal of the American Chemical Society 135 (2013) 648-650.

[38] M. Rezaei, S.M. Alavi, S. Sahebdelfar, Z.-F. Yan, Journal of Natural Gas Chemistry 15 (2006) 327-334.

[39] H.-S. Roh, K.-W. Jun, W.-S. Dong, J.-S. Chang, S.-E. Park, Y.-I. Joe, Journal of Molecular Catalysis A: Chemical 181 (2002) 137-142.

[40] Z. Zhang, X.E. Verykios, J. Chem. Soc., Chem. Commun. (1995,) 71-72.

[41] N. Laosiripojana, S. Assabumrungrat, Applied Catalysis A: General 290 (2005) 200-211.

[42] J.A.C. Ruiz, F.B. Passos, J.M.C. Bueno, E.F. Souza-Aguiar, L.V. Mattos, F.B. Noronha, Applied Catalysis A: General 334 (2008) 259-267.

[43] G. Vlaic, P. Fornasiero, S. Geremia, J. Kašpar, M. Graziani, Journal of Catalysis 168 (1997) 386-392.

[44] G. Balducci, J. Kašpar, P. Fornasiero, M. Graziani, M.S. Islam, The Journal of Physical Chemistry B 102 (1998) 557-561.

[45] D. Goodman, R. Kelley, T. Madey, J. Yates, Journal of Catalysis 63 (1980) 226-234.

[46] T. Minowa, F. Zhen, T. Ogi, The Journal of Supercritical Fluids 13 (1998) 253-259.

[47] W.-S. Dong, K.-W. Jun, H.-S. Roh, Z.-W. Liu, S.-E. Park, Catal Lett 78 (2002) 215-222.

[48] X.E. Verykios, International Journal of Hydrogen Energy 28 (2003) 1045-1063.

[49] S. Wang, G. Lu, Industrial & Engineering Chemistry Research 38 (1999) 2615-2625.

[50] C. Song, W. Pan, Catalysis Today 98 (2004) 463-484.

[51] M.M. Yung, S. Cheah, K. Magrini-Bair, J.N. Kuhn, ACS Catalysis 2 (2012) 1363-1367.

[52] V.V. Chesnokov, V.I. Zaikovskii, R.A. Buyanov, V.V. Molchanov, L.M. Plyasova, Catalysis Today 24 (1995) 265-267.

[53] C. Crisafulli, S. Scirè, R. Maggiore, S. Minicò, S. Galvagno, Catal Lett 59 (1999) 21-26.

[54] B. Steinhauer, M.R. Kasireddy, J. Radnik, A. Martin, Applied Catalysis A: General 366 (2009) 333-341.

[55] J. Chen, C. Yao, Y. Zhao, P. Jia, International Journal of Hydrogen Energy 35 (2010) 1630-1642.

[56] S.C. Dantas, J.C. Escritori, R.R. Soares, C.E. Hori, Chemical Engineering Journal 156 (2010) 380-387.

[57] D.P. Chynoweth, J.M. Owens, R. Legrand, Renewable Energy 22 (2001) 1-8.

[58] N. Altawell, LinkedIn slidshare, http://www.slideshare.net/Altawell/combustible-gas-from-gasification-anaerobic-digestion-and-pyrolysis, 2011, 11/03/2016.

[59] Z. Abedeen, LinkedIn Slideshare, http://www.slideshare.net/zakiabedeen/anaerobic-aerobic-digestion, 2010, 11/03, Anaerobic Aerobic Digestion.

[60] M. Ni, D.Y.C. Leung, M.K.H. Leung, K. Sumathy, Fuel Processing Technology 87 (2006) 461-472.

[61] A.V. Bridgwater, D. Meier, D. Radlein, Organic Geochemistry 30 (1999) 1479-1493.

[62] D. Baudouin, J.-P. Candy, U. Rodemerck, F. Krumeich, L. Veyre, P.B. Webb, C. Thieuleux, C. Copéret, Catalysis Today 235 (2014) 237-244.

[63] A. Yamaguchi, E. Iglesia, Journal of Catalysis 274 (2010) 52-63.

[64] S.M. Stagg-Williams, F.B. Noronha, G. Fendley, D.E. Resasco, Journal of Catalysis 194 (2000) 240-249.

[65] Q. Yu, W. Chen, Y. Li, M. Jin, Z. Suo, Catalysis Today 158 (2010) 324-328.

[66] G. Kim, D.-S. Cho, K.-H. Kim, J.-H. Kim, Catal Lett 28 (1994) 41-52.

[67] S. Rossignol, F. Gérard, D. Duprez, Journal of Materials Chemistry 9 (1999) 1615-1620.

[68] J.C. Escritori, S.C. Dantas, R.R. Soares, C.E. Hori, Catalysis Communications 10 (2009) 1090-1094.

[69] S. Pengpanich, V. Meeyoo, T. Rirksomboon, K. Bunyakiat, Applied Catalysis A: General 234 (2002) 221-233.

[70] C.E. Hori, H. Permana, K.Y.S. Ng, A. Brenner, K. More, K.M. Rahmoeller, D. Belton, Applied Catalysis B: Environmental 16 (1998) 105-117.

[71] K.S. Devi, S. Jayashree, Reaction Kinetics, Mechanisms and Catalysis 108 (2013) 183-192.

[72] N. Kamiuchi, M. Haneda, M. Ozawa, Catalysis Today 201 (2013) 79-84.

[73] L.F. Liotta, A. Macaluso, A. Longo, G. Pantaleo, A. Martorana, G. Deganello, Applied Catalysis A: General 240 (2003) 295-307.

[74] F. Giordano, A. Trovarelli, C. de Leitenburg, M. Giona, Journal of Catalysis 193 (2000) 273-282.

[75] H.-S. Roh, W.-S. Dong, K.-W. Jun, S.-E. Park, Chemistry Letters 30 (2001) 88-89.

[76] A. Goguet, F. Meunier, J.P. Breen, R. Burch, M.I. Petch, A. Faur Ghenciu, Journal of Catalysis 226 (2004) 382-392.

[77] E. Rogemond, R. Fréty, V. Perrichon, M. Primet, S. Salasc, M. Chevrier, C. Gauthier, F. Mathis, Journal of Catalysis 169 (1997) 120-131.

[78] V. Pitchon, J.F. Zins, L. Hilaire, G. Maire, React Kinet Catal Lett 59 (1996) 203-209.

[79] A.M. Diskin, R.H. Cunningham, R.M. Ormerod, Catalysis Today 46 (1998) 147-154.

[80] P. Fornasiero, J. Kašpar, M. Graziani, Journal of Catalysis 167 (1997) 576-580.

[81] F.B. Passos, E.R. de Oliveira, L.V. Mattos, F.B. Noronha, Catalysis Today 101 (2005) 23-30.

[82] S.M. de Lima, A.M. Silva, I.O. da Cruz, G. Jacobs, B.H. Davis, L.V. Mattos, F.B. Noronha, Catalysis Today 138 (2008) 162-168.

[83] X. Wu, J. Fan, R. Ran, D. Weng, Chemical Engineering Journal 109 (2005) 133-139.

[84] R.C. Egeberg, S. Ullmann, I. Alstrup, C.B. Mullins, I. Chorkendorff, Surface Science 497 (2002) 183-193.

[85] A. Kambolis, H. Matralis, A. Trovarelli, C. Papadopoulou, Applied Catalysis A: General 377 (2010) 16-26.

[86] J. Wei, E. Iglesia, The Journal of Physical Chemistry B 108 (2004) 4094-4103.

[87] Ş. Özkara-Aydınoğlu, A. Erhan Aksoylu, Chemical Engineering Journal 215–216 (2013) 542-549.

[88] M.C.J. Bradford, M.A. Vannice, Journal of Catalysis 173 (1998) 157-171.

[89] M.C. Bradford, M. Albert Vannice, Catalysis today 50 (1999) 87-96.

[90] T. Osaki, T. Horiuchi, K. Suzuki, T. Mori, Catal Lett 35 (1995) 39-43.

[91] M. Sigl, M.C. Bradford, H. Knözinger, M.A. Vannice, Topics in Catalysis 8 (1999) 211-222.

[92] A. Erdőhelyi, K. Fodor, F. Solymosi, Studies in Surface Science and Catalysis 107 (1997) 525-530.

[93] Y. Li, Y. Wang, X. Zhang, Z. Mi, International Journal of Hydrogen Energy 33 (2008) 2507-2514.

[94] M. Boaro, M. Vicario, C. de Leitenburg, G. Dolcetti, A. Trovarelli, Catalysis Today 77 (2003) 407-417.

[95] U. Roland, T. Braunschweig, F. Roessner, Journal of Molecular Catalysis A: Chemical 127 (1997) 61-84.

[96] D. Qin, J. Lapszewicz, Catalysis Today 21 (1994) 551-560.

[97] EPA, https://www.epa.gov/ghgemissions/inventory-us-greenhouse-gas-emissions-and-sinks-1990-2014 (2016) Last accessed 1/6/2017.

[98] N.H. Elsayed, N.M. Roberts, B. Joseph, J. Kuhn, Topics in Catalysis (2015) 138-146.

[99] J. Álvarez-Flórez, E. Egusquiza, Engineering Failure Analysis 50 (2015) 29–38.

[100] O. Sevimoglu, B. Tansel, Waste Management 33 (2013) 74-80.

[101] S.C. Surita, B. Tansel, Renewable Energy 80 (2015) 674-681.

[102] W. Urban, H. Lohmann, J.I. Salazar Gómez, Journal of Power Sources 193 (2009) 359-366.

[103] K. Haga, S. Adachi, Y. Shiratori, K. Itoh, K. Sasaki, Solid State Ionics 179 (2008) 1427-1431.

[104] A. Ohannessian, V. Desjardin, V. Chatain, P. Germain, Water Science and Technology 58 (2008) 1775-1781.

[105] J. Läntelä, S. Rasi, J. Lehtinen, J. Rintala, Applied Energy 92 (2012) 307–314.

[106] M. Schweigkofler, R. Niessner, Environmental Science & Technology 33 (1999) 3680-3685.

[107] D. Papurello, A. Lanzini, P. Leone, M. Santarelli, S. Silvestri, Waste Management 34 (2014) 2047-2056.

[108] D.D. Papadias, S. Ahmed, R. Kumar, Energy 44 (2012) 257-277.

[109] Q. Sun, H. Li, J. Yan, L. Liu, Z. Yu, X. Yu, Renewable and Sustainable Energy Reviews 51 (2015) 521-532.

[110] T.J. Bandosz, M. Seredych, J. Allen, J. Wood, E. Rosenberg, Chemistry of materials 19 (2007) 2500-2511.

[111] H.-C. Shin, J.-W. Park, K. Park, H.-C. Song, Environmental Pollution 119 (2002) 227-236.

[112] D.R. Ortega, A. Subrenat, Environmental Technology 30 (2009) 1073-1083.

[113] O. Sevimoğlu, B. Tansel, Journal of Environmental Management 128 (2013) 300-305.

[114] D.M. Walker, S. Pettit, J.T. Wolan, J.N. Kuhn, Applied Catalysis A: General 445 (2012) 61-68.

[115] R. Chakrabarti, J.L. Colby, L.D. Schmidt, Applied Catalysis B: Environmental 107 (2011) 88-94.

[116] R. Chakrabarti, S.A. Tupy, L.D. Schmidt, Energy & Fuels 25 (2011) 4763-4769.

[117] E. Finocchio, G. Garuti, M. Baldi, G. Busca, Chemosphere 72 (2008) 1659–1663.

[118] M. Schweigkofler, R. Niessner, Journal of Hazardous Materials B83 (2001) 183–196.

[119] P. Cheng, M. Zheng, Y. Jin, Q. Huang, M. Gu, Materials Letters 57 (2003) 2989-2994.

[120] S.B. Rasmussen, A. Kustov, J. Due-Hansen, B. Siret, F. Tabaries, R. Fehrmann, Applied Catalysis B: Environmental 69 (2006) 10-16.

[121] K. Liu, Q. Feng, Y. Yang, G. Zhang, L. Ou, Y. Lu, Journal of Non-Crystalline Solids 353 (2007) 1534-1539.

[122] Z. Zhang, X.E. Verykios, J. Chem. Soc., Chem. Commun. (1995) 71-72.

[123] Z. Zhang, X.E. Verykios, Applied Catalysis A: General 138 (1996) 109-133.

[124] U. Cimenler, B. Joseph, J.N. Kuhn, Applied Catalysis A: General 505 (2015) 494-500.

[125] U. Cimenler, B. Joseph, J.N. Kuhn, Energy & Fuels 30 (2016) 5300-5308.

[126] M.F. Philip Budzik, EIA: US Energy Information Administration, http://www.eia.gov/todayinenergy/detail.cfm?id=18451, 2014, North Dakota aims to reduce natural gas flaring.

[127] W. Pan, J. Zheng, C. Song, Fuel Chem. Div. Prep 47 (2002) 262-264.

[128] V.R. Choudhary, B.S. Uphade, A.S. Mamman, Applied Catalysis A: General 168 (1998) 33-46.

[129] L. Pino, A. Vita, F. Cipitì, M. Laganà, V. Recupero, Applied Catalysis B: Environmental 104 (2011) 64-73.

[130] G.A. Olah, Catal Lett 143 (2013) 983-987.

[131] N. Kumar, A. Roy, Z. Wang, E.M. L'Abbate, D. Haynes, D. Shekhawat, J.J. Spivey, Applied Catalysis A: General 517 (2016) 211-216.

[132] G.A. Olah, A. Goeppert, M. Czaun, T. Mathew, R.B. May, G.K.S. Prakash, Journal of the American Chemical Society 137 (2015) 8720-8729.

[133] Y. Lim, C.-J. Lee, Y.S. Jeong, I.H. Song, C.J. Lee, C. Han, Industrial & Engineering Chemistry Research 51 (2012) 4982-4989.

[134] D.S.A. Simakov, M.M. Wright, S. Ahmed, E.M.A. Mokheimer, Y. Roman-Leshkov, Catalysis Science & Technology 5 (2015) 1991-2016.

[135] S.D. Angeli, L. Turchetti, G. Monteleone, A.A. Lemonidou, Applied Catalysis B: Environmental 181 (2016) 34-46.

[136] S. Chilukoti, F. Gao, B.G. Anderson, J.H. Niemantsverdriet, M. Garland, Physical Chemistry Chemical Physics 10 (2008) 5510-5520.

[137] J.C. Wu, C.-W. Huang, Frontiers of Chemical Engineering in China 4 (2010) 120-126.

[138] G. Jacobs, L. Williams, U. Graham, D. Sparks, B.H. Davis, The Journal of Physical Chemistry B 107 (2003) 10398-10404.

[139] A. Goguet, F.C. Meunier, D. Tibiletti, J.P. Breen, R. Burch, The Journal of Physical Chemistry B 108 (2004) 20240-20246.

[140] X. Wang, H. Shi, J.H. Kwak, J. Szanyi, ACS Catalysis 5 (2015) 6337-6349.

[141] T. Bunluesin, R.J. Gorte, G.W. Graham, Applied Catalysis B: Environmental 15 (1998) 107-114.

[142] R.L. Espinoza, A.P. Steynberg, B. Jager, A.C. Vosloo, Applied Catalysis A: General 186 (1999) 13-26.

[143] A.P. Steynberg, R.L. Espinoza, B. Jager, A.C. Vosloo, Applied Catalysis A: General 186 (1999) 41-54.

[144] S. Li, S. Krishnamoorthy, A. Li, G.D. Meitzner, E. Iglesia, Journal of Catalysis 206 (2002) 202-217.

[145] H.M. Torres Galvis, J.H. Bitter, T. Davidian, M. Ruitenbeek, A.I. Dugulan, K.P. de Jong, Journal of the American Chemical Society 134 (2012) 16207-16215.

[146] S.A. Gardezi, J.T. Wolan, B. Joseph, Applied Catalysis A: General 447–448 (2012) 151-163.

[147] K.-W. Jun, H.-S. Roh, K.-S. Kim, J.-S. Ryu, K.-W. Lee, Applied Catalysis A: General 259 (2004) 221-226.

[148] S. Eliason, C. Bartholomew, Applied Catalysis A: General 186 (1999) 229-243.

[149] K. Cheng, V. Ordomsky, M. Virginie, B. Legras, P. Chernavskii, V. Kazak, C. Cordier, S. Paul, Y. Wang, A. Khodakov, Applied Catalysis A: General 488 (2014) 66-77.

[150] E. van Steen, M. Claeys, Chemical engineering & technology 31 (2008) 655-666.

APPENDIX A: COPYRIGHT PERMISSIONS

A.1 Permission for Use of Material in Chapter 1

Copyright permission
2 messages

Schert,John D <jschert@ufl.edu> Wed, Sep 28, 2016 at 6:34 PM
To: Nada Elsayed <nelsaye2@mail.usf.edu>
Cc: John Kuhn <jnkuhn@usf.edu>

Hi Nada,
Yes. You have permission to use any or all of the report "Single Step Conversion of Landfill Gas to Liquid Hydrocarbon Fuels" in your dissertation.

Best regards,
jds
John Schert
Executive Director
The Bill Hinkley Center for Solid and Hazardous Waste Management
A Statewide Center for Research, Education and Public Service
Created by the Florida Legislature and Hosted by the University of Florida College of Engineering
528 Nuclear Science Building | Gainesville, FL 32611
jschert@ufl.edu | 352-392-6264 | www.hinkleycenter.org

On Sep 28, 2016, at 4:10 PM, Nada Elsayed <nelsaye2@mail.usf.edu> wrote:

Good afternoon John

How are you? I hope you are well. I am writing you this e-mail to request permission to use portions of the "Single Step Conversion of Landfill Gas to Liquid Hydrocarbon Fuels" report in my dissertation. As per university guidelines, I must include a written consent (e-mail will suffice), to use portions of the report. I would also like to point out that my dissertation will be available online for readers. Both the report and the Hinkley center will be referenced in my dissertation so readers are able to locate the original report on the Hinkley website.

Have a wonderful day!

Regards,

Nada Elsayed

Doctoral Candidate
Heterogeneous Catalysis & Materials Chemistry Group
Department of Chemical & Biomedical Engineering
University of South Florida
4202 E. Fowler Avenue
Office: IDRB 202A/Mail to: ENB 118

A.2 Permission for Use of Material in Chapter 2

My Orders | My Library | My Profile | Welcome nelsaye2@mail.usf.edu | Log out | Help

My Orders > Orders > All Orders

License Details

This Agreement between Nada Elsayed ("You") and Elsevier ("Elsevier") consists of your license details and the terms and conditions provided by Elsevier and Copyright Clearance Center.

printable details

License Number	3998890465520
License date	Nov 30, 2016
Licensed Content Publisher	Elsevier
Licensed Content Publication	Applied Catalysis B: Environmental
Licensed Content Title	Low temperature dry reforming of methane over Pt–Ni–Mg/ceria–zirconia catalysts
Licensed Content Author	Nada H. Elsayed,Nathan R.M. Roberts,Babu Joseph,John N. Kuhn
Licensed Content Date	December 2015
Licensed Content Volume	179
Licensed Content Issue	n/a
Licensed Content Pages	7
Type of Use	reuse in a thesis/dissertation
Portion	full article
Format	both print and electronic
Are you the author of this Elsevier article?	Yes
Will you be translating?	No
Order reference number	
Title of your thesis/dissertation	Catalytic Upgrading of Biogas to Fuels: Role of Reforming Temperature, Oxidation Feeds, and Contaminants
Expected completion date	Jan 2017
Estimated size (number of pages)	135
Elsevier VAT number	GB 494 6272 12
Requestor Location	Nada Elsayed 4202 e fowler ave TAMPA, FL 33620 United States Attn: Nada Elsayed
Total	**0.00 USD**

BACK

A.3 Permission for Use of Material in Chapter 3

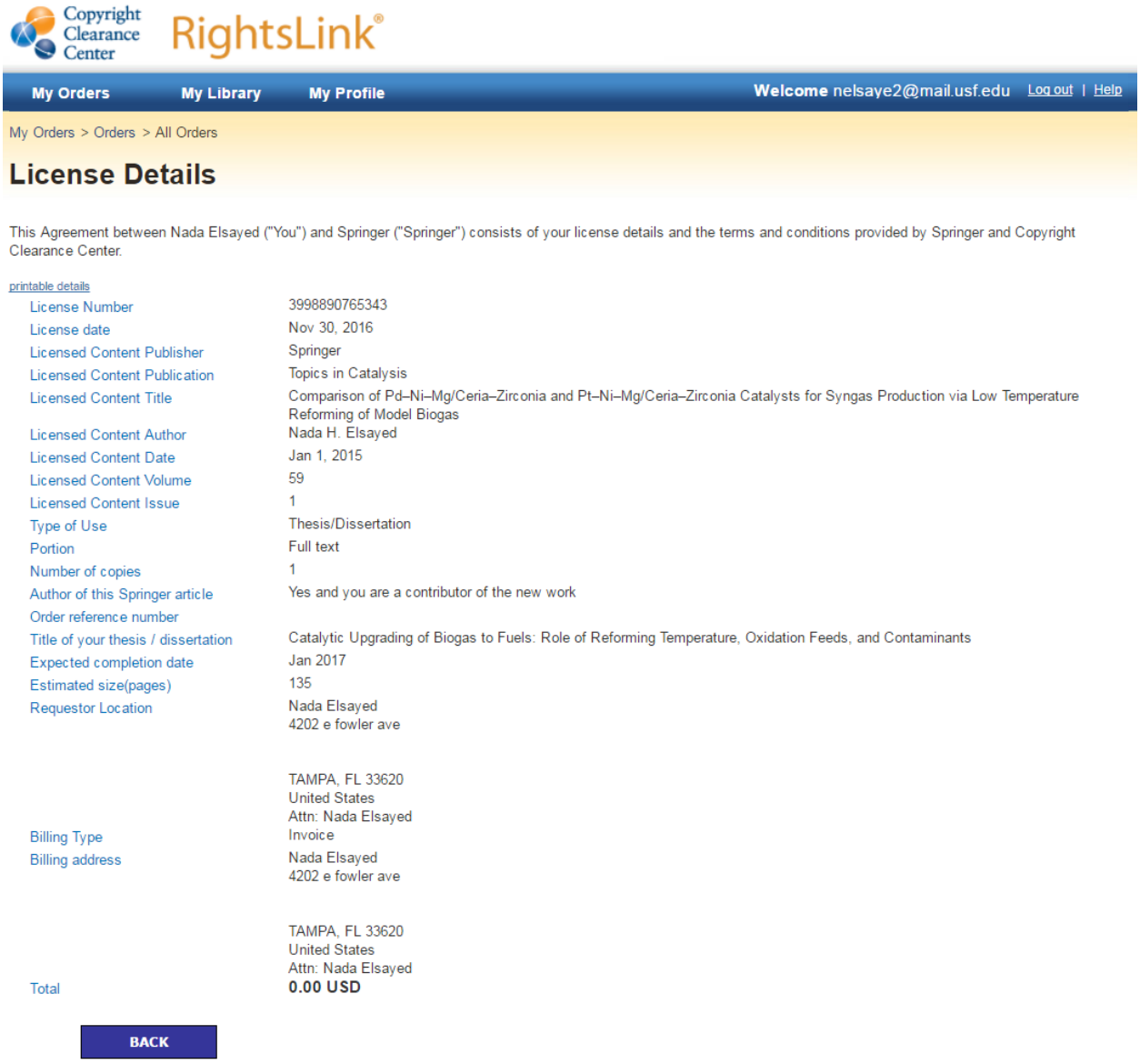

Copyright Clearance Center RightsLink®

My Orders | My Library | My Profile | Welcome nelsaye2@mail.usf.edu | Log out | Help

My Orders > Orders > All Orders

License Details

This Agreement between Nada Elsayed ("You") and Springer ("Springer") consists of your license details and the terms and conditions provided by Springer and Copyright Clearance Center.

printable details

License Number	3998890765343
License date	Nov 30, 2016
Licensed Content Publisher	Springer
Licensed Content Publication	Topics in Catalysis
Licensed Content Title	Comparison of Pd–Ni–Mg/Ceria–Zirconia and Pt–Ni–Mg/Ceria–Zirconia Catalysts for Syngas Production via Low Temperature Reforming of Model Biogas
Licensed Content Author	Nada H. Elsayed
Licensed Content Date	Jan 1, 2015
Licensed Content Volume	59
Licensed Content Issue	1
Type of Use	Thesis/Dissertation
Portion	Full text
Number of copies	1
Author of this Springer article	Yes and you are a contributor of the new work
Order reference number	
Title of your thesis / dissertation	Catalytic Upgrading of Biogas to Fuels: Role of Reforming Temperature, Oxidation Feeds, and Contaminants
Expected completion date	Jan 2017
Estimated size(pages)	135
Requestor Location	Nada Elsayed 4202 e fowler ave TAMPA, FL 33620 United States Attn: Nada Elsayed
Billing Type	Invoice
Billing address	Nada Elsayed 4202 e fowler ave TAMPA, FL 33620 United States Attn: Nada Elsayed
Total	**0.00 USD**

BACK

APPENDIX B: CALCULATIONS

B.1 Assumptions and Calculations for Chapter 4

The estimate of accelerated poisoning, general assumptions are:

- Plant operates 24/7.
- GHSV= 68,000h^{-1}
- Density of catalyst= 1704.5 kg/m^3
- Flowrate=Q= 2500ft^3/min
- Assuming a 4mg/m^3 siloxane concentration

The sample calculations for silica % weight gain based on the previous assumptions are:

$$Volume\ Catalyst\ Bed = \frac{4248 \frac{m^3}{hr}}{68000\ hr^{-1}} = 0.0625\ m^3 \quad (1)$$

$$Mass\ Catalyst\ Bed = 0.0625\ m^3 \times 1704.5\ \frac{kg}{m^3} = 106.5\ \text{kg} \quad (2)$$

$$Silica\ Flow = 4248\ \frac{m^3}{hr} \times 4E^{-6}\ \frac{kg}{m^3}(SiO2) = 0.01699\ \frac{kg}{hr} \quad (3)$$

$$Silica\ Mass\ After\ 6\ months = 0.01699\ \frac{kg}{hr} \times \left(180\ days \times 24\ \frac{hr}{day}\right) = 73.41\ kg \quad (4)$$

$$6\ month\ Silica\ \%\ mass\ gain: = \frac{73.41\ kg}{106.5\ kg} = 68.9\% \quad (5)$$

Table B1: Mass gain of silica and error calculations

Sample	Nomenclature	Theoretical Mass gain SiO_2	Actual Mass Gain SiO_2	%error
1 week NiMg	1W-NiMg	2.6%	1.5%	-43.5%
1 month NiMg	1M-NiMg	11.1%	11.9%	7.5%
6 month NiMg	6M-NiMg	66.7%	65.7%	-1.5%
1week Pt	1W-Pt	2.6%	1.1%	-59.4%
1 month Pt	1M-Pt	11.1%	10.5%	-5.4%
6 month Pt	6M-Pt	66.7%	61.9%	-7.2%

Table B2: Effect of changing GHSV (h^{-1})

2X GHSV			
GHSV	136000		h^{-1}
6 months silica % mass gain	Mass of silica/mass of catalyst bed	138	%
0.5X GHSV			
GHSV	35000		h^{-1}
6 months silica % mass gain	Mass of silica/mass of catalyst bed	35.8	%

Table B3: Effect of changing initial siloxane amount

2X siloxane			
6 months silica % mass gain	Mass of silica/mass of catalyst bed	138	%
0.5X siloxane			
6 months silica % mass gain	Mass of silica/Mass of bed	34.5	%